Sodium Borohydride As a Circular Hydrogen Carrier

An Energy Efficient Link Between Hydrogen Release and Sodium Borohydride Synthesis.

SET3901: Graduation Project

Tim Wesselingh

Delft University of Technology

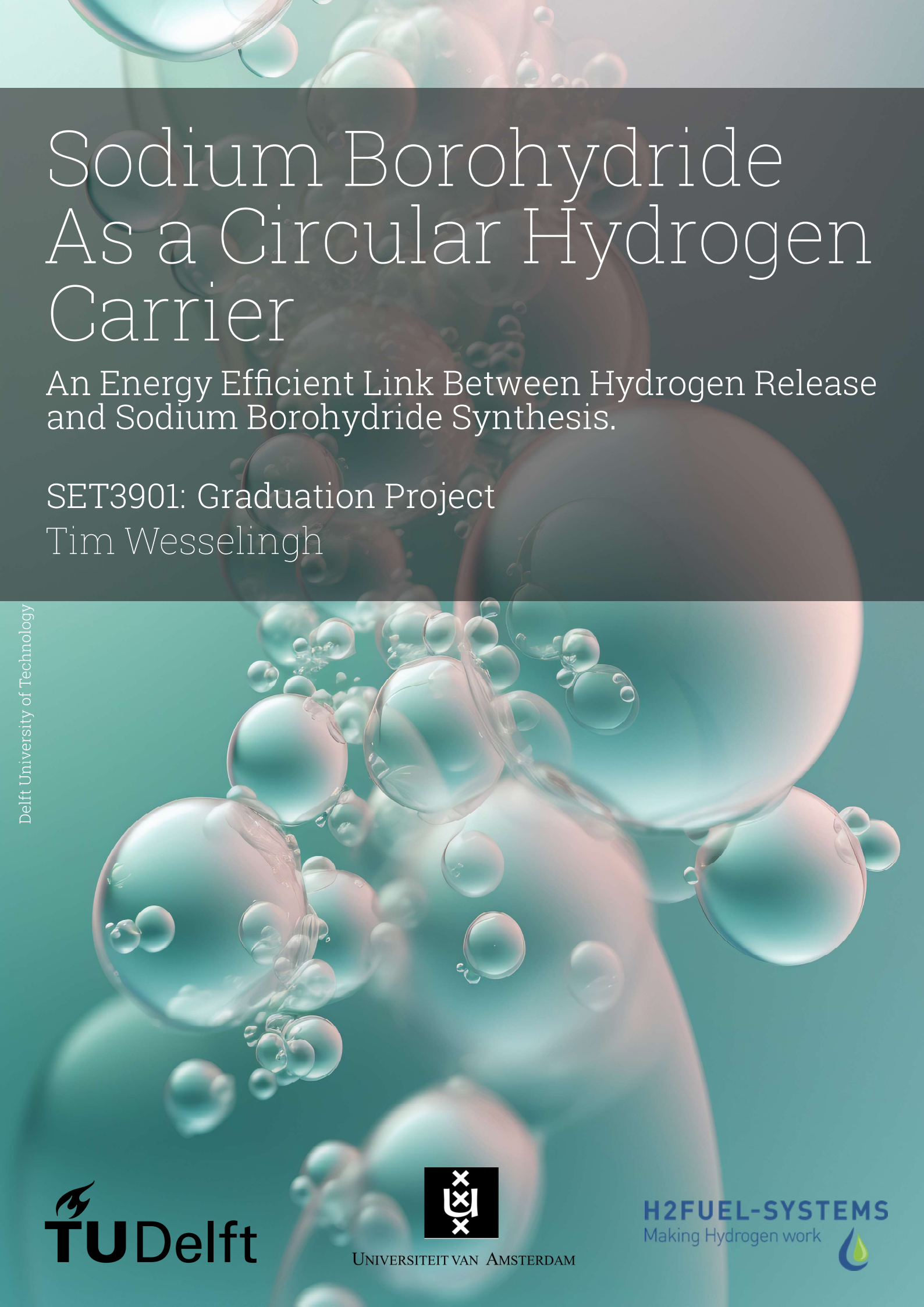

TU Delft

Universiteit van Amsterdam

H2FUEL-SYSTEMS
Making Hydrogen work

Sodium Borohydride As a Circular Hydrogen Carrier

An Energy Efficient Link Between Hydrogen Release and Sodium Borohydride Synthesis.

by

Tim Wesselingh

to obtain the degree of Master of Science
at the Delft University of Technology,
to be defended on Monday September 11, 2023 at 10:00 AM.

Student number:	4480155	
Project duration:	November, 2022 – August, 2023	
Thesis committee:	Prof. Dr. Ir. J.T. Padding,	TU Delft
	Dr. C. Slootweg,	UvA
	Dr. F. Buß,	UvA

This thesis is confidential and cannot be made public until September 1st, 2025.

An electronic version of this thesis is available at `http://repository.tudelft.nl/`.

TU Delft

Universiteit van Amsterdam

H2FUEL-SYSTEMS
Making Hydrogen work

Preface

This report presents a novel method for circular hydrogen storage in sodium borohydride ($NaBH_4$). All experiments that have been conducted in this thesis are performed by Tim Wesselingh, as well being the author of this thesis. All experiments are performed within the Synthetic Organic Chemistry research group (SOC) as part of the Van 't Hoff Institute for Molecular Sciences at the University of Amsterdam during the period of 11/2022 until 09/2023 under the supervision of Florenz Buß. This research is part of a joint research project between the Slootweg Research Group within SOC and the research group of Complex Fluid Processing in the Department of Process and Energy (P&E) at Delft University of Technology.

During my studies in molecular sciences and chemical engineering for my Bachelors, together with environmental sciences during my masters, I became inspired by the fundamental ideas in chemistry and the technological assets that facilitates its implementation. This project is a reflection of the combination between finding a fundamental solution for a societal problem in chemistry and trying to implement it on large scale through chemical engineering assets. I am truly grateful that I have been given the opportunity to contribute to this field of research from such a close perspective.

I would like to thank people who played an important role in the realization of this master thesis. First of all, I would like to thank my main supervisors at the University of Amsterdam: Chris Slootweg, Assistant professor at the SOC research group and Florenz Buß, Post-doc researcher at the SOC research group. Without them and their enthusiasm and constructive feedback this research would not have been possible. I have always been motivated and thrived on this topic thanks to their guidance on this project. The same holds for the supervisor from the TU Delft: Prof.Dr.Ir. Johan Padding, Chair of Complex Fluid Processing in the Department of Process and Energy (P&E) of Delft University of Technology. I want to thank Johan extensively. Without him, this research would definitely have not been possible as he started the joint research project between the UvA and the TU Delft. His guidance and feedback helped me a lot in the realization of this master thesis. Thirdly, I want to thank all members of the SOC research group, specifically Valentin Geiger, Bas de Jong, Pier Wessels, Joost van Gaalen and Philip Germanecos with whom I sparred a lot and who made going to the lab everyday very enjoyable. Fourthly, I would like to thank all attendees of the 'H2Fuel Systems B.V.', with special thanks to Marieke Palm, who got me involved with the research project in the first place. Thereafter, I like to thank my friends and family who supported me during my thesis.

Tim Wesselingh
Delft, September 2023

Summary

This thesis presents a novel method for using sodium borohydride ($NaBH_4$) as a circular hydrogen carrier, addressing the current lack of commercially viable approaches for hydrogen storage in $NaBH_4$. Conventional methods for storing hydrogen in $NaBH_4$ suffer f rom h igh e nergy r equirements d ue t o h igh r eaction temperatures and having multiple reaction steps. This research aims to optimize the release of hydrogen from $NaBH_4$ and the regeneration of spent fuel, with the objective of minimizing the energy intensity associated with the potential use of $NaBH_4$ as a circular hydrogen carrier.

The traditional approach of using $NaBH_4$ for circular hydrogen storage through hydrolysis was reevaluated, leading to the development of a novel reaction system consisting of solely a one-pot reaction for the hydrogen release process. Alcoholysis reactions were performed using methanol and isopropyl alcohol (IPA) along with stoichiometric amounts of an acid. This resulted in the selective formation of trimethylborate ($B(OCH_3)_3$) and triisopropylborate ($B(OiPr)_3$), respectively. Notably, the focus was centered on alcoholysis through IPA and stoichiometric amounts of H_2SO_4, as $NaBH_4$ and IPA could be premixed without premature reaction occurring in the absence of a stabilizer and because the $B(OiPr)_3$/IPA mixture was assumed to be easier separable compared to the $B(OCH_3)_3$/methanol mixture. Subsequently, successful regeneration of $B(OiPr)_3$ to $NaBH_4$ was achieved by adopting reaction conditions from the Brown-Schlesinger process, thus realizing a complete circular hydrogen storage process for the proposed system. Attempts were made to minimize the energy intensity of $NaBH_4$ synthesis by exploring alternate reaction pathways that could potentially lower reaction temperatures. This involved the use of radical sources such as sodium naphthalenide and sodium biphenyl, leading to the formation of boron radical anions that facilitated homolytic hydrogen cleavage which initiated borohydride formation. The formation of BH, BH_2, BH_3 compounds, as well as selective formation of BH compounds, was observed. These findings serve as a foundation for selective borohydride synthesis through radical activation, enabling borohydride formation at mild reaction conditions and ultimately estab-lishing a potential economically viable method for $NaBH_4$ synthesis.

To address the challenge of heat transfer during hydrogen release, a heat transfer limitation model was developed. Real-time data was collected to extrapolate temperature profiles for different $NaBH_4$ quantities and their respective proportions of IPA, H_2SO_4, and reactor volumes for predicting temperature trajectories. This data was functionalized and used for the prediction of cooling water temperature profiles and minimum cooling water flow rates upon up scaling. It was seen that heat transfer in this system has a linear correlation to the amount of reacting $NaBH_4$ upon scaling. Therefore, the envisioned hydrogen release process is not assumed to be forming a problem for the reactor design upon up scaling with regards to heat transfer limitations. The minimum scaling factor for the model to be in effect was 580 due to the threshold of reaching turbulent flow regimes in the cooling mantle, corresponding to a minimum turnover number of 12 kg $NaBH_4$/batch reaction of 20 minutes, requiring 812 L of cooling water.

Furthermore, an economic assessment was conducted to evaluate the viability of the envisioned system. A process flow diagram of the alcoholysis reaction pathway was initially constructed. Subsequently, this diagram served as the foundation for establishing an energy balance for both the hydrogen release process and the $NaBH_4$ regeneration process, which enabled a comparative examination between the hydrolysis pathway and the proposed alcoholysis pathway. It was observed that the energy requirement of the hydrolysis pathway being 360.2 kWh/kg of H2, was decreased to 253.1 kWh/kg of H_2, required by the proposed alcoholysis system.

In conclusion, this thesis proposes a fully circular reaction pathway for hydrogen storage in $NaBH_4$ and introduces a novel potential reaction pathway for borohydride formation through radical chemistry. Additionally, a comprehensive analysis of scale-up potential is presented, incorporating a heat transfer limitation model and a techno-economic analysis. By doing so, this research aims to overcome barriers associated with the application of $NaBH_4$ as a circular hydrogen carrier, ultimately establishing an e icient, economically viable, scalable, and sustainable reaction pathway for circular hydrogen storage in $NaBH_4$.

Contents

Nomenclature

Abbreviations

Abbreviation	Definition
$B(OCH_3)_3$	Trimethylborate
$B(O\textit{i}Pr)_3$	Triisopropylborate
FLP	Frustrated Lewis Pair
H_2SO_4	Sulfuric Acid
H_3PO_4	Phosphoric Acid
HCl	Hydrochloric Acid
IPA	Isopropanol/Isopropyl Alcohol
IR	Infrared
LuHOTf	Lutidinium Triflate
LAB	Lewis Acidic Boranes
$NaBH_4$	Sodiumborohydride
$NaBO_2 \cdot H_2O$	Sodium metaborate
$NaB(OCH_3)_4$	Sodium tetra methoxyborate
NaH	Sodiumhydride
$NaOCH_3$	Sodium metoxide
NaOH	Sodium Hydroxide
$NaO\textit{i}Pr$	Sodium isopropoxide
NMR	Nuclear Magnetic Resonance
PEM	Proton Exchange Membrane
RBF	Roundbottom Flask
THF	Tetrahydrofuran

Symbols

Symbol	Definition	Unit
A	Area	m^2
C_p	Heat capacity	J/kg*K
D	Diameter or thickness	m
h	Thermal conductance	J/m*K
H	Enthalpy	J/mol
L	Length	m
m	Mass	kg
Q	Heat	J
T	Temperature	K
V	Volume	m^3
v	Velocity	m/s
μ	Kinetic viscosity	Pa*s
ρ	Density	kg/m^3
ϕ_q	Heat flow rate	J/s
ϕ_m	Mass flow rate	kg/s
ϕ_v	Volumetric flow rate	m^3/s

1 Introduction

The energy market experiences heightened volatility due to the increasing unpredictability of energy load, attributed to the widespread adoption of wind and solar energy [1]. Efficient use and distribution of energy are basic requirements for a prospective energy economy. As an important matter in this respect, the infrastructure of modern energy systems requires innovative and renewable storage capabilities, one of such being energy storage through hydrogen. Hydrogen is a highly promising alternative energy source to traditional fuels, including fossil fuels, and has the potential to function as a suitable energy carrier. With a calorific value of $1.4{\cdot}10^8$ J/kg [2], hydrogen has a higher energy potential in comparison to all fossil and biofuels. Additionally, hydrogen is a potential sustainable fuel with zero carbon emission upon combustion. However, the production of hydrogen still has a significant carbon footprint since 96% of commercially produced hydrogen originates from the steam reformation of light hydrocarbons or coal gasification, which releases substantial amounts of carbon dioxide (CO_2) [3]. Only 4% of the global commercial hydrogen is produced sustainably through the electrolysis of water [4].

While hydrogen has multiple advantages compared to conventional energy carriers, it has certain drawbacks with regard to storage. Various methods exist for storing hydrogen on a larger scale. The conventional method of hydrogen storage is through liquefaction [5]. However, it is energetically challenging to store liquefied hydrogen as it requires high pressures and low temperatures [6, 7]. Another storage vector which can be employed as an alternative to conventional energy carriers is hydrogen storage through ammonia. Ammonia provides an alternative storage option as it is a liquid with mild pressurization and cryogenic constraints [8]. Nevertheless, releasing hydrogen from ammonia and separating hydrogen gas from nitrogen gas after the hydrogen release requires significant amounts of energy [9]. Moreover, ammonia has a substantial nitrogen footprint and high environmental toxicity [10]. Another way of storing hydrogen is through the use of Liquid Organic Hydrogen Carriers (LOHCs), in which hydrogen is chemically bound in organic compounds that can absorb and release hydrogen through external stimuli such as temperature, pressure, or the presence of a catalyst [11]. Although LOHCs offer a potentially valuable alternative as a hydrogen storage vector with a higher energy density than both ammonia and liquid hydrogen, they still have a relatively low energy density when compared to conventional energy carriers such as diesel or gasoline. Another promising strategy for storing hydrogen is by binding hydrogen to a metal or metalloid in the form of metal hydrides. Metal hydrides can function as solid hydrogen carriers and can be stored at atmospheric pressure at room temperature. Metal hydrides are non-flammable and mostly have no severe toxic properties [12]. One of the more intesively investigated metal hydrides is sodiumborohydride ($NaBH_4$). $NaBH_4$ is a metal hydride which is widely used as a reducing agent for pharmaceuticals and as a bleaching agent [3]. It also functions as a metalhydride potentially suitable for hydrogen storage [12]. $NaBH_4$ is relatively cheap and lightweight compared to other metal hydrides [13, 14, 15]. It is stated in literature that hydrogen released from $NaBH_4$ is suitable for feeding into a proton-exchange membrane (PEM) fuel cell to generate electricity [12]. Additionally, $NaBH_4$ has a high energy density compared to other alternative and conventional energy carriers. A comparison of energy densities between such alternate and conventional energy carriers is depicted in Figure 1.1.

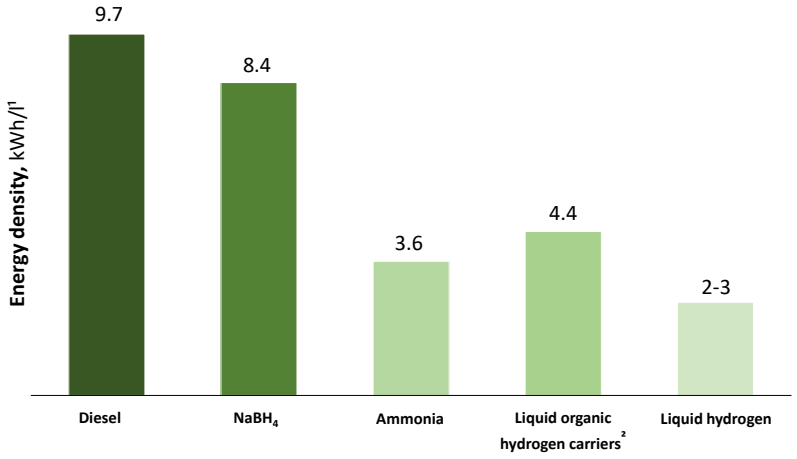

Figure 1.1: Energy densities of various energy carriers [16]. [1]$NaBH_4$ is stored as a solid. [2]Based on methanol.

Despite that $NaBH_4$ has a comparable energy density to that of diesel and in view of the various advantages of $NaBH_4$ and metal hydrides in general, the industrial application of using $NaBH_4$ for hydrogen storage has not yet been realized. Persistent problems are the weight of hydrogen that $NaBH_4$ carries and the reversibility of the storage process [17]. The release of hydrogen from $NaBH_4$ can be achieved in a simple manner by chemical treatment. However, synthesizing $NaBH_4$ by storing hydrogen has only be realised through severe reaction conditions and the use of expensive reducing agents [18], which make industrial application as an energy storage vector challenging.

A main driver for the use of $NaBH_4$ was the potential implementation in personal transportation, e.g. cars and other vehicles. However, in 2007 the US department of Energy has declared that $NaBH_4$ is not a feasible fuel substitute due to the barriers mentioned earlier. Therefore, research in this area has become more scarce [19]. However, these claims were made on conventional non-circular reaction pathways. If the reversibility of the storage process is realised in a circular way, $NaBH_4$ as an energy carrier could potentially be used as a competitive method for storing hydrogen.

1.1. Hydrogen release from metalhydrides

In the published literature, several alternative metal hydrides have been identified as potential candidates for hydrogen storage, including potassium borohydride [20, 21], lithium borohydride [22], magnesium hydride [23], and lithium aluminium hydride [24]. It has been suggested that $NaBH_4$ could serve as a suitable circular storage vector due to its relatively favorable reactivity and high gravimetric hydrogen storage capacity. Over 60% of the mass of $NaBH_4$ consists of sodium (Na). Na being an alkali metal with an atomic number of 11, it represents one of the lightest metals used in metal hydrides for potential commercial hydrogen storage, second only to lithium (Li) used in lithiumborohydride ($LiBH_4$) [13]. While $LiBH_4$ offers a higher gravimetric hydrogen storage capacity than $NaBH_4$, it is considerably more expensive and less sustainable due to the relative abundance of Na as a metal resource.

Various methods for hydrogen release from metal hydrides are documented in the literature, including hydrolysis [12, 25], alcoholysis [22], and semi-alcoholysis [26, 27], typically initiated by external stimuli such as heat or the presence of a catalyst, depending on the specific fuel mixture. For the hydrolysis and (semi-)alcoholysis of $NaBH_4$, two main hydrogen release pathways have been proposed [12]: under employment of acid or under employment of a catalyst under alkaline conditions.

1.1.1. Hydrogen release from $NaBH_4$ in aqueous solutions

The hydrolysis of $NaBH_4$ is a reaction between $NaBH_4$ and water. The reaction is depicted in Equation 1.1. The hydrolysis of $NaBH_4$ releases 4 equivalents of dihydrogen. However, the release rate of hydrogen is slow and does not suffice for an adequate hydrogen release rate for industrial application [25]. Therefore, the release rate of hydrogen has to be increased. As previously mentioned, an accelerated release of hydrogen through hydrolysis can be initiated through two reaction pathways. The first pathway is the alkaline/catalytic pathway where $NaBH_4$ reacts with water in an alkaline environment over a metal catalyst forming dihydrogen and sodium metaborate as shown in Equation 1.2.

$$NaBH_4 + 4\,H_2O \xrightarrow[RT]{} NaB(OH)_4 + 4\,H_2 \tag{1.1}$$

$$NaBH_4 + 4\,H_2O \xrightarrow[RT]{\text{Catalyst}} NaB(OH)_4 + 4\,H_2 \tag{1.2}$$

The second pathway is the the acid activated hydrolysis of $NaBH_4$. In the latter reaction, $NaBH_4$ is brought in contact with an acid/water mixture to form H_2 and boric acid (H_3BO_3) (see Equation 1.3).

$$NaBH_4 + 3\,H_2O + HCl \xrightarrow[RT]{} H_3BO_3 + NaCl + 4\,H_2 \tag{1.3}$$

1.1.1.1. Hydrolysis of $NaBH_4$ through the alkaline/catalytic pathway

Equation 1.2 depicts the hydrolysis reaction through the alkaline/catalytic pathway in which $NaBH_4$ is brought in contact with H_2O over a catalyst to form H_2 and sodium tetrahydroxyborate ($NaB(OH)_4$). If $NaBH_4$ can be considered 'fuel', the latter product can be considered 'spent fuel'. Henceforth, the term 'spent fuel' refers to the resulting mixture formed after the H_2 release reaction using the respective 'fuel' mixture. In terms of spent fuel, literature description on the nature of the spent fuel is inconsistent as the primary existence of $NaB(OH)_4$ in solution has been claimed but not consistently reported [28]. By adding stochiometric amounts of an acid, the spent fuel is converted to H_3BO_3 and the respective sodium salt (see Equation 1.4). H_3BO_3 can subsequently be used for the regeneration of $NaBH_4$.

$$NaB(OH)_4 + HCl \xrightarrow[RT]{} H_3BO_3 + H_2O + NaCl \tag{1.4}$$

Various catalysts have been shown to accelerate the release of hydrogen from $NaBH_4$ in water (see Table 1.1). The hydrogen release rate with the use of a catalyst is increased substantially in comparison to the uncatalysed reaction. Also, within this route, the $NaBH_4$ is premixed with water and sodiumhydroxide (NaOH) before the hydrogen release [29]. The latter is possible because $NaBH_4$ is stable in an aqueous alkaline solution with a pH above 10 [29]. In this way, the release of hydrogen is more controllable with regards to process design as premixing generally prevents mass transfer limitations because $NaBH_4$ is dissolved before making contact to the surface of the catalyst [29, 30]. In Table 1.2, some examples of premixed liquid to solid reactions of the hydrolysis of $NaBH_4$ are shown.

Noble metal catalysts usually exhibit superior catalytic activity in comparison to non-metal catalysts with regards the the hydrolysis of $NaBH_4$ [31, 32, 33, 34]. However, most of these used catalysts are more cost-intensive and less abundant [35, 36, 37, 31, 38]. In previous studies, no full recyclability and no sufficient yields could be achieved, implicating another disadvantage to this strategy. Other disadvantages have been found in the recovery of the catalytic material which ends up in the reaction mixture and again later in the process has to be removed [12]. This makes both product characterization and catalyst recovery challenging.

Table 1.1: A selection of catalysts used for the hydrogen release of $NaBH_4$ through hydrolysis.

Catalyst type	Hydrogen release rate ($ml/min/g_{cat}$)
$CoCl_2$ with Guanidinium Borohydride	692.3 [39]
Co composite	1179 [40]
Ru-particles	3100 [41]
Poly(4-vinylpyridine)-based polymer	9125 [42]
Pt-/Ru-$LiCoO_2$	7200 [43]
Pt/Co_3O_4	120 [44]
$Au_{50}Ni_{50}$	2597 [45]
SiO_2-OSO_3H	6219 [46]

Table 1.2: A selection of catalytic systems using premixed alkaline solutions with $NaBH_4$ used for the hydrogen release of $NaBH_4$ through hydrolysis.

Catalyst type	Hydrogen release rate ($ml/min/g_{cat}$)
Sepiolite clay with CoB	5025 [47]
$Ru/CoFe_2O_4$	93,500 [48]
$Pd/CoFe_2O_4$	74800 [48]
Ni_xB	333,333 [49]
$NiCo_2O_4$/zeolite	6219 [50]
Fe-Co-B-Ni	22,000 [51]
Mn-CeO_2	7142 [52]
Zn-Co-B/G	2180 [53]

1.1.1.2. Hydrolysis of $NaBH_4$ through the acidic pathway

It is known in literature that the hydrolysis of $NaBH_4$ in the presence of an acid elevate the hydrogen release [54]. Acids react with $NaBH_4$ and overall increase the hydrogen generation this way. In this reaction, side product formation depends on the acid concentration in the reaction mixture [55]. It is postulated that as the concentration of acid increases, protons react with the borohydride anion to form an intermediate complex H_2BH_3 (or $H^+xBH_4^-$) which decomposes to hydrogen and borane (see Equation 1.5) [56, 57, 58, 59]. Borane subsequently dimerizes to diborane (see Equation 1.6).

$$H_2BH_3 \rightleftharpoons BH_3 + H_2 \tag{1.5}$$

$$2\,BH_3 \rightleftharpoons B_2H_6 \tag{1.6}$$

Both borane and diborane are gaseous compounds and contaminate the hydrogen gas purity. In addition, it decreases hydrogen yield as the proton sources in a concentrated acidic environment are $NaBH_4$ and the acid (see Equation 1.7) instead of $NaBH_4$ and water as in a diluted acidic environment (Equation 1.8). This reaction therefore requires a diluted acid concentration realized by an excess of water in order to prevent

diborane formation.

$$2\,NaBH_4 + 2\,HCl \xrightarrow[RT]{} 2\,NaCl + B_2H_6 + 2\,H_2 \tag{1.7}$$

$$NaBH_4 + 3\,H_2O + HCl \xrightarrow[RT]{} H_3BO_3 + NaCl + 4\,H_2 \tag{1.8}$$

Therefore, excessive amounts of solvent are required to dilute the solution sufficiently in order reach full conversion to the respective spent fuel, which might cause mass or volume limitations. By adding a stochiometric amount of protons in a diluted solution it is seen that H_3BO_3 is solely formed [60]. The formed H_3BO_3 can be isolated through crystallization and subsequent filtration. Subsequently, further transformation to trimethylborate ($B(OCH_3)_3$) can be achieved through a reaction with methanol (Equation 1.9). $B(OCH_3)_3$ can function as a starting material for the regeneration of $NaBH_4$ through the Brown-Schlesinger Process (see section 3.2).

$$H_3BO_3 + 3\,CH_3OH \xrightarrow[RT]{} B(OCH_3)_3 + 3\,H_2O \tag{1.9}$$

Examples in previous literature have demonstrated that release rates of hydrogen by using an acid competes with release rates achieved by expensive noble-metal catalysts [54]. Increasing the release rate through an acid has various advantages in contrast to the use of a catalyst. First of all, cheap acids can be used for the reaction as any strong enough proton source suffices which minimizes process costs. Secondly, there is no catalytic material that erodes in the reaction mixture which again has to be separated from the desired product. A disadvantage of the acidic pathway is that a salt is formed during the reaction. However, most salts are easily removable through evaporation or filtration and could be of commercial value depending on the acid used and the potential formation of other side-products effecting the purity of the latter salt. A selection of hydrolysis reactions with different acids are shown in Table 1.3.

Table 1.3: A selection of hydrolysis reactions and different acids for the hydrogen release of $NaBH_4$. [1]This reaction is performed with KBH_4.

Acid	Hydrogen release rate (ml/min/g of $NaBH_4$)	Equivalents ($NaBH_4$-Acid)	Hydrogen yield (%)
H_2SO_4	384,000	1.5	83 [54]
HNO_3	192,000	3	50 [54]
H_3PO_4	188,000	0.333	52 [54]
HCl	24,640	1	100 [61]
CH_3COOH	16,000	1	91 [61]
H_3BO_3	190	1	88 [62]
H_3PO_4[1]	1875	1	$\sim$100 [27]

The catalytic pathway for the hydrolysis of $NaBH_4$ is shown in Scheme 1. First, a premixed solution of $NaBH_4$ in caustic releases hydrogen under the presence of a catalyst to form $NaB(OH)_4$. Then, an acid is added to the spent fuel to form H_3BO_3. The H_3BO_3 is subsequently converted to $B(OCH_3)_3$ upon addition of methanol. $B(OCH_3)_3$ is then transformed back to $NaBH_4$ according to the Brown-Schlesinger process (see section 3.2).

The acidic pathway for the hydrolysis of $NaBH_4$ is shown in Scheme 2. Here, $NaBH_4$ is directly converted to H_3BO_3 through the use of an acid without being premixed initially. The H_3BO_3 is then converted to $B(OCH_3)_3$ upon addition of methanol and transformed to $NaBH_4$ in the same manner as in the catalytic

pathway. Despite the fact that the hydrolysis of $NaBH_4$ in the presence of an acid seems like a viable circular alternative, it still contains too many reaction steps and purification steps for it to be commercially attractive [19]. In addition, multiple drying steps are required that demand high temperatures due to the relatively high heat capacity of water. The circular hydrolysis pathway is therefore regarded as too energy demanding for industrial use. This circular process of hydrogen storage thus needs to be optimised.

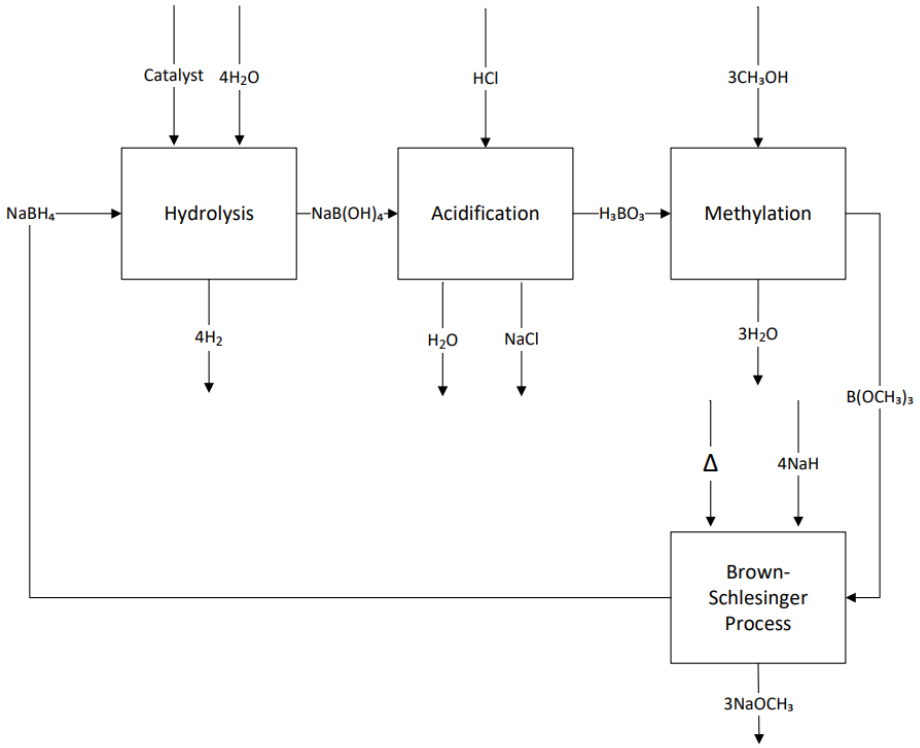

Scheme 1: The circular alkaline/catalytic hydrolysis reaction pathway.

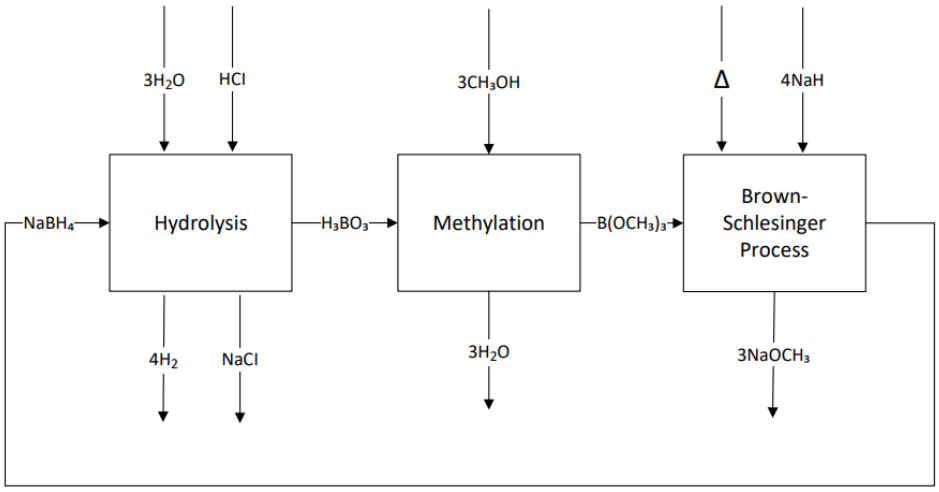

Scheme 2: The circular acidic hydrolysis reaction pathway.

1.1.2. H_2 release from $NaBH_4$ through (semi-)alcoholysis

The hydrogen release through alcoholysis of $NaBH_4$ has been discussed as an alternative to the hydrolysis of $NaBH_4$ in literature [63]. Various alcohols, including methanol, ethanol, and ethylene glycol, have been investigated for their ability to release hydrogen during alcoholysis of $NaBH_4$ [20, 21, 26, 27, 62, 64, 65, 66, 67]. However, limited research has been done on the product characterization. The latter only provides theoretical mechanisms for the products that are formed during the alcoholysis of $NaBH_4$.

The existing studies primarily focus on the methanolysis of $NaBH_4$ due to the high solubility of $NaBH_4$ in methanol and the favorable hydrogen release characteristics of methanol compared to other alcohols, attributed to its acidic nature [21]. Furthermore, methanol, being the alcohol with the lowest molecular weight, offers the advantage of minimizing weight during storage. In addition, the methanolysis of $NaBH_4$ offers two benefits over the hydrolysis pathway. Firstly, the self-methanolysis of $NaBH_4$ exhibits faster kinetics, potentially enabling a more rapid hydrogen production [20]. Secondly, the methanolysis reaction demonstrates enhanced performance also in the presence of catalysts at lower temperatures due to the relatively lower melting point of methanol. Nonetheless, the methanolysis of $NaBH_4$ alone remains insufficiently efficient for industrial applications without the use of an accelerator [68]. In literature, accelerating the methanolysis reaction using a catalyst has proven to work in a similar fashion as with the hydrolysis reaction. Several catalysts have been identified for accelerating the methanolysis of $NaBH_4$, as presented in Table 1.4. However, the cost and limited availability of catalysts pose significant drawbacks, as discussed in Section 1.1.1.

Table 1.4: A selection of catalysts used for the hydrogen release of $NaBH_4$ through methanolysis.

Catalyst type	Hydrogen release rate (ml/min/g)
Ruthenium on Al_2O_3 pellets	209 [69]
$CoCl_2$ with Guanidinium Borohydride	9961.5 [39]
Cell-EPC-DETA-HCl natural polymer	3125 [70]
P(AAGA) hydrogel with in situ Cobalt	799 [71]
Magnetic cobalt/carbon composite derived from a zeolitic imidazolate	4900 [72]
Ni_2P/SiO_2	3700 [73]
O doped metal-free catalyst	14,443 [66]
SiO_2 particles treated with HCl	34,840 [74]

The methanolysis of $NaBH_4$ can also be accelerated through the use of an acid similar to the hydrolysis pathway [20, 26, 27, 65]. A selection of alcoholysis reactions using an acid is provided in Table 1.5. However, the acids used are in an aqueous solution which does not exclude the undesired hydrolysis reaction proceeding in parallel. Hence, these reactions are referred to as 'semi-alcoholysis' reactions.

Table 1.5: A selection of semi-alcoholysis reactions with various acids for the hydrogen release of $NaBH_4$ with reaction specifications.

Acid	Reaction	Hydrogen release rate (ml/min/g of $NaBH_4$)	Equivalents ($NaBH_4$-Acid)	Hydrogen yield (%)
H_3BO_3	Semi-Methanolysis	-	1	99 [62]
HCl	Semi-Methanolysis	4875	1	100 [20]
CH_3COOH	Semi-Methanolysis	3960	1	100 [20]
H_3PO_4	Semi Methanolysis	11684	0.5	$\sim$ 100 [65]
H_3PO_4	Semi-Methanolysis	5779	1	100 [27]
H_3PO_4	Semi-Ethanolysis	9981	0.5	$\sim$ 100 [65]
H_3PO_4	Semi-Ethanolysis	6423	1	100 [27]
H_3BO_3	Semi-Ethanolysis	-	1	62 [62]
H_3PO_4	Semi-Glycolysis	5800	1	100 [67]
CH_3COOH	Semi-Glycolysis	4542	1	100 [67]

Only one literature example was found investigating the alcoholysis with an acid which excludes water from the reaction mixture to effectively produce hydrogen [64]. Here, hydrogen is released from $NaBH_4$ through ethanolysis and various acids. However, product isolation and characterization has not been performed. The focus in the latter work lies on the release rate of hydrogen instead of realising the possibility of recycling the spent fuel to $NaBH_4$. To date, there is no known reaction pathway for the release of hydrogen through alcoholysis using stochiometric amounts of an acid yielding to an isolated, recyclable product. The reaction pathway for the hydrogen through alcoholysis with an acid therefore remains unknown including the characterization of the reaction products to enable an efficient recycling of the spent fuel (vide infra, section 3.2).

Table 1.6: An overview of ethanolysis reactions with the used acids for the hydrogen release of $NaBH_4$.

Acid	Hydrogen release rate (ml/min/g of $NaBH_4$)	Equivalents ($NaBH_4$-Acid)	Hydrogen yield (%)
HCl	5020	1	77 [64]
CH_3OOH	2000	1	90 [64]
Citric acid	460	1	80 [64]
Ftalic acid	400	1	71 [64]
H_3BO_3	360	1	72 [64]

1.2. $NaBH_4$ Regeneration after H_2 release

The most dominant barrier for the application of hydrogen storage through metalhydrides is the recycling of the spent fuel after the hydrogen has been released. The spent fuel for the catalytic/alkaline hydrolysis reaction is $NaB(OH)_4$ as depicted in Scheme 1. The spent fuel for the acidic hydrolysis reaction is generally considered to be H_3BO_3 as depicted in Scheme 2. In both reaction pathways, the boron compounds acidificate to H_3BO_3. Esterification of methyl groups can be performed through the addition of methanol which results in the formation of $B(OCH_3)_3$ as shown in Equation 1.10.

$$H_3BO_3 + 3\,CH_3OH \xrightarrow[RT]{} B(OCH_3)_3 + 3\,H_2O \tag{1.10}$$

$B(OCH_3)_3$ can be used as a starting material for $NaBH_4$ synthesis through the Brown-Schlesinger process (see Equation 1.11) [18], which has been developed in the early 1950s and has been proven to work efficiently on industry scale since, concomitant with an enormous energy input.

$$4\,NaH + B(OCH_3)_3 \xrightarrow[225\text{-}275\,^\circ C]{} NaBH_4 + 3\,NaOCH_3 \tag{1.11}$$

The Brown-Schlesinger process consists of five steps, shown in Scheme 3, which require high pressures and temperatures and produce various side products. Therefore, the Brown-Schlesinger process is energy demanding. However, the process is employed for $NaBH_4$ synthesis on industrial scale and therefore serves as an initial starting point for the envisioned circular use of $NaBH_4$. With this in mind, $NaBH_4$ can be used again for hydrogen release.

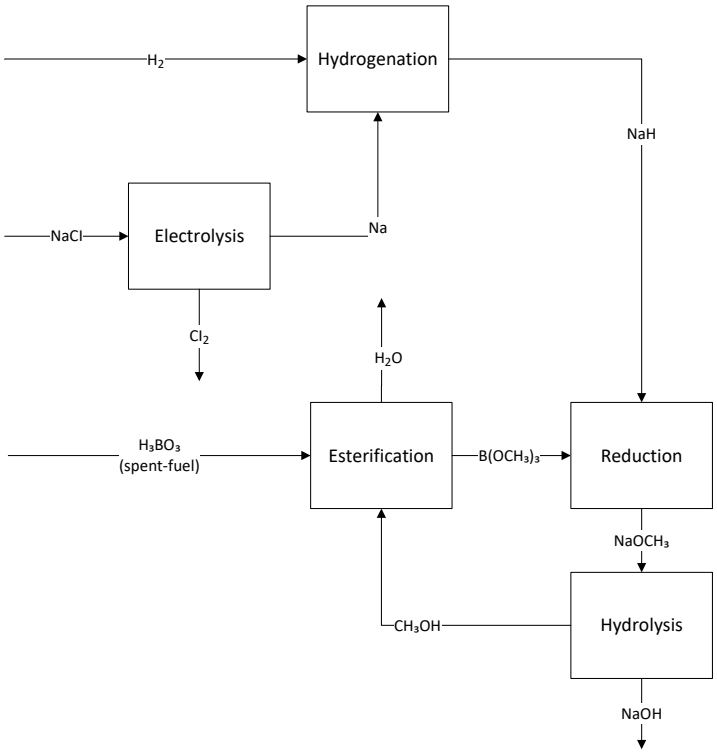

Scheme 3: Block diagram of the Brown-Schlesinger process [16].

1.3. Activation of H_2 via boron radical anion

The regeneration of $NaBH_4$ is the most energy demanding step within the envisioned circular use of $NaBH_4$ as an option for hydrogen storage as stated in the latter. The high energy demand originates from the high reaction temperature and the 4 equivalents of NaH needed to form one equivalent of sodium borohydride. In literature, no pathway is proposed to circumvent the 4 equivalents of NaH to synthesize $NaBH_4$ from borates. However, multiple attempts have been made to lower the reaction temperature of $NaBH_4$ synthesis, thereby decreasing the energy demand for the regeneration of $NaBH_4$ [75, 76]. In literature, $NaBH_3(OR)$ can be synthesized at room temperature through the use of $NaAlH_4$ as a hydride donor [76]. It is observed that only the addition of the fourth hydride to the boron defines the energy barrier for $NaBH_4$ synthesis. If this energy threshold could be compromised by external stimuli such as electrochemical hydride addition, catalytic activation or activation through a radical pathway, the required temperature needed for $NaBH_4$ regeneration could potentially be decreased.

The idea of using a radical pathway is based on a paper written by Slootweg and co-workers in which borohydride compounds are synthesized at room temperature from Lewis-acidic boranes (LAB's) [77]. LAB's are often used in Frustrated Lewis Pair (FLP) chemistry where a mixture contains a Lewis acid and a Lewis base that cannot combine to form a traditional adduct because of steric hindrance [78]. If LAB's are exposed to H_2 in the presence of common reducing agents, such as alkali metals, instead of the Lewis bases required in FLP chemistry [78], then homolytic H_2 cleavage occurs. It was shown that this activation is done through a radical mechanism in which triphenylborane and sodium form a boron radical anion, which is capable of homolytic hydrogen cleavage, shown in Scheme 4.

Literature also showed that hydriding the B–O-bond using a Li/naphthalene-system is possible [79]. Despite the promising result of forming a B-H bond from a B-O compound, such reaction mechanism was not applied to trialkylborates to form borohydrides. In this thesis, the idea of using an initial radical source to stimulate hydrogen cleavage and subsequently form borohydrides is adopted to the use of trialkylborates ($B(\text{-}OR)_3$ compounds) instead of trialkylboranes ($B(\text{-}R)_3$ compounds). In this way, a one pot synthesis of borohydrides can potentially be realized with the ultimate goal of synthesizing $NaBH_4$.

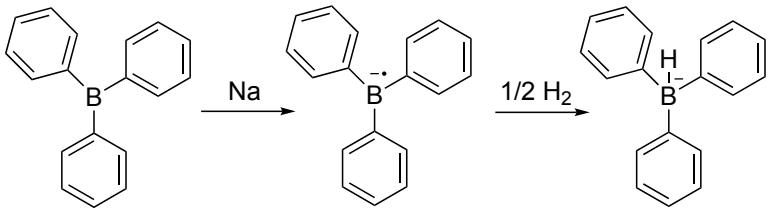

Scheme 4: Reaction scheme for the use of boron radical anions to perform homolytic hydrogen cleavage using triphenylborane [77].

1.4. Heat Transfer Limitation Modeling

When evaluating the complete cycle of hydrogen storage in $NaBH_4$ for potential complications related to heat transfer limitations, it is important to acknowledge that the regeneration of $NaBH_4$ through the Brown-Schlesinger process has been successfully implemented in industry since the 1950s as it is used as reductant and bleaching agent [18], in contrary to the hydrogen release reaction. Table 1.7 illustrates the reaction enthalpy associated with the hydrogen release reaction via hydrolysis, as well as the reaction enthalpy involved in the synthesis of $NaBH_4$ through the Brown-Schlesinger process. These values are determined based on the heat of formation of the various compounds (see Equation 1.12). It can be seen that the enthalpy change is the highest during the hydrogen release, thus imposing the highest risk for heat transfer limitations. From this observation, it is worth noting that the primary risk for scale-up implementation lies in the constraint imposed by heat transfer during hydrogen release, also with regards to the alcoholysis of $NaBH_4$.

Hydrogen release via alcoholysis and/or hydrolysis is an exothermic reaction [12]. According to the Arrhenius equation (see Equation 1.13), an elevation in temperature leads to an accelerated reaction rate, resulting in greater heat release. This phenomenon of thermal runaway quickly gives rise to complications associated with adequate heat transfer when scaling up the amount of reacting $NaBH_4$. Currently, there are limited models available in literature that can predict the heat generation during $NaBH_4$ hydrolysis or (semi-)alcoholysis. Nonetheless, it is crucial to develop a comprehensive model that can accurately forecast heat generation from $NaBH_4$ to assess the extent to which heat transfer limitations pose a threat to the overall feasibility of the application and what cooling it requires to function properly.

$$\Delta_r H^\circ = \Sigma\nu\Delta_r H^\circ(products) - \Sigma\nu\Delta_r H^\circ(reactants) \tag{1.12}$$

$$k = A \cdot e^{\frac{-Ea}{RT}} \tag{1.13}$$

Table 1.7: The heat of formation for the different reactions within the circular hydrolysis pathway.

Reaction	Heat of Reaction, $\Delta_r H^\circ (kJ/mol)$
$NaBH_4 + 2\,H_2O \longrightarrow NaBO_2 + 4\,H_2$	-217 [16]
$NaBO_2 + H_2O + HCl \longrightarrow H_3BO_3 + NaCl$	-11.0 [80]
$H_3BO_3 + 3\,CH_3OH_3 \longrightarrow B(OCH_3)_3 + 3\,H_2O$	72.6 [80, 81]
$4\,NaH + B(OCH_3)_3 \longrightarrow NaBH_4 + 3\,NaOCH_3$	-210 [80, 81, 82]

1.5. Techno-Economic Analysis

The reason for the absence of large scale implementation of hydrogen storage in $NaBH_4$ is due to the fact that current strategies are too cost- and energy intensive to be competitive compared to other hydrogen storage methodologies [19]. This is mainly due to current proposed methods for storing hydrogen in $NaBH_4$ being non-circular [12, 83]. However, developing a circular method for using $NaBH_4$ as a hydrogen storage vector is associated with a potential for minimizing energy requirements through compound recycling and heat integration. This could potentially be realized to such an extend that large scale implementation might be possible in the future. To asses how the novel process described in this thesis is optimized in terms of energy consumption, a techno-economic analysis is required for the envisioned circular method of storing hydrogen in $NaBH_4$.

Conventional reaction steps have been altered within this research to optimize energy usage. By quantifying the proposed alterations in the alcoholysis process in terms of energy requirements, one can compare the envisioned alcoholysis system with pre-existing methodologies for storing H_2 in $NaBH_4$, specifically focussing on the hydrolysis reaction pathway for comparison. It is crucial to develop a techno economic analysis to assess whether the proposed alterations in the alcoholysis process achieves a reduction in energy requirement relative to the hydrolysis system. Within this techno-economic analysis, a mass and energy balance are required, thereby creating insight in the energy consumption and the subsequent monetary enhancement of such improvements of both processes.

2

Thesis Scope

In recent years, numerous studies have investigated the hydrolysis and (semi-)alcoholysis of $NaBH_4$ in view of its potential useage as a hydrogen storage vector. However, to date, no comprehensive study has been investigated on the alcoholysis reaction utilizing stoichiometric amounts of acid to selectively produce spent fuel suitable for synthesizing $NaBH_4$, thus establishing circular hydrogen storage through metal hydrides.

The primary objective of this thesis is to optimize the recyclability of the spent fuel from the hydrogen release of $NaBH_4$ via alcoholysis and to achieve a more efficient synthesis of $NaBH_4$ from spent fuel. The central focus of this thesis lies in the synthesis of $B(OCH_3)_3$ and triisopropylborate ($B(O\mathit{i}Pr)_3$) from spent fuel for integration into the Brown-Schlesinger process, accompanied by the envisioned circular pathway for the alcoholysis reaction. Next to the envisioned circularity of the optimized process, the minimization of energy and purification requirements that ultimately arises from the latter potentially establishes an efficient, economically viable, scalable, and sustainable reaction pathway for circular hydrogen storage in $NaBH_4$. Accordingly, the primary research question is formulated as follows:

"How can the recyclability of the spent fuel from the hydrogen release via the alcoholysis of $NaBH_4$ and the regeneration of 'spent fuel' be optimised to minimize the energy intensity of the use of $NaBH_4$ as a circular hydrogen carrier?"

Upon answering this research question in an adequate manner, this thesis could lay the foundation for a novel scalable circular reaction pathway for using $NaBH_4$ as a solid hydrogen carrier. Here, an optimized hydrogen release and a new approach to the regeneration of spent fuel, while simultaneously minimizing energy requirements and process costs, could potentially form a start for a new industrial circular strategy of hydrogen storage in $NaBH_4$. This framework thus establishes a foundation for the realization of the latter.

3

Results and Discussion

Despite the numerous advantages and extensive literature available on the hydrogen release from $NaBH_4$ and the regeneration of $NaBH_4$ from spent fuel, there remains a need for comprehensive analytical understanding of the various reactions involved and the resulting products that are formed. Additionally, limited knowledge exists regarding the influence of reaction parameters on these reactions. As mentioned in chapter 1, to date, there is no comprehensive study on the release of hydrogen through alcoholysis using stochiometric amounts of an acid, including characterization of the formed products. Performing experiments to investigate the latter is the starting point of this research.

3.1. Hydrogen release through alcoholysis

As discussed in chapter 1, there is no known reaction pathway for the release of hydrogen through alcoholysis using stochiometric amounts of an acid. As explained in subsection 1.1.2, methanol is the alcohol with the lowest molecular weight which saves storing additional weight compared to other alcohols. Therefore, methanolysis reactions of $NaBH_4$ with stochiometric amounts of an acid were performed to indicate whether a method can be found to selectively synthesize trimethylborate $(B(OCH_3))_3$ in a one-pot synthesize, circumventing multiple process steps with regards to spent fuel formation and hydrogen release when compared to the hydrolysis reaction pathway.

3.1.1. Methanolysis towards the selective formation of trimethylborate

Experiments with $NaBH_4$, an excess of methanol and stochiometric amounts of Hydrochloric acid (HCl), phosphoric acid (H_3PO_4) and sulfuric acid (H_2SO_4) were initially aimed for in order to investigate the spent fuel formation of the methanolysis of $NaBH_4$. These acids were chosen for the present study as HCl has an advantage with regards to its molecular weight. H_3PO_4 is a powder, thereby being easy to dry. H_2SO_4 was used as it is a pure acid that is not dissolved or diluted in an excess of solvent. In addition, all three acids are commercially viable on larger scale. However, an initial NMR reaction was performed with $NaBH_4$ and lutidinium triflate (LuHOTf) as a proton source (see Equation 3.1). LuHOTf was used because it is a solid acid with a non-coordinating counter ion which makes it easier to add in stochiometric ratios when compared to the use of a liquid acid and simplifies the characterization and separation of the formed salt. The reaction was performed with an excess of methanol and stochiometric amounts of the acid. 11.7 mg of $NaBH_4$ and 80 mg of LuHOTf were added in a quartz NMR tube under inert condition, followed by addition of 0.7 mL dry methanol. Subsequently, a NMR measurement was carried out. A singlet at 18.52 ppm was observed in the ^{11}B NMR spectrum, which corresponds to the signal of trimethylborate $(B(OCH_3)_3)$, as described in literature [84] (see Figure 3.1). ^{13}C NMR and ^{1}H NMR confirmed $B(OCH_3)_3$ as the formed product [85], which serves as the starting compound for the Brown-Schlesinger process used for the regeneration of $NaBH_4$.

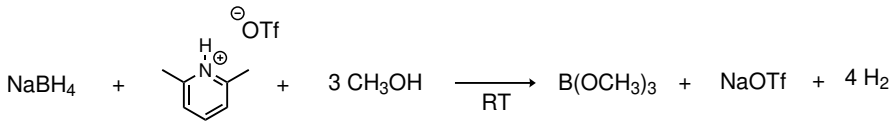

(3.1)

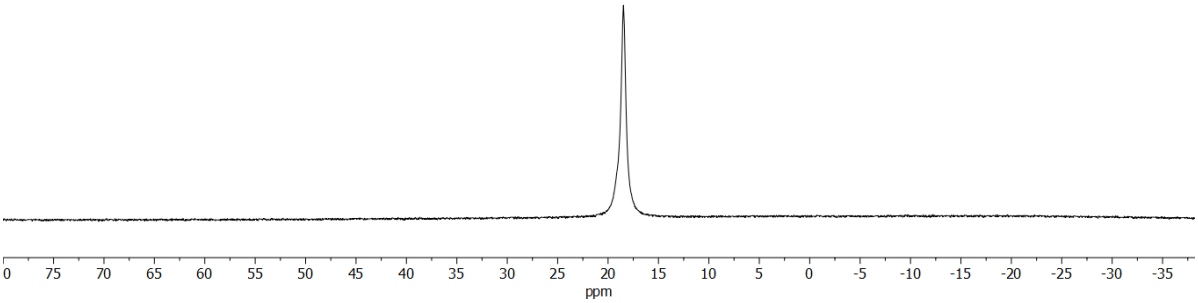

Figure 3.1: ^{11}B NMR of the reaction mixture of $NaBH_4$ with an excess of methanol and stochiometric amounts of LuHOTf after hydrogen release.

This methanolysis reaction operates through a similar mechanism as the hydrolysis reaction. However, unlike the hydrolysis reaction, wherein boric acid replaces protons through a condensation reaction, leading to the subsequent synthesis of $B(OCH_3)_3$, the methanolysis reaction directly forms the borate ester. This direct synthesis of $B(OCH_3)_3$ bypasses the intermediate formation of boric acid, thereby minimizing the number of reaction steps involved.

Reactions with $NaBH_4$ in 5 mL of methanol and stochiometric amounts of H_2SO_4, H_3PO_4 and HCl were performed based on the initial result described above. For these reactions with H_2SO_4, HCl and H_3PO_4, respectively 0.07 mL H_2SO_4, 2.2 mL of 1.25 M HCl in methanol and 86.3 mg H_3PO_3 was added to 100 mg of $NaBH_4$. The reactions with HCl and H_3PO_4 showed a broad peak in the ^{11}B NMR spectrum. It can be postulated that the reason for this peak broadening is the coordination of the chlorine and phosphate anion. The methanolysis reaction with H_2SO_4 did show one clear signal in the ^{11}B NMR spectrum corresponding to $B(OCH_3)_3$ after the reaction was finished (see Equation 3.2 and Figure 3.2) [86]. The formation of Na_2SO_4 makes the solution significantly more viscous, henceforth the need for such an excess of methanol. H_2SO_4 was used as the proton donor for further reactions.

$$2\,NaBH_4 + H_2SO_4 + 6\,CH_3OH \xrightarrow[RT]{} 2\,B(OCH_3)_3 + Na_2SO_4 + 8\,H_2 \tag{3.2}$$

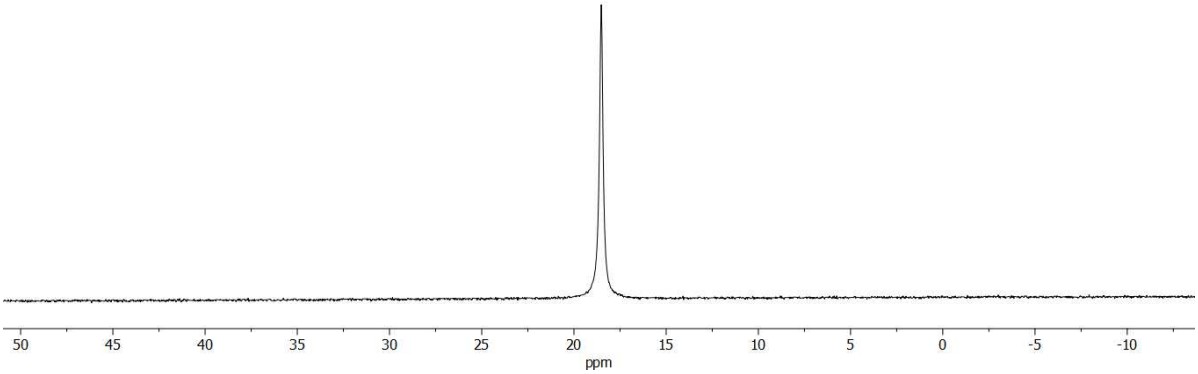

Figure 3.2: ^{11}B NMR of the reaction mixture of $NaBH_4$ with an excess of methanol and stochiometric amounts of H_2SO_4 after hydrogen release.

An additional challenge encountered in the methanolysis of $NaBH_4$ is the formation of an azeotrope between methanol and $B(OCH_3)_3$ after hydrogen release, wherein both substances have boiling points in close proximity to one another (64.7 °C and 68.7 °C, respectively) [87]. In the Slootweg research group, as well as in literature, several attempts have been made to separate this azeotrope and obtain pure $B(OCH_3)_3$ on laboratory scale [88, 89, 90]. The isolation of $B(OCH_3)_3$ is crucial, as it serves as the starting material for the Brown-Schlesinger process. However, achieving a satisfactory separation of $B(OCH_3)_3$ on lab scale has proven elusive thus far. An azeotrophic distillation has to be conducted to break the azeotrope and separate the methanol from the $B(OCH_3)_3$ [87]. Notably, breaking the azeotrope requires highly specific reaction conditions and involves the deployment of two distinct columns: an extractive column and a solvent recovery column [91]. Consequently, the implementation of this circular process at an industrial scale increases initial investment costs.

3.1.2. Methanolysis towards the selective formation of sodiumtetramethoxyborate

As mentioned in subsection 1.1.2, the methanolysis reaction is too slow without the presence of an acid. Nevertheless, the reaction rate increases substantially at increased temperatures. Furthermore, given the exothermic nature of the reaction, the temperature of the solution rises as more $NaBH_4$ reacts. Hence, it can be said that the hydrogen is released at sufficient rates once the reaction is scaled up. As known in literature, a condensation reaction between methanol and $NaBH_4$ without adding an acid occurs to form sodiumtetramethoxyborate ($NaB[OCH_3]_4$) and release hydrogen [92, 93], as depicted in Equation 3.3. If $B(OCH_3)_3$ is formed after adding a stochiometric amount of acid to $NaB[OCH_3]_4$, the reaction can be separated into two distinct stages when larger quantities of $NaBH_4$ are involved. First, the hydrogen release could be performed by synthesizing $NaB(OCH_3)_4$. Secondly, $B(OCH_3)_3$ could be formed after adding stochiometric amounts of an acid. In fact, according to Brown et al, $NaB(OCH_3)_4$ can also function as a starting material for the Brown-Schlesinger process [18]. In the latter publication, the reaction of NaH with $NaB(OCH_3)_4$ yielded 66% of $NaBH_4$ in 91% purity. This circumvents the subsequent addition of acid to form $B(OCH_3)_3$, and therefore circumvents the formation of the azeotrope between methanol and $B(OCH_3)_3$, making the separation of the release process a potential tool for circumventing process complications.

As a starting point of this study, the literature known reaction of methanol and $NaBH_4$ was reproduced to synthesize $NaB(OCH_3)_4$ [92, 93]. The reaction was performed on 5 gram scale and showed 100% conversion according to ^{11}B NMR after 1 hour and 20 minutes (see Figure 3.3). The product was obtained as a white powder in 97% yield.

$$NaBH_4 + 4\,CH_3OH \xrightarrow[RT]{} NaB(OCH_3)_4 + 4\,H_2 \tag{3.3}$$

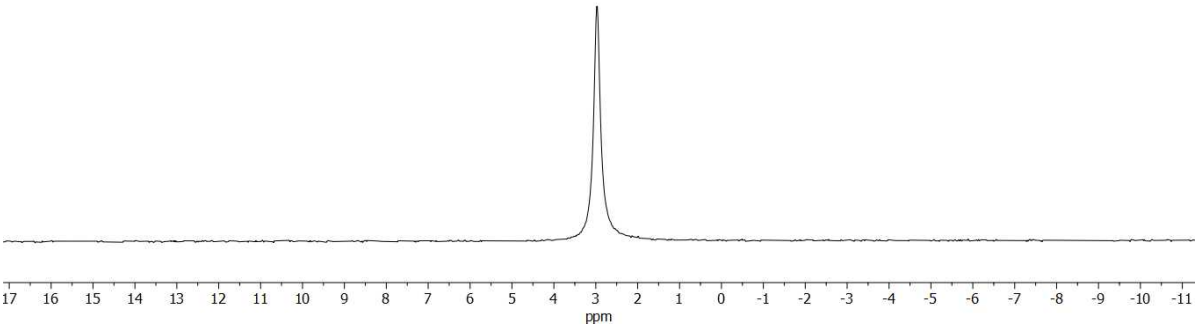

Figure 3.3: ^{11}B NMR of the reaction mixture of $NaBH_4$ with an excess amount of methanol after 1 hour and 20 minutes. The spectrum indicates the full conversion from $NaBH_4$ to $NaB(OCH_3)_4$.

Adding a stoichiometric amount of protons to $NaB(OCH_3)_4$ after the hydrogen release also resulted in selective product formation to a signal corresponding to $B(OCH_3)_3$ according to ^{11}B NMR [84] (see Equation 3.4 and Figure 3.4). This means that $B(OCH_3)_3$ synthesis is possible in two steps by first subjecting $NaBH_4$ to an excess of methanol to form $NaB(OCH_3)_4$, and subsequently adding stochiometric amounts of an acid to form $B(OCH_3)_3$.

$$2\,NaB(OCH_3)_4 + H_2SO_4 \xrightarrow[RT]{} 2\,B(OCH_3)_3 + 2\,CH_3OH + Na_2SO_4 \tag{3.4}$$

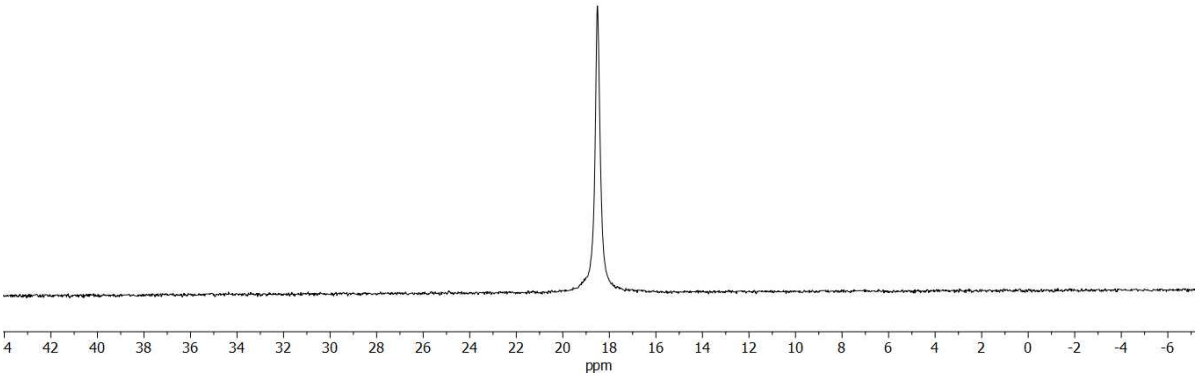

Figure 3.4: ^{11}B NMR of the reaction mixture of $NaB(OCH_3)_4$ with an excess of methanol and stochiometric amounts of H_2SO_4 after hydrogen release.

A reaction with stochiometric amounts of methanol in the absence of an acid was also performed using isopropanol (IPA) and tetrahydrofuran (THF) as solvents. $NaBH_4$ is stable in both THF and IPA as known in literature [94, 95]. According to ^{11}B NMR, the reaction in IPA showed 7% conversion to a signal corresponding to $NaB(OCH_3)_4$ after 150 minutes. The reaction in THF showed higher conversions (65% and 91% after 5 and 24 hours, respectively) to the same product according to ^{11}B NMR. This illustrates that solely an excess of methanol results in a fast enough conversion time.

In order to gain more control over the methanolysis reaction, a series of stabilizer experiments were conducted to facilitate the premixing of sodium borohydride ($NaBH_4$) and methanol. Potassium hydroxide (KOH) and sodium methoxide (NaOMe) were used as stabilizers, using varying molar percentages, with the aim of assessing their effectiveness in preventing self-methanolysis upon the addition of $NaBH_4$ and methanol. KOH was selected as the initial stabilizer due to its established role as a stabilizer in hydrolysis reactions [29]. However, the formation of water when protonating hydroxides through acid addition makes it unfavorable for this purpose in the proposed system. Consequently, NaOMe was proposed as a potential stabilizer, as it forms methanol upon protonation, which is the solvent used in the methanolysis reaction.

A total of ten round-bottom flasks (RBFs) with a volume of 25 mL were prepared, each containing 10 mL of methanol. Five of the RBFs were assigned for the addition of various amounts of KOH to achieve concentrations of 0, 2, 5, 7, and 10 mol% of KOH, respectively. The same procedure was followed for the remaining five RBFs with NaOMe. Once the stabilizer had completely dissolved through stirring, 100 mg of $NaBH_4$ was added to all RBFs. Measurements were taken after 5 hours and 24 hours. The respective conversions are presented in Figure 3.5. The results indicate that both NaOH and NaOMe failed to realize the desired stabilizing effect. This outcome can potentially be attributed to the acidity of methanol, which reacts with the alkaline stabilizer, thereby resulting in minimal changes to the pH of the reaction mixture and, consequently, an insufficient stabilizing effect. Initial experiments involving alternative organic bases, such as pyridine and triethylamine, were also conducted, but failed to demonstrate any significant stabilizing effect. Consequently, the possibility of premixing $NaBH_4$ and methanol in the presence of a stabilizer prior to initiating the reaction is precluded.

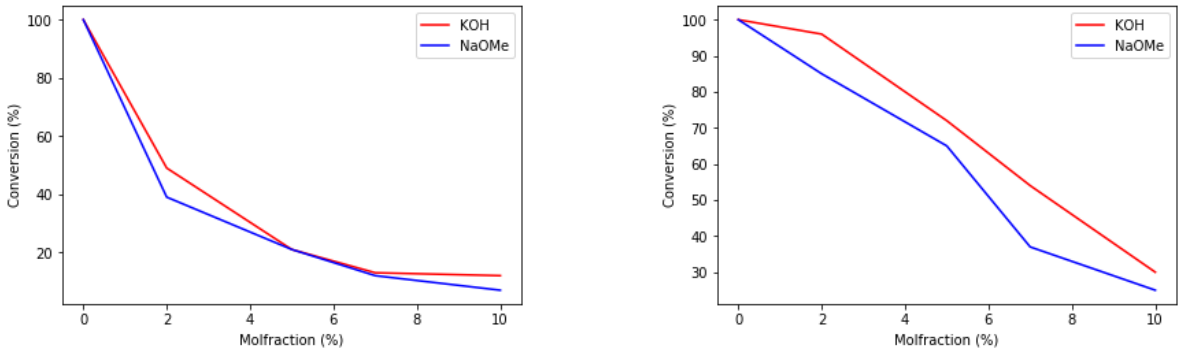

(a) **(b)**

Figure 3.5: a) Conversion of $NaBH_4$ with a stabilizer after 5 hours. b) Conversion of $NaBH_4$ with a stabilizer after 24 hours.

3.1.3. Alcoholysis towards the selective formation of triisopropylborate

As mentioned in the previous section, premixing of $NaBH_4$ in methanol is not possible as using a stabilizer for this reaction such as strong bases like methoxides and hydroxides as well as organic bases like pyridine and triethylamine have insufficient effect on conversion to $NaB(OCH_3)_4$, despite having sufficient effect on conversion in the hydrolysis of $NaBH_4$ [29]. In addition, the requirement of using an excess of methanol in the methanolysis reaction as explained in subsection 3.1.1 forms an azeotrope with trimethylborate and methanol which unsuccessfully has been separated in lab scale. Both issues prompted the author to search for alternative alcoholysis routes to circumvent these complications.

In literature, it has been shown that $NaBH_4$ is stable in isopropanol (IPA) [94]. Brown et al. showed that no hydrogen release was observed over a period of 24 hours when mixing IPA and $NaBH_4$. No conversion has been observed over a 5 day period according to ^{11}B NMR when reproducing $NaBH_4$ and IPA addition. This means that premixing of $NaBH_4$ and IPA would be possible without an additional stabilizer. This would however only pose a process-technical advantage if the alcoholysis reaction with stochiometric amounts of an acid releases the same amount of hydrogen as in the methanolysis reaction and forms the respective borate ester, which is triisopropylborate ($B(OiPr)_3$), through the same condensation reaction shown in Equation 3.5. If so, another advantage of using IPA as reacting alcohol would be that the separation between $B(OiPr)_3$ and IPA would potentially require less effort as the boiling points of IPA (82.5 °C) and $B(OiPr)_3$ (140 °C) are more apart from each other relative to methanol and trimethylborate.

$$2\,NaBH_4 + H_2SO_4 + 6\,IPA \xrightarrow[RT]{} B(OiPr)_3 + Na_2SO_4 + 8\,H_2 \tag{3.5}$$

A similar reaction set-up was proposed for the reaction with IPA as for the methanolysis reaction. 212 mg of $NaBH_4$ was dissolved in 10 mL IPA. An excess of IPA was necessary due to solubility limitation of $NaBH_4$

as the solubility of $NaBH_4$ in IPA is 3.7 g/L at room temperature [94]. Higher temperatures do increase the solubility of $NaBH_4$, but still do not suffice for adequate reaction conditions. In addition, the formation of Na_2SO_4 makes the solution significantly more viscous as stated in the latter. The minimum amount of IPA required was observed to be 6 equivalents for 1 equivalent of $NaBH_4$.

Upon straight addition of stochiometric amounts of H_2SO_4 (0.15 mL) to the reaction mixture, the reaction showed product formation with a signal that corresponds to the signal of $B(OiPr)_3$ according to ^{11}B NMR [96]. However, also intermediate product formation occurred upon straight addition of acid, which degraded to $B(OiPr)_3$ over a period of 20 hours (see Figure 3.6). As the decoupled ^{11}B NMR spectrum showed a singlet and the boron NMR spectrum showed a duplet, it can be derived that this side product contains a B-H bond. Thus, attempts to selectively form the intermediate product by performing a reaction with a large excess of H_2SO_4 were carried out. However, the intermediate compound could not be isolated due to $B(OiPr)_3$ still being present in solution. However, despite the unsuccessful attempt of separating this intermediate compound, it was observed in follow-up experiments that H_2SO_4 addition rates less then 0.45 mL/h did not show any intermediate product formation for this particular system. Slow addition of H_2SO_4 was carried out through the use of a syringe pump (see Figure 6.40 in section 6.2). The intermediate product was not investigated further as selective formation of $B(OiPr)_3$ could be achieved by lowering H_2SO_4 addition rates (see Figure 3.7).

Upon optimizing the reaction time and temperature correlation of the latter alcoholysis reaction, full conversion was achieved after 20 minutes for 50°C, 60°C and 70°C as depicted in Table 3.1.

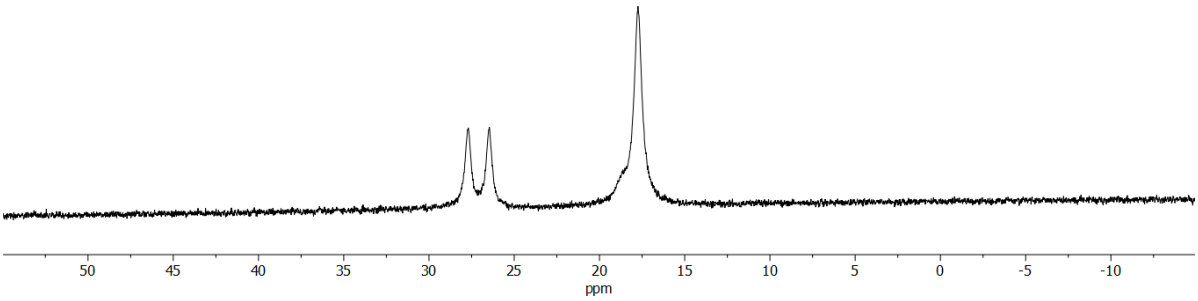

Figure 3.6: ^{11}B NMR spectrum of a duplet (A) corresponding to the intermediate B-H compound and a singlet (B) corresponding to $B(OiPr)_3$

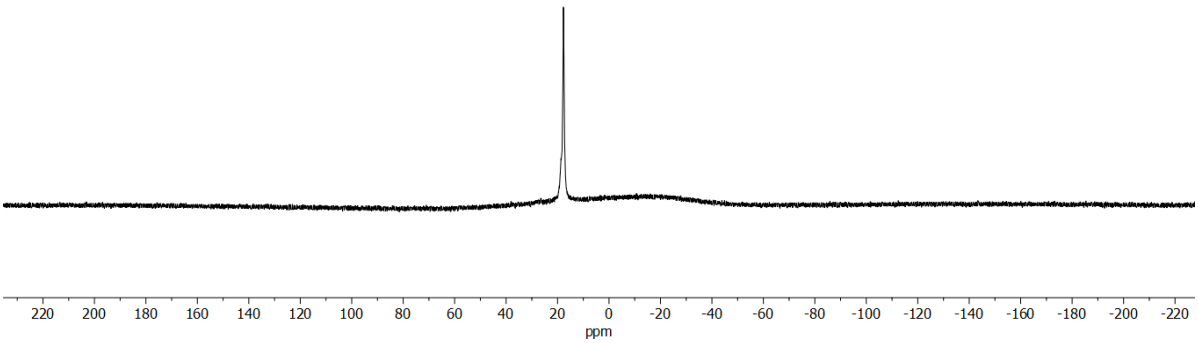

Figure 3.7: ^{11}B NMR spectrum corresponding to $B(OiPr)_3$

Time (min)	RT	30°C	40°C	50°C	60°C	70°C
20	88%	88%	85%	100%	100%	100%
30	95%	95%	100%	-	-	-
35	100%	100%	-	-	-	-

Table 3.1: Conversion of $NaBH_4$ with H_2SO_4 in an excess of IPA at different temperatures for different reaction times.

It is known in literature that $B(OiPr)_3$ and IPA still form an azeotrope [97]. However, IPA and $B(OiPr)_3$ is also known to be separated through fractional distillation [86], which is by definition contradictory. Therefore, experiments were performed in which attempts were made of separating $B(OiPr)_3$ and IPA through fractional distillation.

Initially, separation of $B(OiPr)_3$ from IPA through fractional distillation showed pure $B(OiPr)_3$ according to ^{1}H NMR, with a yield of 46% for one particular case as depicted in Figure 3.8. However, after performing multiple attempts to reproduce this particular experiment, no pure $B(OiPr)_3$ according to ^{1}H NMR was obtained. Subsequent separation attempts resulted in an IPA/$B(OiPr)_3$ molar ratio of 1:10 in the distillate according to ^{1}HNMR (see Figure 3.9). A longer distillation column and a packed bed column (see Figure 6.41 in section 6.2) were used in an attempt to separate $B(OiPr)_3$ from IPA by respectively increasing the vapor retention and the surface area. Both attempts did not show superior results with regards to the separation of IPA and $B(OiPr)_3$. According to [98], saturating the mixture with lithiumchloride (LiCl) could be used to separate a trialkylborate from its corresponding alcohol. However, the same IPA/$B(OiPr)_3$ molar ratio of 1:10 was observed in the distillate according to ^{1}H NMR using a saturated LiCl solution.

Even though the isolation of $B(OiPr)_3$ from IPA was successful in one performed experiment, it was stated that this experiment was not reproducible as multiple follow-up experiments showed an IPA fraction in the corresponding distillate. Despite that the separation of $B(OiPr)_3$ and IPA shows complications on lab scale, it is advantageous when compared to the separation of $B(OCH_3)_3$ and methanol which has a molar ratio of 1:1.2, according to experiments that were performed by Pier Wessels, member of the SOC research group. This represents a significantly higher fraction of alcohol in the distillate, indicating the requirement for a higher separation power to separate $B(OCH_3)_3$ from methanol relative to the separation of $B(OiPr)_3$ and IPA. The use the alcoholysis pathway using IPA therefore still poses an advantage relative to the methanolysis pathway with regards to alcohol/trialkylborate separation. Notably, as the separation of $B(OCH_3)_3$ and methanol has proven to successfully function on industrial scale [87], it is assumed that the separation of $B(OiPr)_3$ and IPA will also be achieved on industrial scale as relatively less separation power is required to separate the $B(OiPr)_3$/IPA mixture relative to the $B(OCH_3)_3$/methanol mixture.

Conclusively, the alcoholysis reaction to $B(OiPr)_3$ yields the same respective alkylborate as for the methanolysis reaction. In addition, the separation of $B(OiPr)_3$ requires less separation power relative to the separation of $B(OCH_3)_3$ and methanol. Moreover, premixing of $NaBH_4$ and IPA is possible without an additional stabilizer, which simplifies process design. Despite these various advantages, using the alcoholysis reaction pathway with IPA only makes sense if conversion from $B(OiPr)_3$ back to $NaBH_4$ would also be possible.

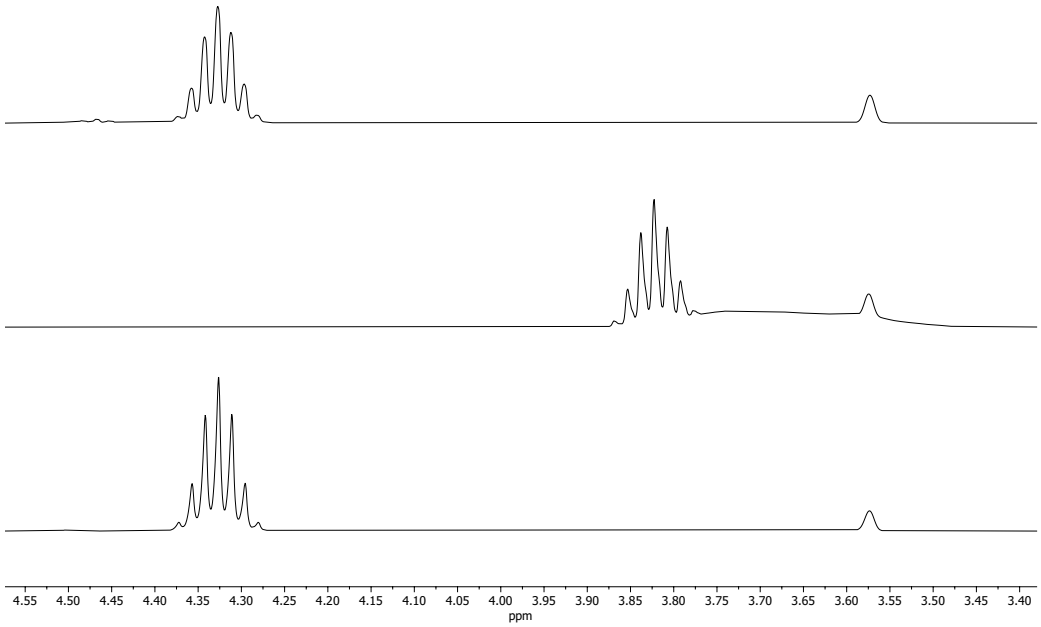

Figure 3.8: Stacked ^{1}H NMR spectra for the distillate (top), IPA (middle) and pure B(O*i*Pr)$_3$ (bottom). A signal was observed that corresponds to pure B(O*i*Pr)$_3$.

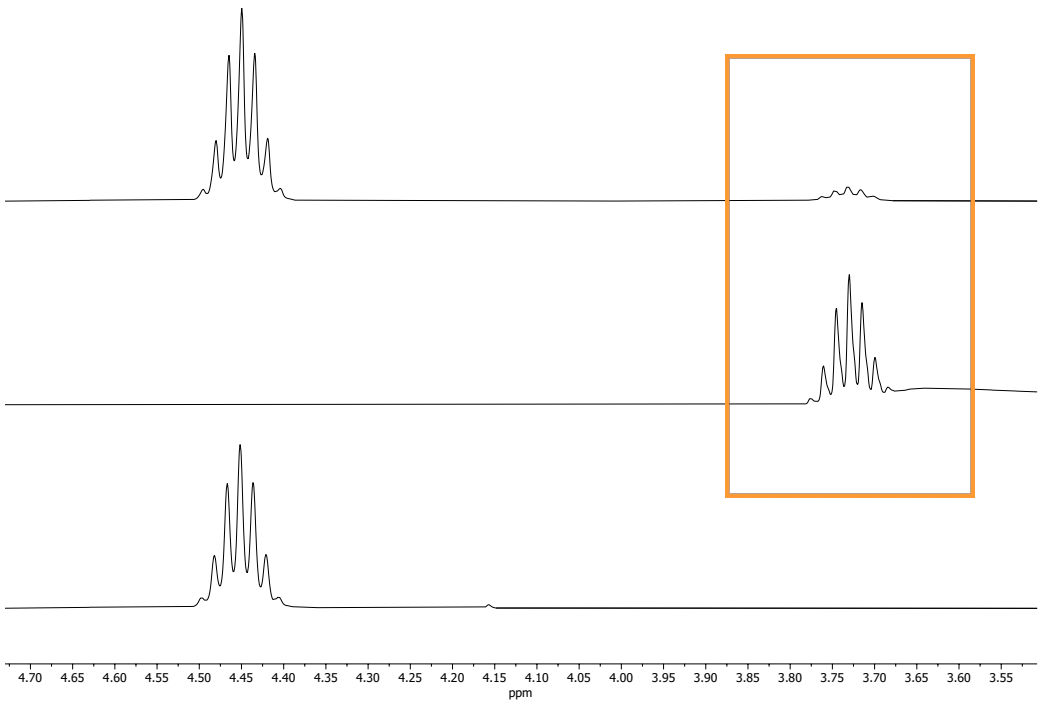

Figure 3.9: Stacked ^{1}H NMR spectra for the distillate (top), IPA (middle) and pure B(O*i*Pr)$_3$ (bottom) of a subsequent experiment to separate IPA from B(O*i*Pr)$_3$. A signal was observed in the distillate that corresponds to a mixture of IPA and B(O*i*Pr)$_3$ with a ratio of 1:10 respectively. The IPA fraction is highlighted in the orange rectangle.

3.2. Regeneration of $NaBH_4$ through the Brown-Schlesinger Process

To acquire a fully circular methodology for storing hydrogen in $NaBH_4$, conversion from spent fuel back to $NaBH_4$ must be realised. In the alcoholysis pathway, the spent fuel refers to the alkylborate of the respective alcohol used as mentioned in subsection 1.1.2. For methanol and IPA, its respective spent fuels are thus $B(OCH_3)_3$ and $B(O\mathit{i}Pr)_3$. Conversion from $B(OCH_3)_3$ to $NaBH_4$ has been done successfully through the Brown-Schlesinger process [18]. As stated in chapter 1, the process includes a reaction between $B(OCH_3)_3$ and 4 equivalents of NaH to $NaBH_4$ and 3 equivalents of $NaOCH_3$ (see Equation 3.6).

$$4\,NaH + B(OCH_3)_3 \xrightarrow[225\text{-}275\,^\circ C]{} NaBH_4 + 3\,NaOCH_3 \tag{3.6}$$

However, the successful formation of $NaBH_4$ in Equation 3.6 by using $B(OCH_3)_3$ as a reagent does not imply its universality to arbitrary alkylborates. As indicated, the preferred reaction pathway involves the alcoholysis of $NaBH_4$ with IPA, yielding triisopropylborate ($B(O\mathit{i}Pr)_3$). This pathway is preferred due to the potentially easier separation between IPA and $B(O\mathit{i}Pr)_3$, relative to the methanolysis pathway. Moreover, the premixing of $NaBH_4$ and IPA can be accomplished without the need for a stabilizer. However, the literature does not contain any known instances of converting $B(O\mathit{i}Pr)_3$ back to $NaBH_4$ through the Brown-Schlesinger process as depicted in Equation 3.7. If this reaction were to be feasible, it would establish a circular reaction pathway through the use of IPA as the solvent, reactant, and energy carrier in combination with metal borohydrides and hydrogen.

Expanding on this point, it is essential to recognize the essential role played by the alcohol used in the alcoholysis pathway, as it serves as both the reaction solvent and the alcohol participating in the esterification reaction responsible for the formation of the borate ester. Additionally, the alcohol in question acts as an energy carrier because the hydrogen atoms released during the reaction originate from both $NaBH_4$ and the respective alcohol (refer to Equation 3.8).

$$4\,NaH + B(O\mathit{i}Pr)_3 \xrightarrow[225\text{-}275\,^\circ C]{} NaBH_4 + 3\,NaO\mathit{i}Pr \tag{3.7}$$

$$2\,NaBH_4 + H_2SO_4 + 6\,IPA \xrightarrow[RT]{} B(O\mathit{i}Pr)_3 + Na_2SO_4 + 8\,H_2 \tag{3.8}$$

46 mg (4.4 equivalents) of NaH was added in a standard shlenck flask under inert conditions together with 2 mL of mineral oil. 0.1 mL of $B(O\mathit{i}Pr)_3$ was slowly added so a double layer was formed between the mineral oil and the $B(O\mathit{i}Pr)_3$. This precautionary step was undertaken to prevent any premature reactions within the glovebox. The reaction mixture was then transferred outside the glovebox and subjected to isocratic heating. The temperature was incrementally raised to 230 °C, increasing by 20 °C every 20 minutes. After a duration of 5 hours, complete conversion to $NaBH_4$ was confirmed by ^{11}B NMR analysis, as depicted in Figure 3.10, closing the loop for circular hydrogen storage in the proposed novel reaction system.

The subsequent extraction of $NaBH_4$ was initially carried out using IPA as this would circumvent drying $NaBH_4$ after extraction and potentially enabling a continuing process flow from the extraction of $NaBH_4$ straight to the H_2 release reaction again. However, when performing the extraction with IPA, a suspension of IPA in mineral oil occurred that did not form a polar-apolar double layer over time, which made the work-up by IPA extraction elusive. Therefore, the extraction was done through stabilized D_2O (40 wt% NaOD). By using D_2O, the $NaBH_4$ has to be fully dried again and has to be separated from the NaOD in order to be reused again which is severely energy intensive [16]. The isolation of NaOH from $NaBH_4$ during the work-up procedure represents an inherent challenge associated with the Brown-Schlesinger process. Consequently, in industrial applications, the alkaline solution is often used in its entirety, rather than distil the solution to evaporate the water and subsequently extract NaOH to obtain pure solid $NaBH_4$ [99]. However, despite the inherent barriers posed by this work-up methodology for $NaBH_4$, the successful extraction of $NaBH_4$ has nonetheless realized a closed cycle for circular hydrogen storage within the envisioned system, either with or

without the presence of NaOH.

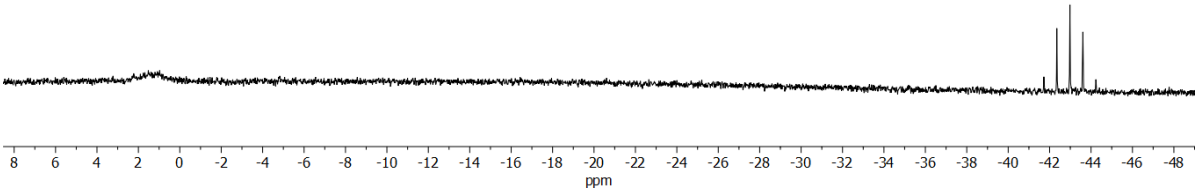

Figure 3.10: ^{11}B NMR of the reaction mixture after the reaction had completed. A clear signal of $NaBH_4$ can be observed. A small signal is observed at 1.38 ppm which corresponds to sodium tetrahydroxyborate which is formed due to the extraction with D_2O.

A small peak was oberseved in the ^{11}B NMR at 1.38 ppm (see Figure 3.10), which corresponds to sodium tetrahydroxyborate which is formed due to the extraction with D_2O [100], which slightly causes the formation of spent fuel of the hydrolysis reaction even though the D_2O is stabilized.

Despite that a circular system for the alcoholysis pathway using IPA has been provided, it still requires energy intensive reaction steps which would not be commercially viable when scaling up. First, 4 equivalents of NaH are needed to produce 1 equivalent of $NaBH_4$ which requires a substantial amount of energy. NaH is a reducing agent produced from Na and pressurized hydrogen at high temperatures (see Equation 3.9) [101]. Second, the Brown-Schlesinger process requires high temperatures (230 °C), which preferably would be decreased to minimize process costs at large scale. Note, that the proposed circular alcoholysis process with IPA still requires a drying step after the extraction of $NaBH_4$ with stabilized water as described in the latter. However, separation of oil-based compounds and IPA has been done excessively on larger scale through centrifuging or membrane pervaporation [102, 103].

$$2\,Na + H_2 \xrightarrow{400\,^{\circ}C} 2\,NaH \tag{3.9}$$

3.3. Regeneration of $NaBH_4$ through H_2 activation via boron radical anions

The regeneration of $NaBH_4$ from various alkylborates can be achieved via the Brown-Schlesinger process as described in the previous sections. This reaction pathway entails the use of four equivalents of NaH in combination with a trialkylborate to produce three equivalents of NaO*i*Pr and one equivalent of $NaBH_4$. While this method exhibits complete conversion to $NaBH_4$ for both $B(OCH_3)_3$ and $B(OiPr)_3$, it requires elevated reaction temperatures and demonstrates relatively inefficient use of NaH for the synthesis of one equivalent of $NaBH_4$. Given that circumventing the requirement of four equivalents of NaH is a too ambitious undertaking for the scope of this thesis, experiments were conducted with the objective of reducing the operating temperature for $NaBH_4$ synthesis.

As mentioned in chapter 1, an alternative reaction mechanism is proposed, involving the formation of borohydrides through radical activation which aims to achieve comparable outcomes to the Brown-Schlesinger process but at lower reaction temperatures. Literature showed that homolytic hydrogen cleavage occurs when Lewis-acidic boranes (LABs) are exposed to common reducing agents, such as alkali metals, resulting in borohydride product formation [77]. Prior literature also reported that hydriding the B–O-bond using a Li/naphthalene-system is possible [79]. However, despite the formation of a B-H bond from a B-C bond or a B-O bond, it is not proven that borohydrides also are formed from trialkylborates within this used

system. Based on this observation, it is postulated that hydroboron bonding could occur at milder reaction temperatures in the presence of an initial radical source for trialkylborates as well. It is assumed that this initial radical source would induce boron radical formation, thereby enhancing the reactivity of the boron and facilitating hydroboron sigma bonding.

Naphthalene and sodium have long been recognized for their ability to form a naphthalene radical anion when combined in an ethereal solvent since the early 1930s [104]. Literature indicates that this radical system is capable of realizing homolytic hydrogen cleavage, leading to the formation of sodium hydride under mild reaction conditions [18]. This radical system could serve as the initial radical source for the reaction discussed above. In an initial attempt to activate this initial radical source, stoichiometric amounts of naphthalene (111 mg) and sodium (20 mg) were combined under inert conditions in mineral oil, which serves as the solvent used in the Brown-Schlesinger process described in section 3.2. Subsequently, 0.1 mL of $B(OiPr)_3$ was added to the solution. The resulting reaction mixture was subjected to 4 bar hydrogen pressure in an autoclave at 120 °C for 4 hours. However, no conversion to any perceptible products was observed according to ^{11}B NMR and ^{1}H NMR spectroscopy (Figure 3.11). Furthermore, no noticeable change in color, which typically indicates radical formation within a reaction mixture, was observed. As indicated earlier, the formation of a naphthalene radical necessitates the presence of an ethereal solvent. Among the commonly used ethereal solvents for this system, monoglyme, diglyme, and THF are frequently used [105, 106]. However, it is important to note that monoglyme and diglyme, when in contact with metallic sodium at higher temperatures, pose a significant risk of explosion, making them less preferable solvents for this particular application [107]. On the other hand, THF, despite its affinity to form coordination adducts with boron compounds [108], remains the solvent of choice due to its demonstrated ability to initiate radical activation in the described system, as supported by the existing literature [106].

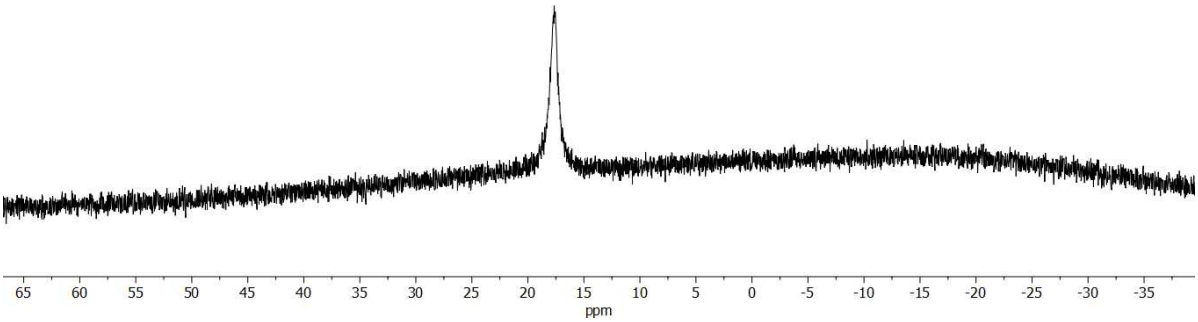

Figure 3.11: ^{11}B NMR of the reaction mixture of $B(iOPr_3)$ with 4 equivalents of Na and napthalene in mineral oil under 4 bar H_2 pressure after 4 hours at 120 °C. No conversion from $B(iO)Pr_3$ to any other boron products is observed.

To induce boron radical activation and potentially initiate hydride transfer to the boron centre, an experiment was conducted with $B(OCH_3)_3$ and 4 equivalents of sodium and napthalene in THF at 120 °C under 4 bar hydrogen pressure in an autoclave. No B-H containing products were observed. This can be attributed to two potential reasons. First, it is possible that the energy barrier required for the hydroboration of methylborate compounds was not overcome through radical activation. Alternatively, hydroboration may have occurred, but the resulting product reacted with formed methanol to reform trimethylborate. It is known in literature that borohydride reacts spontaneously with methanol, supporting this potential explanation.

The same reaction was repeated using $B(OiPr)_3$ instead of $B(OCH_3)_3$. In a small autoclave reactor (Büchi-glas Tinyclave, see chapter 4), 0.1 mL of $B(OiPr)_3$, 111 mg of naphthalene (4 equivalents), and 20 mg of sodium (4 equivalents) were combined in 3 mL of THF under 4 bar hydrogen pressure at 120 °C for 4 hours. The recorded ^{11}B NMR and $^{11}B\{^{1}H\}$ NMR spectra of the reaction mixture showed various signals corresponding to -BH, $-BH_2$, and $-BH_3$ compounds (see Figure 3.12). However, no signal corresponding to a $-BH_4$ compound was observed in the spectra. As discussed in chapter 1, the fourth hydride transfer step has the highest energy barrier, which aligns with the observed results. Despite the successful hydride transfer to

the boron center of triisopropylborate, the signal in the ^{11}B NMR and $^{11}B\{^1H\}$ NMR spectra at -15.42 ppm exhibited a singlet pattern in the $^{11}B\{^1H\}$ NMR spectrum and a multiplet in the ^{11}B NMR spectrum that can not be immediately attributed to the expected borohydride products (BH, BH_2, BH_3 or BH_4 compounds). It is postulated that these signals may originate from boron-naphthalene adducts as a result of a hydroboration reaction (see Figure 3.13). Modifying the hydrogen pressure (from 3 to 6 bar) or adjusting the reaction temperature (ranging from 80 to 160 °C) did not result in any variation in product formation, as indicated by ^{11}B NMR and $^{11}B\{^1H\}$ NMR spectroscopy. Similarly, altering the reaction time (ranging from 3 to 12 hours) or crosslinking the mentioned parameters did not yield any differences in product formation. In addition, blank reactions were performed in which either sodium or naphthalene were excluded from the reaction mixture to confirm that no initial radical forms to induce boron radicals, thereby preventing homolytic hydrogen cleavage and detaining hydride transfer to the boron centre. As expected, no reaction was observed for the reactions with either no naphthalene or no sodium in the reaction mixture according to ^{11}B NMR spectroscopy.

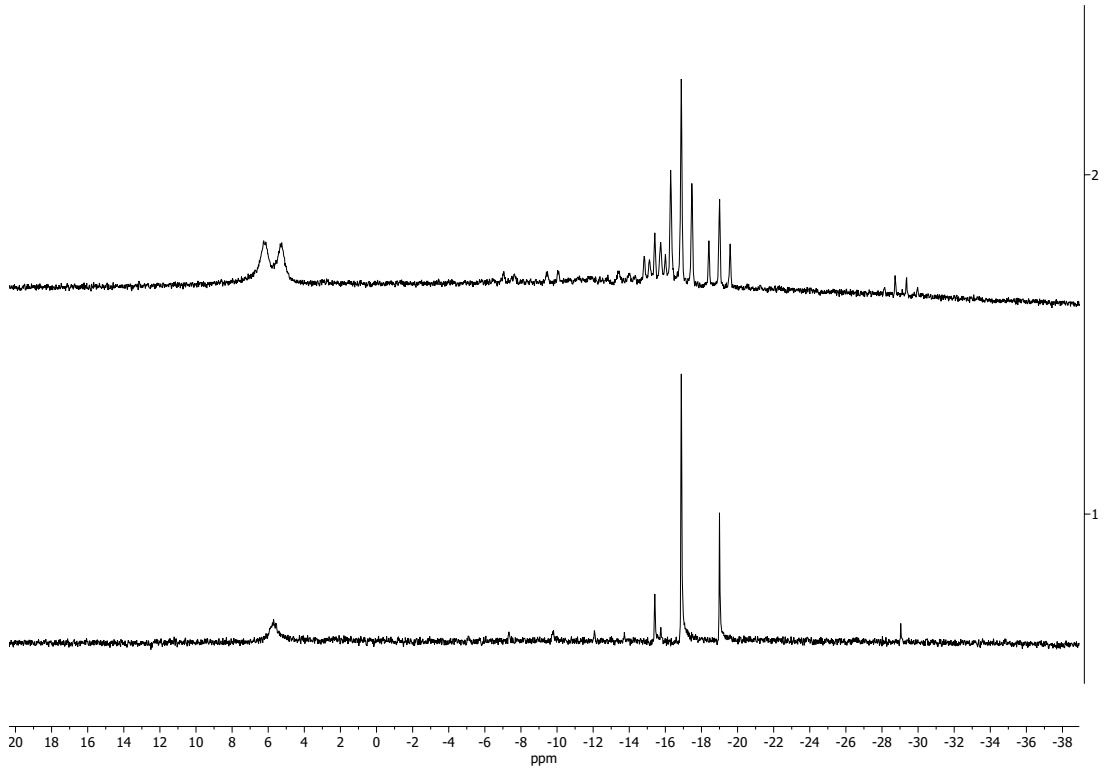

Figure 3.12: Stacked ^{11}B NMR (top) and $^{11}B\{^1H\}$ NMR (bottom) spectra of the reaction between B(*i*OPr)$_3$, Na and H_2 in THF with napthalene as initial radical source. Multiple signals occurred that correspond to a -BH compound at 5.70 ppm, -7.14 ppm and -9.78 ppm. In addition, two signals that correspond to a -BH_2 compound were observed at 16.88 ppm and 19.00 ppm and one signal occurred that correspond to a BH_3 compound at -29.04 ppm.

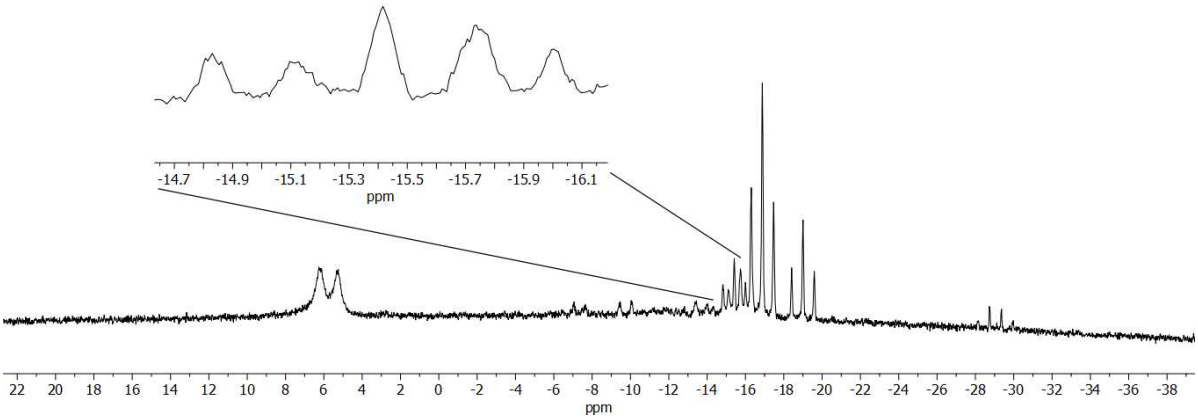

Figure 3.13: ^{11}B NMR spectrum of the reaction between B(*i*OPr)$_3$, Na and H_2 in THF with 4 equivalents of napthalene. Five signals between -14.7 ppm and -16.1 ppm were not clearly assigned and could be the result of hydroboration to a boron-naphtalene adduct.

To avoid the potential formation of boron-naphthalene adducts, a similar reaction was performed. However, biphenyl was used as the radical source instead of naphthalene. The use of biphenyl aimed to minimize boron adduct formation, but still generate a radical anion upon contact with sodium. Likely, the formation of boron adducts is less probable due to the loss of aromaticity in the phenyl rings in a potential hydroboration product. This is in contrast to naphthalene, which retains its pi-system due to the connection with the second phenyl ring within the aromatic system. Adopting the previously used reaction conditions, 133 mg of biphenyl (4 equivalents) was combined with 20 mg of sodium (4 equivalents) in 3 mL of THF. Subsequently, 0.05 mL of B(O*i*Pr)$_3$ was added. The solution was stirred after which the autoclave was assembled and the reaction mixture was put under 4 bar of hydrogen pressure and subjected to 120 °C for 4 hours, after which ^{11}B NMR measurements were taken. Figure 3.14 shows an increase in selectivity towards signals that correspond to the tetra coordinated salt (NaB(O*i*Pr)$_4$) and a B-H compound relative to the product formation of the naphtalene system. Less reaction products were formed despite that no signals were observed that correspond to BH_2 or BH_3 compounds, which does indicate a more selective product formation relative to the reaction with naphtalene as a radical source. Increasing the reaction time to 12 hours did show a shift in product formation as no peak occurs that correspond to the quartenary salt. Instead, a peak occurred at -16.07 ppm that correspond to a BH_2 compound. Increasing the amount of hydrides in the solution present by doubling the amount of sodium and biphenyl did show similar results with respect to selectivity compared to the 12 hour reaction described above. Increasing the amount of hydrides by using 16 equivalents of sodium and biphenyl showed a selective formation of a product that corresponds to a BH compound according to ^{11}B NMR (see Figure 3.14).

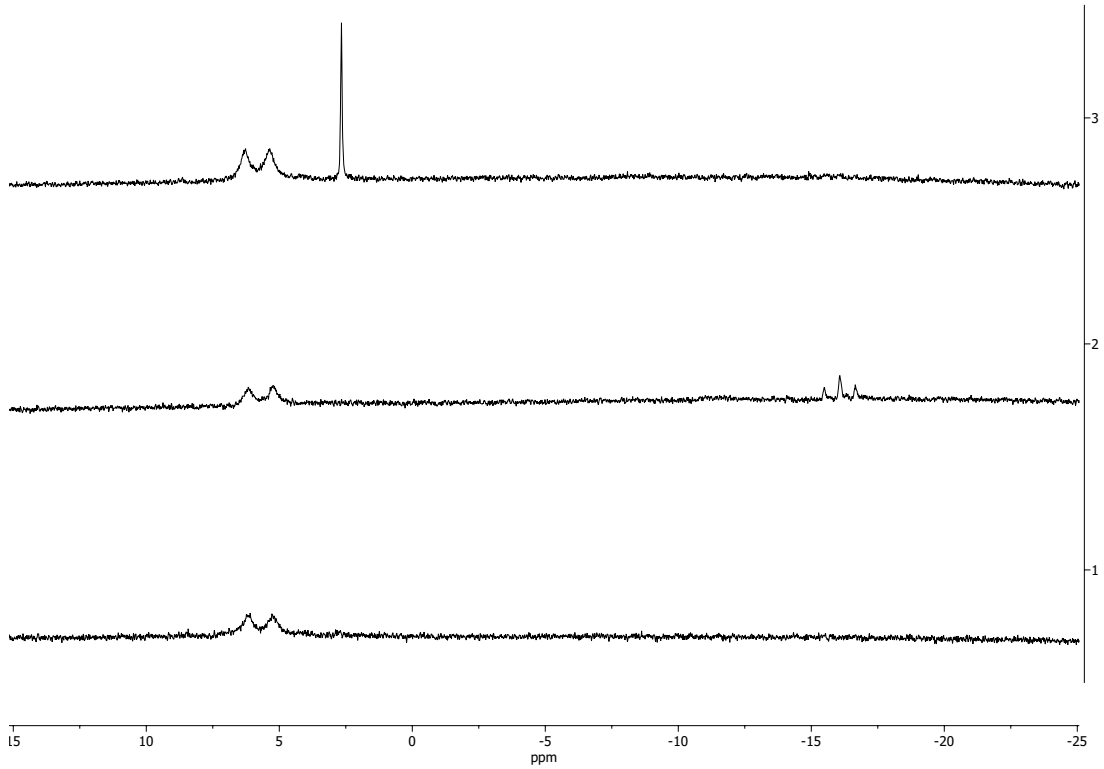

Figure 3.14: Stacked ^{11}B NMR spectra of the reaction between B(*i*OPr)$_3$, Na and H_2 in THF with 4 equivalents of biphenyl (top), 8 equivalents of biphenyl (middle) and 16 equivalents of biphenyl (bottom). No signal that corresponds to a B(OR)$_4$ compound is observed upon increasing the amount of hydrides in solution to 8 equivalents. In addition, a signal occurred at -16.07 ppm that correspond to the formation of a BH_2 compound. Upon increasing the amount of hydrides in solution to 16 equivalents relative to B(O*i*Pr)$_3$, a signal that corresponds to the selective formation of a BH compound was observed.

To see whether an increase in hydrides present in the reaction mixture also results in a deviation of product formation for the naphtalene system, autoclave reactions in THF at 80 °C under 4 bar of hydrogen pressure were performed with 8 and 16 equivalents of naphtalene and sodium. The reaction time was 4 hours for both experiments. A shift in product formation was observed upon increasing the amount of hydrides to 8 equivalents. Figure 3.15 shows the comparison between the product formation of the naphtalene system in Figure 3.12 and the naphtalene system with 8 equivalents of hydrides. No signal that correspond to a BH compound was observed upon increasing the amount of hydrides in solution. In addition, signals were observed that indicated additional formation of BH_2 and BH_3 compounds in comparison to the reaction with only 4 equivalents of hydrides in solution. Finally, no signal was observed that potentially is attributed to the hydroboration of the boron and the naphtalene when doubling the amount of hydrides. However, no difference in product formation was seen when performing an autoclave reaction using 16 equivalents of naphtalene and sodium. This indicates that increasing the amount of hydrides with more than 8 equivalents does not increase product selectivity or alter product mixture composition in general, according to ^{11}B NMR.

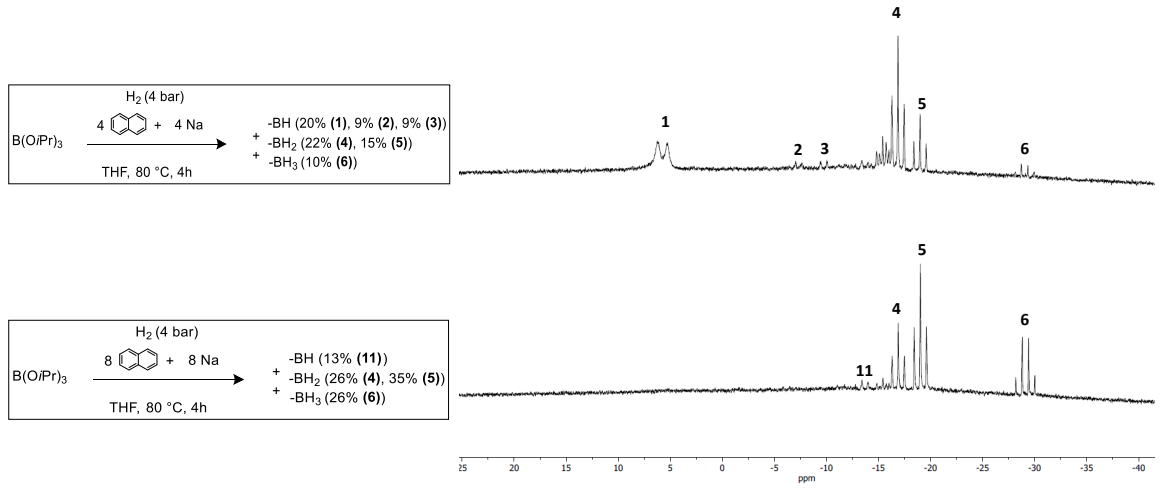

Figure 3.15: Stacked ^{11}B NMR spectra of the reaction between B(*i*OPr)$_3$, Na and H_2 in THF with 4 equivalents of hydrides (top) and 8 equivalents of hydrides (bottom). No signal that corresponds to a BH compound (1) was observed upon increasing the amount of hydrides in solution. In addition, signals were observed that indicated relatively higher amounts of compound (5) and compound (6).

In order to acquire an increase in selectivity towards BH_2 compounds and simplify the reaction system, an autoclave experiment was performed adopting the previous conditions in THF. To archive this, a mono alkoxy substituted diethylmonomethoxyborate was used instead of the tri alkoxy substituted B(O*i*Pr)$_3$ (see Equation 3.10). The basic motivation for using monosubstituted borates is that these compounds differ in a way that only either a monohydride boron compound, quartenary monohydride salt or quartenary dihydride salt can be formed due to the inert boron-carbon bonds under these conditions in contrast to triisopropylborate, which has three substitutable alkoxy groups (see Table 3.2). This might drive the reaction to a more selective product formation. In order to test this hypothesis, 17.5 mg of sodium was added to 97.7 mg of naphtalene in 3 mL of THF in the glass reactor of the autoclave in the glovebox under inert atmosphere. Subsequently, 0.1 mL of the diethylmonomethoxy borate was added and the reaction mixture was stirred. Then, the autoclave was assembled and brought under 4 bar hydrogen pressure in the fumehood. The reaction was stirred for 4 hours at 120 °C. According to ^{11}B NMR and $^{11}B\{^1H\}$ NMR spectroscopy, four signals were observed as depicted in Figure 3.16. A singlet at 6.58 ppm indicates the formation of sodium diethyldimethoxyborate in alignment with similar monosubstituted alkylborate compounds in literature [109]. Furthermore, the spectrum indicates the formation of two monohydride compounds and one dihydride compound. As expected, the reaction showed a higher selectivity than the reactions with B(O*i*Pr)$_3$ as a reagent, but still did not show the desired selective formation of only one borohydride compound. The same reaction was carried out and a subsequent ^{11}B NMR spectrum was recorded after 12 hours to see whether a longer reaction time could drive the reaction to a more selective product formation. However, it was confirmed by ^{11}B NMR spectroscopy that the products in the previously described reaction mixture degrade over time (see Figure 3.17).

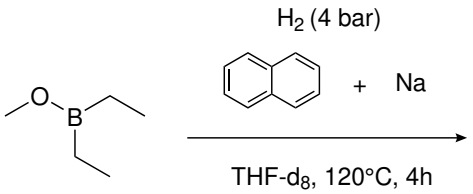

(3.10)

Table 3.2: Potential boron containing compounds which can be formed for a mono-alkoxy substituted reagent and a trialkylborate as a reagent under the selected reaction conditions.

Reactant	Potential products			
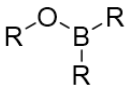		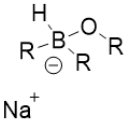	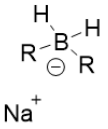	
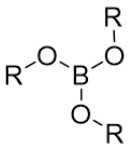	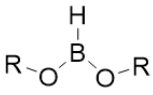	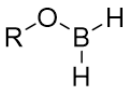		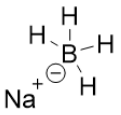
	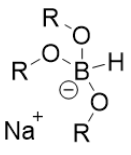	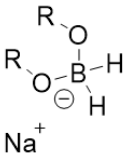	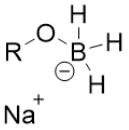	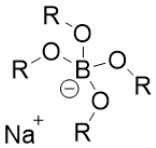

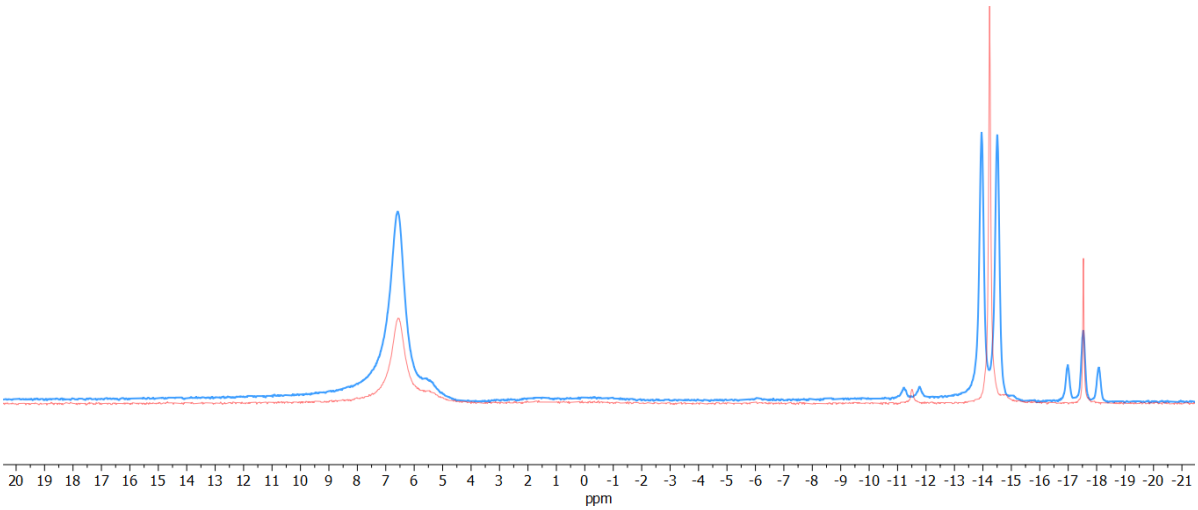

Figure 3.16: Stacked ^{11}B NMR spectrum (blue) and $^{11}B\{^1H\}$ NMR spectrum (red) of the reaction between diethylmonomethoxyborate, 4 equivalents of naphtalene, 4 equivalents of Na and H_2 in THF.

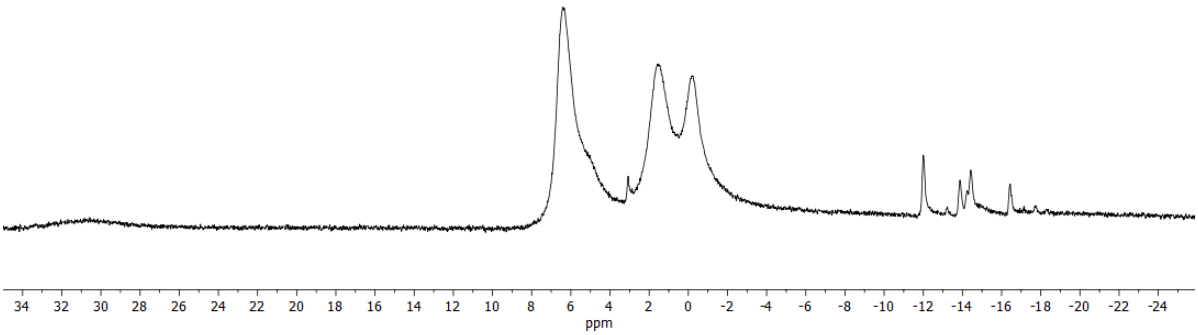

Figure 3.17: ^{11}B NMR spectrum of the reaction between diethylmonomethoxyborate, 4 equivalents of naphtalene, 4 equivalents of Na and H_2 in THF with a reaction time of 12 hours. Products could not be identified out of the resulting reaction mixture via ^{11}B NMR and ^{1}H NMR spectroscopy.

The reaction of sodium aluminium hydride with the tri alkoxy substituted $B(OCH_3)_3$ yielding $NaBH_3(OCH_3)$ occurs under mild conditions at room temperature according to literature [76]. However, the transfer of a fourth hydride on the boron centre seems to have the highest energy threshold to overcome to form $NaBH_4$ (vide supra). A neat reaction is described in literature between NaH and a slight excess of $B(OCH_3)_3$ to form $NaBH(OCH_3)_3$ at room temperature [110]. This reaction was adopted and was carried out my members of the Slootweg research group. However, instead of solely forming a BH compound, the ^{11}B NMR spectrum indicated that 30% conversion to a BH_3 containing compound had occurred. By adopting these reaction conditions to the $B(O\mathit{i}Pr)_3$ system, selective BH_3 synthesis could potentially be possible. The basic idea is, by initially driving the reaction to BH_3 formation through the use of NaH, and subsequently introducing additional hydrides through radical formation, the gibbs energy of the reaction might overcome the energy threshold for the association of a fourth hydride and thereby inducing BH_4 formation (see Equation 3.11).

A neat reaction was performed with 2.11 mL (1.1 equivalents) of $B(O\mathit{i}Pr)_3$ and 200 mg of NaH (1 equivalent). The reaction was stirred for 5 hours at room temperature. Figure 3.18 shows similar results for the reaction product of the reactions with $B(OCH_3)_3$, which were carried out by members of the Slootweg research group. The ^{11}B NMR spectrum indicates that 30% conversion to a BH_3 containing compound had occurred. However, in contrast to the result of the $B(OCH_3)_3$ system, a relatively weak signal was observed that might indicate the formation of a BH_4^- ion. Note that this was the result of increasing the temperature during the work up of the reaction mixture in order to evaporate any remaining starting material ($B(O\mathit{i}Pr)_3$) still left in the product mixture. The formation of traces of a BH_4^- ion could therefore be a result of the reaction of any products with remaining NaH in the reaction mixture in a Brown-Schlesinger process fashion. When subsequently introducing 4 equivalents of naphtalene and sodium in THF to this reaction product and subject it to 120 °C under 4 bar H_2 in an autoclave for 5 hours, the same amount of BH_4^- got more concentrated in the NMR sample and therefore resulted in a relatively stronger signal in the ^{11}B NMR spectrum. No signal was observed that correspond to a BH_3 compound anymore upon addition of 4 equivalents of naphtalene and sodium in THF. Figure 3.19 provides an overview of all reactions described above within the pathway of hydrogen activation via boron radicals.

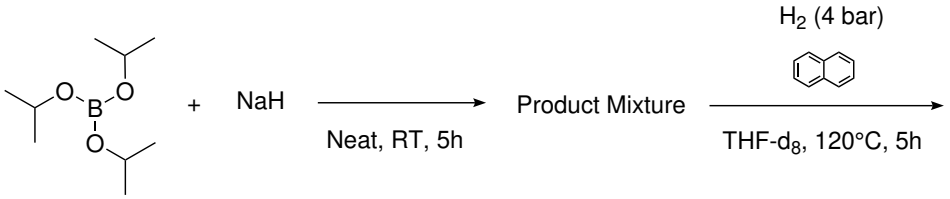

(3.11)

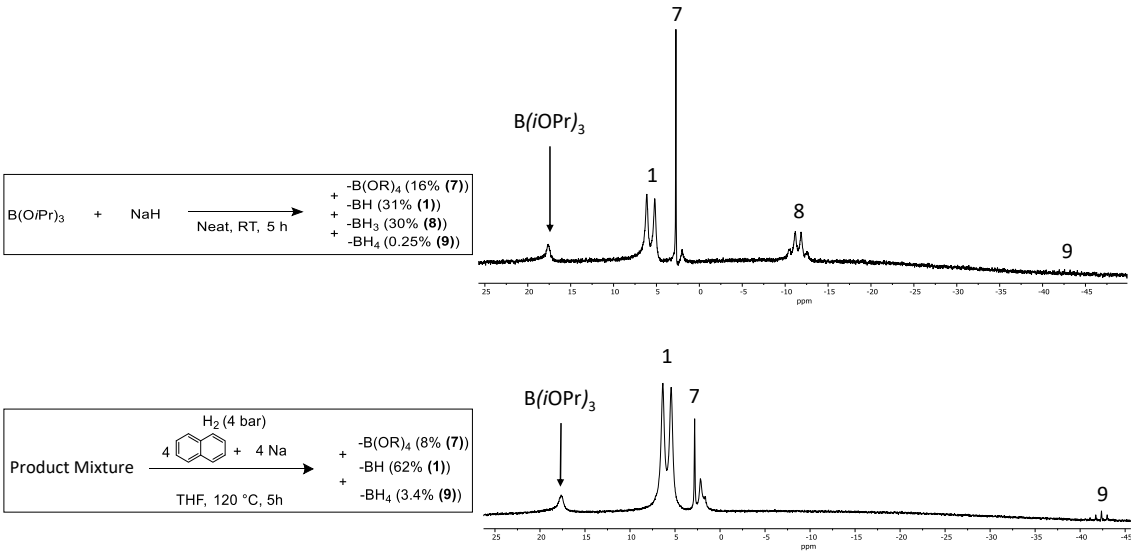

Figure 3.18: Stacked ^{11}B NMR of the neat reaction (top) with similar reaction conditions as for the $B(OCH_3)_3$ system, which is developed by members of the Slootweg research group. 30% of a compound that corresponds to a BH_3 compound is formed (8). A signal was observed that could correspond to BH_4 formation as a result of exposure to higher temperatures during the work up (9). No signal was observed that correspond to a BH_3 compound (8) anymore upon addition of 4 equivalents of naphtalene and sodium in THF (bottom).

Reaction:	Products:
$B(OiPr)_3$ + 4 Naphthalene + 4 Na; H_2 (4 bar); Mineral Oil, 120 °C, 4h	No product formation
$B(OCH_3)_3$ + 4 Naphthalene + 4 Na; H_2 (4 bar); THF, 120 °C, 4h	No product formation
$B(OiPr)_3$ + 4 Naphthalene + 4 Na; H_2 (4 bar); THF, 80 °C, 4h	-BH (20%, 9%, 9%) + $-BH_2$ (22%, 15%) + $-BH_3$ (10%)
$B(OiPr)_3$ + 8 Naphthalene + 8 Na; H_2 (4 bar); THF, 80 °C, 4h	$-BH_2$ (24%, 30%) + $-BH_3$ (24%)
$B(OiPr)_3$ + 16 Naphthalene + 16 Na; H_2 (4 bar); THF, 80 °C, 4h	$-BH_2$ (25%, 37%) + $-BH_3$ (21%)
$B(OiPr)_3$ + 4 Biphenyl + 4 Na; H_2 (4 bar); THF, 120 °C, 4h	$-B(OR)_4$ (34%) + -BH (66%)
$B(OiPr)_3$ + 4 Biphenyl + 4 Na; H_2 (4 bar); THF, 120 °C, 12h	-BH (53%) + $-BH_2$ (47%)
$B(OiPr)_3$ + 8 Biphenyl + 8 Na; H_2 (4 bar); THF, 120 °C, 4h	-BH (59%) + $-BH_2$ (41%)
$B(OiPr)_3$ + 16 Biphenyl + 16 Na; H_2 (4 bar); THF, 120 °C, 4h	-BH (100%)
2-ethoxy-2-ethyl-1,3,2-dioxaborolane + 4 Naphthalene + 4 Na; H_2 (4 bar); THF, 120 °C, 4h	$-B(OR)_4$ (59%) + -BH (5%, 35%) + $-BH_2$ (9%)
2-ethoxy-2-ethyl-1,3,2-dioxaborolane + 4 Naphthalene + 4 Na; H_2 (4 bar); THF, 120 °C, 12h	No selective product formation
$B(OiPr)_3$ + NaH; Neat, RT, 5 h	$-B(OR)_4$ (16%) + -BH (31%) + $-BH_3$ (30%) + $-BH_4$ (0.25%)
Product Mixture + 4 Naphthalene + 4 Na; H_2 (4 bar); THF, 120 °C, 5h	$-B(OR)_4$ (8%) + -BH (62%) + $-BH_4$ (3.4%)

Figure 3.19: An overview of all experiments conducted concerning H_2 activation via boron radical anions and the corresponding borohydride formation according to ^{11}B NMR.

3.4. Heat Transfer Limitation Model

In order to obtain a comprehensive assessment of the feasibility of scaling up the proposed circular hydrogen storage system using $NaBH_4$ as a solid hydrogen carrier, it is crucial to analyze the most energy-intensive steps of the process. As the regeneration of $NaBH_4$ from spent fuel has primarily been achieved through the well-established Brown-Schlesinger Process, which is widely used in industrial applications, its energy demand is thus predictable. The Brown-Schlesinger process is therefore not thoroughly investigated with regards to its energy demand and its corresponding operating costs, despite the question whether the energy requirements of the Brown-Schlesinger process are too substantial or not in the context of competitive circular hydrogen storage. Consequently, this chapter focuses primarily on the hydrogen release stage and the associated energy demands as this reaction system has not been performed on larger scale yet.

The release of hydrogen from $NaBH_4$ involves highly exothermic reactions, both for hydrolysis and alcoholysis. This heat generation and its concomitant cooling requirement represents the most challenging aspect of the circular alcoholysis reaction with regards to heat transfer during the scale-up of $NaBH_4$ quantities, as discussed in chapter 1. As mentioned in subsection 3.1.3, optimization of the hydrogen release reactions using IPA was performed on a 212 mg scale, requiring elevated temperatures to achieve faster conversion times. To comprehensively understand the heat release and the corresponding heat exchange requirements in relation to the quantity of reacting $NaBH_4$, a heat transfer limitation model is introduced which predicts heat flows of upscale reactor configurations which could potentially pose a problem when scaling up reaction parameters.

A schematic drawing of the reactor model has been depicted in Figure 3.20. It is assumed that the reactor is of cylindrical shape. Furthermore, the reactor is cooled through a cooling mantle that covers the entire circumference of the reactor. As the reactor is of cylindrical shape, it allows for assuming the cooling mantle to be a single pipe heat exchanger [111]. In addition, it is assumed that the reactor is made from stainless steel. Assumptions were also made with regards to ideal behavior within the reactor. There assumptions are listed in Table 3.3.

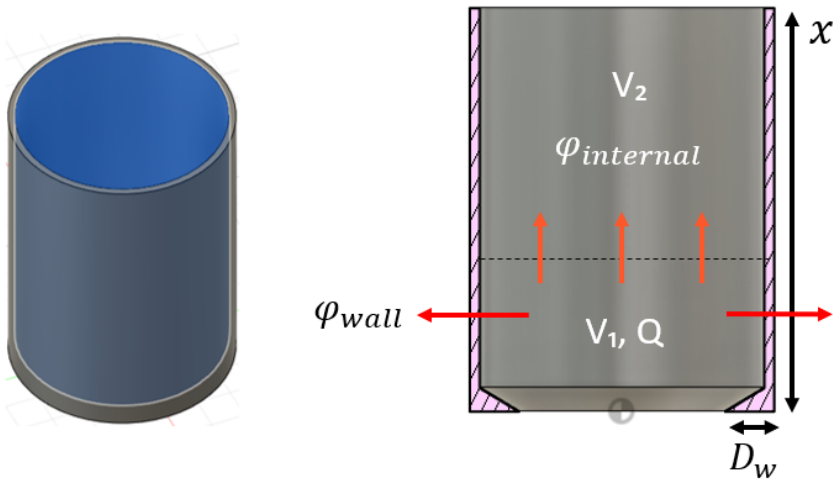

Figure 3.20: A schematic overview of the reactor. V_1 is the volume of the reaction mixture (m^3). V_2 is the excess volume in the reactor (m^3). Q is the heat produced by the reaction mixture (J/s). $\phi_{internal}$ is the heat flux going from V_1 to V_2 (J/s). ϕ_{wall} is the heat flux from V_1 to the reactor wall (J/s). D_w is the thickness of the reactor wall (m). x is the reactor length (m).

Table 3.3: Assumptions made for the demarcation of the heat transfer limitation model.

Assumption	Description
Steady state	The system is considered to be in steady state. The heat produced during the reaction is equal to the rate of removal [112].
Ideal mixture	It is assumed that that the reaction mixture is ideally mixed and therefore the enthalpy of solution (ΔH) is equal to 0. This is done to simplify the modeling of the heat profiles.
Isobaric behavior	The system is assumed to be isobaric. No pressure build up is taken into account in the system.
Inert conditions	the excess reactor volume is assumed to consist solely of N_2 as the excess reactor volume inert with regards to the reaction mixture.

The bottom and top of the reactor are assumed to be isolated. In addition, it is assumed in the model that the heat transfer limiting factor of the reactor wall is the heat transfer between the part of the reactor wall which is in direct contact with the reaction mixture (V_1). It is supposed that the excess volume in the reactor vessel (V_2) will never exceed the temperature of the volume of the reaction mixture where the actual heat is generated. Therefore, the heat transfer from V_2 to through the reactor wall is to be neglected with regards to heat transfer limitations. This does not mean that there is no heat transfer in the reactor vessel between the reaction mixture and the excess volume, V_2. It is assumed that the heat generated can be transferred through either the reactor wall or to the excess volume in the reactor vessel. However, it is also assumed that the heat transferred through the reactor wall is sufficiently larger in comparison to the heat transfer to V_2 as the thermal conductivity of stainless steel is more than 2000 times larger then the thermal conductivity of nitrogen gas ($\phi_{internal} << \phi_{wall}$) [113]. The heat transfer from V_1 to V_2 can therefore also be assumed to be negligible. When combining the latter statements and assumptions, the overall energy balance of the reactor vessel is depicted in Equation 3.12. The heat production term Q is initially investigated, which is defined by Equation 3.13. Here, $\Delta_r H^\circ$ is the heat of reaction and r is the reaction rate. The heat of reaction is defined by the heat of formation of the products and reactants within the reaction (see Equation 3.14). Table 3.4 provides the necessary values to find a value for $\Delta_r H^\circ$. As the alcoholysis reaction with IPA and H_2SO_4 is controlled by the amount of acid which is fed to the reaction mixture by the syringe pump as explained in subsection 3.1.3, the reaction rate is also limited by the addition rate of H_2SO_4. Therefore, it can be assumed that the reaction rate is equal to the addition rate of H_2SO_4, which is provided in Table 3.5. The acid addition rates are based on alcoholysis reactions with IPA corresponding with 10 grams, 15 grams and 20 grams of $NaBH_4$ (vide supra).

$$Q - \phi_{wall} = 0 \tag{3.12}$$

$$Q = \Delta_r H^\circ \cdot r \tag{3.13}$$

$$\Delta_r H^\circ = \Sigma \nu \Delta_f H^\circ(products) - \Sigma \nu \Delta_f H^\circ(reactants) \tag{3.14}$$

Table 3.4: Heat of formation of reactants and products of the alcoholysis reaction with IPA.

Reaction:	$2\,NaBH_4 + H_2SO_4 + 6\,IPA \longrightarrow B(OiPr)_3 + Na_2SO_4 + 8\,H_2$	
Molecule	**Standard heat of Formation** [$\Delta_f H^\circ$ (kJ/mol)]	**Stochiometry**
$NaBH_4$	-192 [114]	2
H_2SO_4	-814 [114]	1
IPA	-319 [114]	6
$B(OiPr)_3$	-1130 [115]	2
Na_2SO_4	-1387 [114]	1
H_2	0	8

Table 3.5: Acid addition rates of sulfuric acid corresponding to the amount of reacting $NaBH_4$. It can be assumed that the acid addition rate is equal to the reaction rate as the acid addition is the limiting factor for the reaction to proceed.

$NaBH_4$ (grams)	**$r_{H_2SO_4,addition}$(mL/s)**	**$r_{reaction}$(mol/s)**
10	0.00592	$1.104 \cdot 10^{-4}$
15	0.00883	$1.656 \cdot 10^{-4}$
20	0.01184	$2.208 \cdot 10^{-4}$

According to Equation 3.12, $Q = \phi_{wall}$. However, ϕ_{wall} also depends on the overall heat transfer coefficient through the reactor wall and on the temperature of the of the cooling water (see Equation 3.15). $U_{overall}$ is the overall heat transfer coefficient through the reactor wall. A_{wall} is the surface of the reactor wall that transfers heat to the cooling water. T_1 is the temperature of the reaction mixture. T_c is the temperature of the cooling water.

$$\phi_{wall} = U_{overall} \cdot A_{wall} \cdot (T_1 - T_c) \tag{3.15}$$

To derive the overall heat transfer coefficient, the heat transfer from the reactor wall to the cooling water can be explained through Figure 3.21, where T_w is the temperature of the wall, T_w, δ being the temperature of the interface between cooling water and the stainless steel wall. In Figure 3.21, it is assumed that the reactor wall adopts the same temperature as the reaction mixture. Deriving Equation 3.16 and Equation 3.17 from Figure 3.21 and combining the two equations to Equation 3.18, the overall heat transfer coefficient can be calculated through Equation 3.19. h refers to the thermal conductivity of a specific material provided in Table 3.6. It is assumed that the change of thermal conductivity between 0 and 70 °C for stainless steel, water and IPA is negligible, enabling the use of thermal conductivity for the relevant substances as a constant.

$$\phi^{"}_{q,wall} = h_{water} * (T_{w,\delta} - T_w) \tag{3.16}$$

$$\phi^{"}_{q,wall} = h_{steel} * (T_2 - T_{w,\delta}) \tag{3.17}$$

$$T_w - T_2 = (\frac{1}{h_{water}} + \frac{1}{h_{steel}}) \tag{3.18}$$

$$\frac{1}{U_{overall}} = \frac{1}{h_{water}} + \frac{1}{h_{steel}} \tag{3.19}$$

Table 3.6: Values for the thermal conductivity of water, IPA and stainless steel.

Substance	**Thermal Conductivity Window, λ (W/m/K)**	**Average Thermal Conductivity, λ (W/m/K)**
Stainless Steel	15 [116]	15
Water	0.55 - 0.65 [113]	0.6
IPA	0.15 - 0.17 [117]	0.16

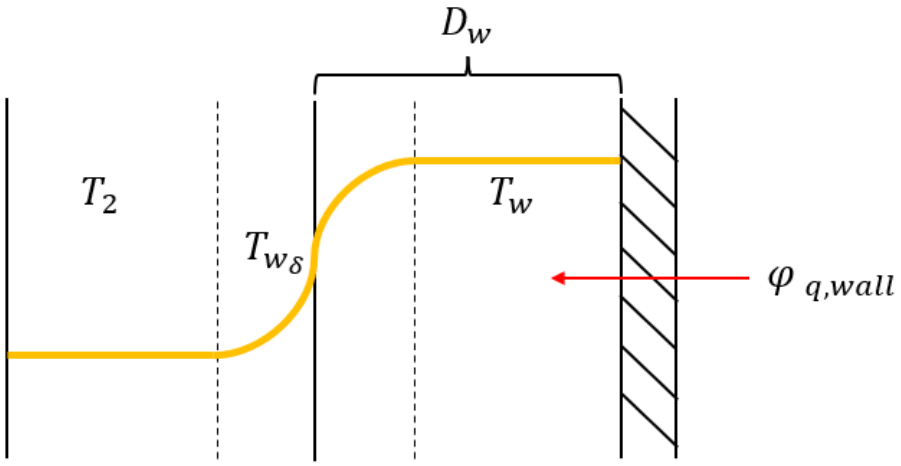

Figure 3.21: A schematic overview of the reactor wall with its correlating temperature profile to predict the overall heat transfer coefficient.

To acquire the temperature profile of the reaction mixture, real-time data tests were performed. Alcoholysis reactions were conducted with $NaBH_4$ in 6 equivalents of IPA with a graduate addition of 1 equivalent of H_2SO_4 over 20 minutes to circumvent side product formation as mentioned in subsection 3.1.3. 6 equivalents of IPA were used as this was regarded as the minimal amount of IPA before the reaction mixture becomes too viscous due to Na_2SO_4 formation upon full conversion to $B(OiPr)_3$, and therefore could cause mass transfer limitations in the reactor piping. Three tests were conducted, respectively using 10, 15 and 20 grams of $NaBH_4$ with the respective amounts of IPA and H_2SO_4 (see Table 3.7). As the laboratory is not suited to facilitate higher amounts of $NaBH_4$ reactions with the corresponding high amounts of hydrogen gas released, the model is used to extrapolate the change in the heat transfer behavior between these 3 data sets. The reactions were respectively performed in a 250 mL, 500 mL or 1000 mL three neck roundbottom flasks (RBF) with attached cooler relative to the excess volume of the reactor with regards to the amount of solvent in the reactor to minimize deviations in internal heat transfer (see Figure 6.40 in section 6.2). A thermocouple was attached to one of the necks of the RBFs to measure the temperature increase in the reaction mixture. No cooling mantle was attached to the reactor in order determine comparable values for the heat elevation of the three different reactions as heat transfer through the reactor wall to the atmosphere could then be assumed to be proportionally similar. From Figure 3.22a, it can be seen that the increase in $NaBH_4$ with proportionate IPA and H_2SO_4, and scaling the reactor volumes accordingly, result in roughly the same amount of temperature elevation. This means that heat transfer in this system has a linear correlation to the amount of reacting $NaBH_4$ upon scaling. Therefore, a mean data set was created from the 3 data sets to which a power regression was done to make a continuous function that corresponds to the real-time data (see Equation 3.20 and Figure 3.22b). This regression function of temperature in the reaction mixture (T_1) together with the calculated heat production in reaction mixture (Q) can then be used to determine the theoretical temperature of the cooling water (T_c) to compensate for this heat flux through Equation 3.15.

The temperature elevation of the cooling water over time is depicted in Figure 3.22c. Note that the cooling water in the cooling mantle in this equation is still stagnant throughout the reaction. Hence the relatively high values for the eventual temperature of the cooling water. Despite it not being realistic to use this value in the actual heat transfer limitation model, this can then be used to calculate the required mass flow rate of the cooling water within the cooling mantle of the reactor.

$$y = -e^{\frac{744.1543-t}{196.4473}+345.5391} \tag{3.20}$$

Table 3.7: Amounts of starting material for the test reactions needed for the heat transfer limitation model. All reactions were performed at room temperature under atmospheric pressure. The standard reaction time was 20 minutes.

Reaction:	$2\,NaBH_4 + H_2SO_4 + 6\,IPA \longrightarrow B(OiPr)_3 + Na_2SO_4 + 8\,H_2$	
$NaBH_4$ (gr)	**IPA (mL)**	**H_2SO_4 (mL)**
10	121	7.1
15	182	10.6
20	242	14.2

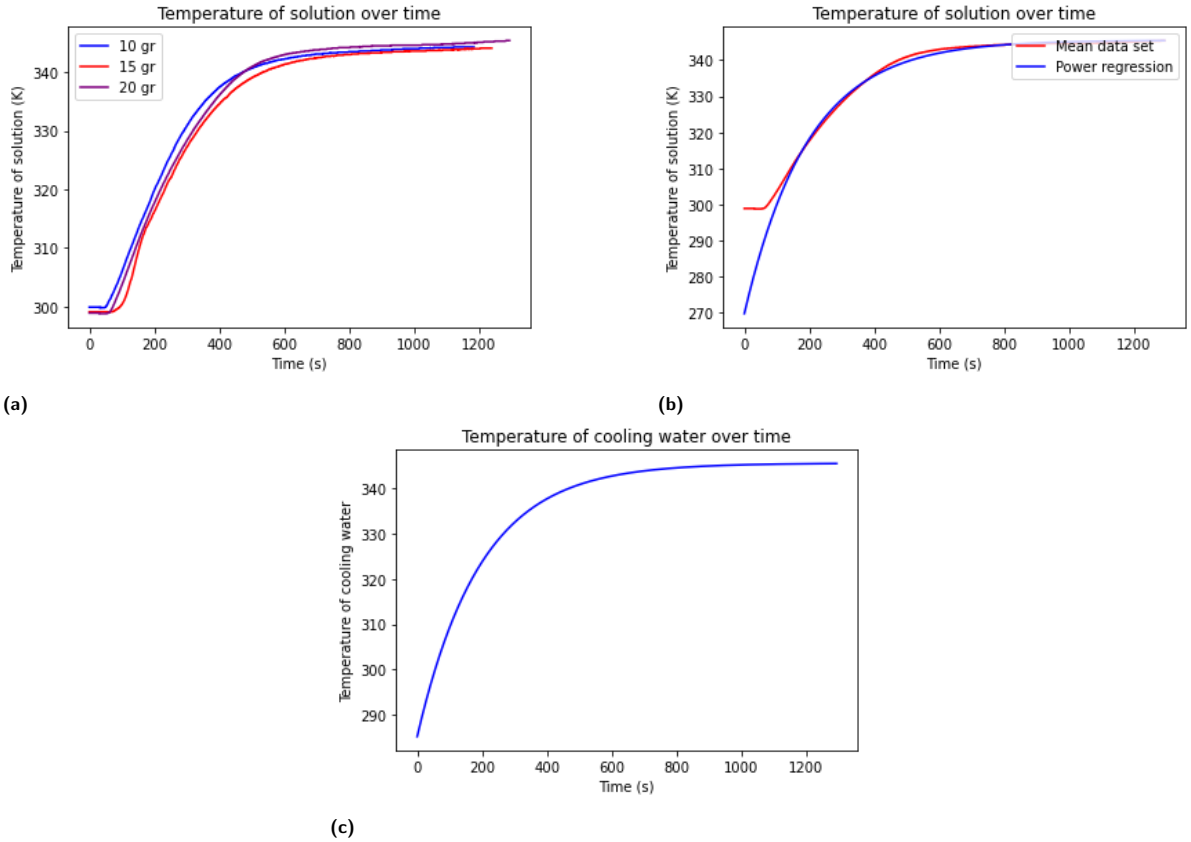

Figure 3.22: a) Temperature elevation in the reaction mixture over time with 10, 15 and 20 grams of $NaBH_4$ with the 6 equivalents of IPA and 1 equivalent of H_2SO_4 fed over time. b) Power regression function to mimic the mean data set of the initial three data sets measured for temperature elevation in $NaBH_4$ alcoholysis. c) The temperature of the stagnant cooling water over time.

Through predicting the heat flow from the reaction mixture through the reactor wall to the cooling water, a temperature profile of the heat exchanger can be derived. This is done by setting up a microbalance over the verticle axis of the cooling mantle. The micro balance is derived from Equation 3.21 to Equation 3.22.

ϕ_m is the mass flow rate of the water (kgs^{-1}), C_p is the heat capacity of water (kJ kg^{-1} K^{-1}), T_w is the temperature of the reactor wall (K), U_w is the overall heat transfer coefficient of the reactor wall (W m^{-2} K^{-1}), D_w is the thickness of the reactor wall (m) and T is the temperature of the cooling water (K). A schematic of the microbalance is provided in Figure 3.23. Setting up such a micro balance is only possible when plug flow behavior can be assumed. Plug flow behavior can be assumed if flow through the heat exchanger is in the turbulent regime [118]. In this way, the laminar sublayer caused by the pipe wall is negligibly thin in comparison to the pipe diameter, realizing uniform compartmentalization throughout the reactor, regardless which section of the heat exchanger is analysed for a microbalance. Whether a flow is turbulent or laminar is determined through the Reynolds number, which depends on the flow velocity (v), the length of the heat exchanger (L) and the dynamic viscosity of water (ν) (see Equation 3.23). In the model, only the reynolds number of the cooling flow is regarded as it is assumed that this is the limiting factor with regards to the Reynolds number of the flow within the reaction mixture. After the mass flow profile has been derived, the minimum scale for this reactor model can be determined to which the flow velocity and reactor dimensions are high enough to reach turbulent flow, therefore enabling plug flow behavior.

$$\frac{d\phi_q}{dt} = \phi_{q,in} - \phi_{q,out} + \phi_{q,wall} \tag{3.21}$$

$$\frac{d\phi_q}{dt} = 0 = [\phi_m C_p T]_x - [\phi_m C_p T]_{x+dx} + U_w D_w dx(T_w - T) \tag{3.22}$$

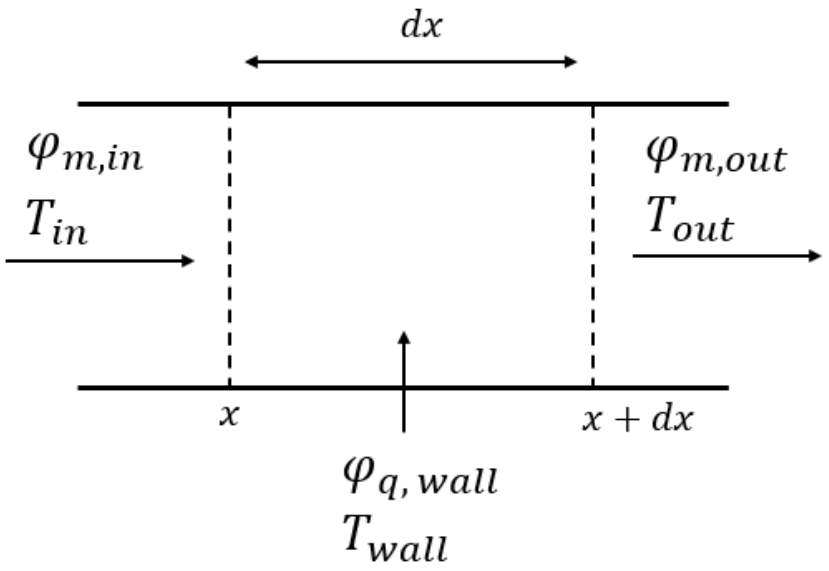

Figure 3.23: Schematic overview of a single pipe heat exchanger. $\phi_{m,in}$ is the mass flow of water entering the heat exchanger (kg/s). $\phi_{m,out}$ is the mass flow of water leaving the heat exchanger (kg/s). $\phi_{q,wall}$ is the heat flux entering the heat exchanger from the reactor wall to the cooling water (J/s). T_{in} is the temperature of the inflowing cooling water (K). T_{out} is the temperature of the outflowing cooling water (K). T_{wall} is the temperature of the reactor wall (K).

$$Re = \frac{v * L}{\nu} \tag{3.23}$$

As steady state is assumed ($\phi_{m,in} = \phi_{m,out} = \phi_m$) within a small interval within the heat exchanger (dx), a Taylor approximation over this very small interval of the length of the pipe (lim x $\rightarrow$ 0) provides us with Equation 3.24. Rewriting Equation 3.24 to Equation 3.25, Equation 3.26, Equation 3.27, and then integrating to Equation 3.28, we obtain an expression for the mass flow (ϕ_m) of the cooling water as a

function of the temperature of the cooling water in Equation 3.29. Devide ϕ_m by the density of water and we obtain the volumetric flow rate of the cooling water (ϕ_v) in Equation 3.30. The trajectory of ϕ_v is depicted in Figure 3.24. The rapid decline in flow rate is due to the increasing difference in temperature between the reaction mixture and the fed cooling water. When integrating Figure 3.24 over the reaction time, the total minimum required cooling water for this particular reaction is 1.4L.

$$lim_{x\to 0}\Big(\frac{[\phi_m C_p T]_x - [\phi_m C_p T]_{x+dx}}{dx}\Big) + U_w D_w dx(T_w - T) = 0 \tag{3.24}$$

$$-\frac{d(\phi_m C_p T)}{dx} + U_w D_w (T_w - T) = 0 \tag{3.25}$$

$$U_w D_w (T_w - T) = \frac{d(\phi_m C_p T)}{dx} \tag{3.26}$$

$$-\frac{d(T_w - T)}{T_w - T} = \frac{U_w D_w}{\phi_m C_p} dx \tag{3.27}$$

$$ln\Big(\frac{T_w - T}{T_w - T_{in}}\Big) = -\frac{U_w D_w}{\phi_m C_p} x \tag{3.28}$$

$$\phi_m = \frac{-U_w D_w x}{C_p ln\Big(\frac{T_w - T}{T_w - T_{in}}\Big)} \tag{3.29}$$

$$\phi_v = \frac{\phi_m}{\rho_{water}} \tag{3.30}$$

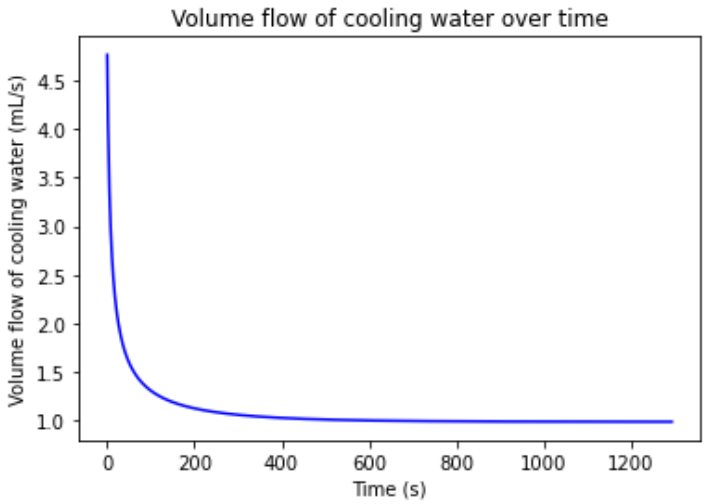

Figure 3.24: The minimum required mass flow of water through the cooling mantle to compensate for the heat flow of the reaction.

It is now possible to see how much the reactor has to be scaled up before the dimensions of the reactor are substantial enough to allow turbulent flow regimes, and therefore for the model to be in effect. The minimum Reynolds number that has to be reached is 2900 to acquire turbulent flow [119]. From Equation 3.23, it is seen that the dynamic viscosity is constant and that the length of the reactor and the flow velocity increase once the dimensions of the reactor proportionately increase. The flow velocity can be derived from the mass flow rate through Equation 3.31, where ρ_{water} is the density of water and A_{mantle} is the intersection of the cooling mantle.

$$v = \frac{\phi_m}{\rho_{water} \cdot A_{mantle}} \tag{3.31}$$

Combining Equation 3.31 and Equation 3.23 gives us an expression for the Reynolds number as a function of the flow velocity (see Figure 3.25). It is seen that the lowest Reynolds number achieved in the flow regime is 5. When defining all the variables in terms of reactor dimensions, it is seen that the Reynolds number is proportionate to the increase in size of the reactor. This means that the minimal reactor size that has to be achieved for the model to be in effect is 580 times larger than the laboratory scale model. This may seem a lot, but with regards to the $NaBH_4$ feed it is roughly 0.01 kg of $NaBH_4$ per second, or 12 kg of $NaBH_4$ for the entire batch reaction, which is less substantial from a process engineering perspective. This would require 812 L of cooling water.

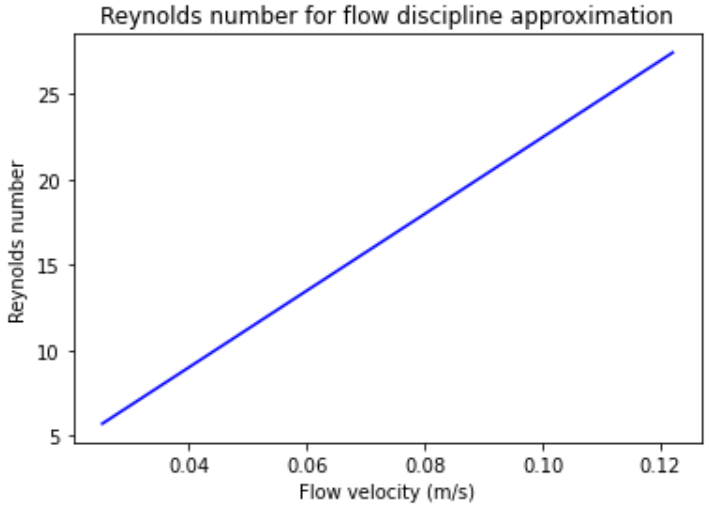

Figure 3.25: The Reynolds number of the flow of cooling water in the cooling mantle of the reactor over the flow velocity of the cooling water.

The mass flow of cooling has been calculated to compensate for the heat flux from the reaction mixture. It is inherent that there is thus a correlation between the temperature of the cooling water and the temperature of the reaction mixture. The temperature between stagnant cooling water and temperature of the uncooled reaction mixture was derived to determine the heat flux, thereby enabling the determination of the required cooling water feed. However, the temperature of the cooling water has a diminishing affect on the temperature of the reaction mixture and vice versa. This interaction was modeled by first deriving a macro energy balance of the heat exchanger to determine the temperature of the out flowing cooling water after heat transfer has occurred (see Equation 3.32). Simplifying and rearranging Equation 3.32 to Equation 3.33, gives us an expression for the temperature of the out flowing cooling water in Equation 3.34.

$$[\phi_m C_{p,water}, T]_{in} - [\phi_m C_{pwater}, T]_{out} + \phi_q = 0 \tag{3.32}$$

$$\phi_q = \phi_m C_p (T_{out} - T_{in}) \tag{3.33}$$

$$T_{out} = \frac{\phi_q}{\phi_m C_p} + T_{in} \tag{3.34}$$

When combining the values for the outflowing cooling water temperature and the calculated heat flux through the reactor wall, the temperature of the cooled reaction mixture can be calculated through Equation 3.35. Rearranging Equation 3.35 provides us with an expression of the temperature of the cooled reaction mixture (see Equation 3.36). Both the temperature of the outflowing cooling water and the temperature of the cooled reaction mixture are plotted in Figure 3.26. In the model, the temperature of the cooled reaction mixture does not exceed 55 °C. The reason for using the temperature of the out-flowing cooling water in the determination of the temperature of the reaction mixture instead of using a differential equation to acquire a temperature profile, is because the temperature of the out-flowing cooling water stagnates at approximately 600 seconds. This indicates that the change in temperature differential between the cooling water and the

reaction mixture is close to zero. This in turn signifies thermodynamic equilibrium within the system. The temperature difference between the cooling water and the reaction mixture is the driving force for the heat flux. The heat flux is in turn dependent on the heat of reaction, which is intrinsic to the reaction. Therefore, it can be assumed that the temperature of the reaction mixture cannot surpass the sum of the temperature of the cooling water and temperature difference imposed by the heat flux. As both these values are constant after 600 s, the temperature of the reaction mixture must be stagnant, therefore indicating a threshold for the maximum temperature of the reaction mixture.

$$\phi_q = U_{tot} A_{wall} (T_{sol} - T_c) \tag{3.35}$$

$$T_{sol} = \frac{\phi_q}{U_{tot} A_{wall}} + T_c \tag{3.36}$$

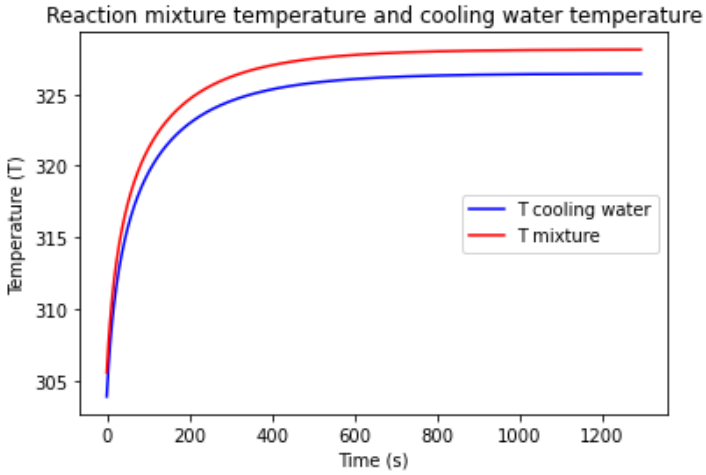

Figure 3.26: The temperature of the cooling water after heat transfer and the temperature of the cooled reaction mixture over time.

3.5. Techno-Economical Analysis

Establishing a sustainable circular method for hydrogen storage in $NaBH_4$ hinges not solely upon the feasibility of the underlying chemical processes or the technological viability of the different process steps. The cost-effectiveness of any novel technological solution is intrinsically correlated upon its successful integration and growth within the targeted market. Market diffusion therefore depends on a viable business case, thereby realizing a technological proposition attractive to potential investors [120]. The main research question in this thesis pursues a solution to a more energy efficient and less energy demanding circular process for storing and releasing hydrogen through $NaBH_4$. The experiments that were performed within this thesis stem from the conceptual framework of realizing such a process. This was done through either diminishing or circumventing energy intensive process steps, thereby lowering process costs. In order to assess the incremental value of the subsequent chapters relative to pre-existing approaches for storing hydrogen in $NaBH_4$, a mass and energy balance was developed of the alcoholysis system with the use of IPA. Both the processes with hydrolysis and alcoholysis were analyzed with respect to their energy consumption to facilitate a comparison of these two systems. Subsequently, an evaluation was conducted to compare the hydrogen production of these systems with competitive market pricing for H_2.

The mass and energy balance entails the results of all latter chapters. Nonetheless, owing to the lack of borohydride formation from H_2 activation through boron radical anions, thereby not capable of closing the cycle for hydrogen storage in $NaBH_4$, said process could not be integrated within the the mass and energy balance. Consequently, the regeneration of $NaBH_4$ is exclusively based upon its synthesis from $B(OiPr)_3$ via the Brown-Schlesinger process. Nevertheless, it is worth noting that H_2 activation through boron radical anions could play an important role in developing an energy efficient, cost-competitive and scalable method

for $NaBH_4$ synthesis from alkylborates in the future.

3.5.1. Mass Balance

To acquire a quantitative evaluation of the assessed systems in terms of energy consumption, it is necessary to develop an overall process flow diagram. This process flow diagram is derived from various reaction steps described in the latter chapters. Summarizing these process steps in terms of chemical equations, the process can be characterized through the release process (Equation 3.37) and the $NaBH_4$ regeneration process (Equation 3.38). Additionally, Equation 3.39 is introduced to facilitate the recycling of the generated $NaOiPr$ from Equation 3.38 back to IPA and NaOH.

$$2\,NaBH_4 + H_2SO_4 + 6\,IPA \longrightarrow 2\,B(OiPr)_3 + Na_2SO_4 + 8\,H_2 \tag{3.37}$$

$$B(OiPr)_3 + 4\,NaH \longrightarrow 3\,NaOiPr + NaBH_4 \tag{3.38}$$

$$NaOiPr + H_2O \longrightarrow IPA + NaOH \tag{3.39}$$

The process flow diagram is derived on the basis of generating 1 kg of hydrogen. The release of hydrogen in Equation 3.37, along with the isolation of $B(OiPr)_3$ and IPA, is integrated in Scheme 5. During the hydrogen release, 6 equivalents of IPA are used. This results in an excess of 3 equivalents of IPA. As discussed in subsection 3.1.3, this surplus of IPA is necessary in counteracting the increase of solution viscosity due to the formation of Na_2SO_4 during hydrogen release, which in turn risks mass transfer limitations and process blockages in piping.

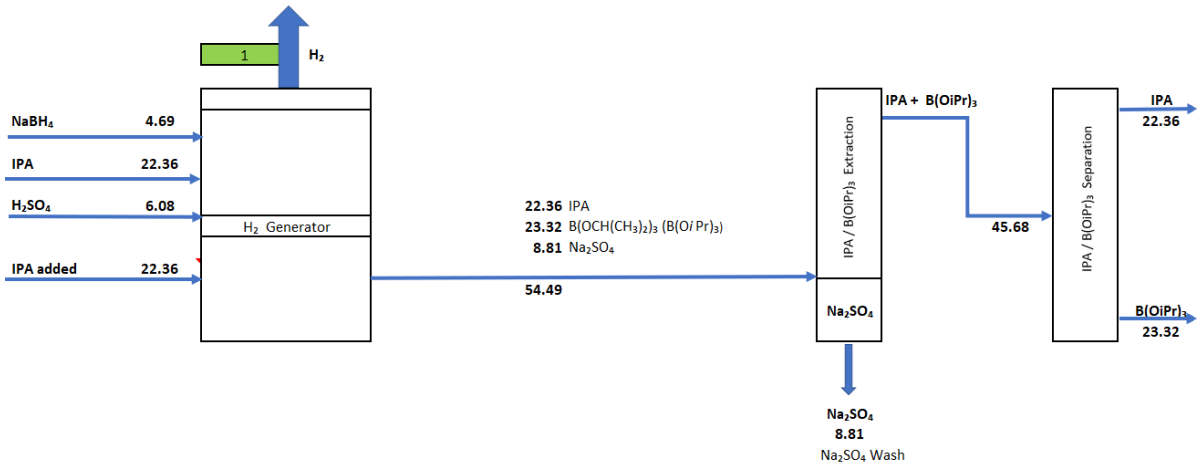

Scheme 5: The process flow diagram of the hydrogen release process from the alcoholysis reaction with IPA. All values in the mass balance are expressed in kg.

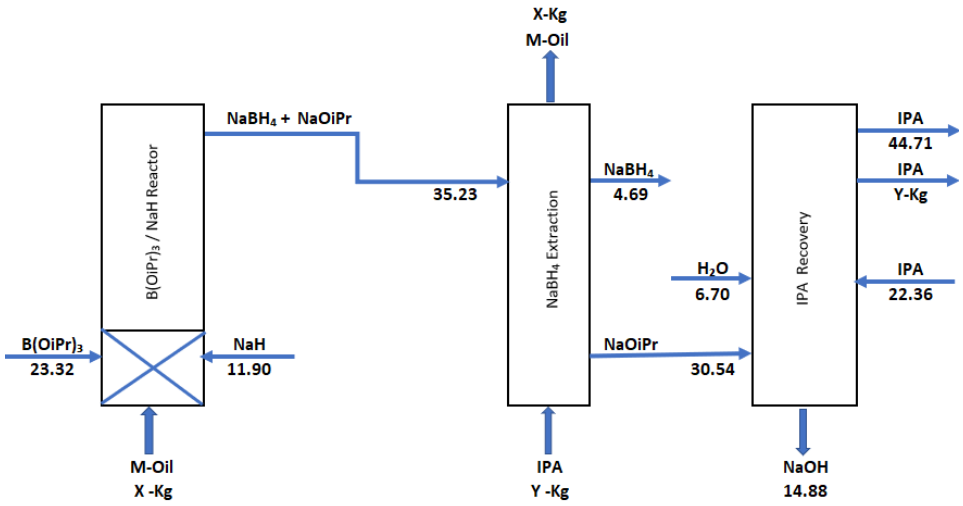

Scheme 6: The process flow diagram of the of the regeneration process of the spent fuel from B(O*i*Pr)$_3$ back to NaBH$_4$ through the Brown-Schlesinger process. All values in the mass balance are expressed in kg.

From Scheme 5, one can deduce the process flow diagram of the regeneration of NaBH$_4$ through the Brown-Schlesinger process, which is shown in Equation 3.38. Note, that IPA does not react with NaBH$_4$, and therefore NaB(O*i*Pr)$_4$ can not be formed as in the presence of stochiometric amounts of protons B(O*i*Pr)$_3$ is formed. In addition, Equation 3.38, it is important to clarify that the extraction of NaBH$_4$ from mineral oil has been done through the use of IPA. As discussed in section 3.2, the extraction process with IPA results a suspension of IPA within the mineral oil. As the mixture does not form a polar-apolar double layer over time upon extraction of IPA, the work-up required when extracting with IPA happens to be elusive on lab scale. However, separation of oil-based substances and IPA has been done excessively on larger scale through centrifuging or membrane pervaporation [102, 103]. Given the overarching objective of extrapolating the mass balance to meet industrial-scale hydrogen production, it can be assumed that extraction of NaBH$_4$ through the use of IPA and subsequent separation through such industrial methods would yield in full extraction of NaO*i*Pr and NaBH$_4$.

3.5.2. Energy Balance

As the process flow diagram has been developed, attention can be directed towards assessing the energy requirements for the implementation of the envisioned alcoholysis system. In addition, these energy requirements can subsequently be compared to the hydrolysis system for storing hydrogen in NaBH$_4$ to access whether the energy requirement of the envisioned alcoholysis system is actually minimized, thereby receding to the research question formulated in chapter 2. Both the hydrolysis pathway, as the alcoholysis pathway are show in Scheme 7 and Scheme 8, respectively.

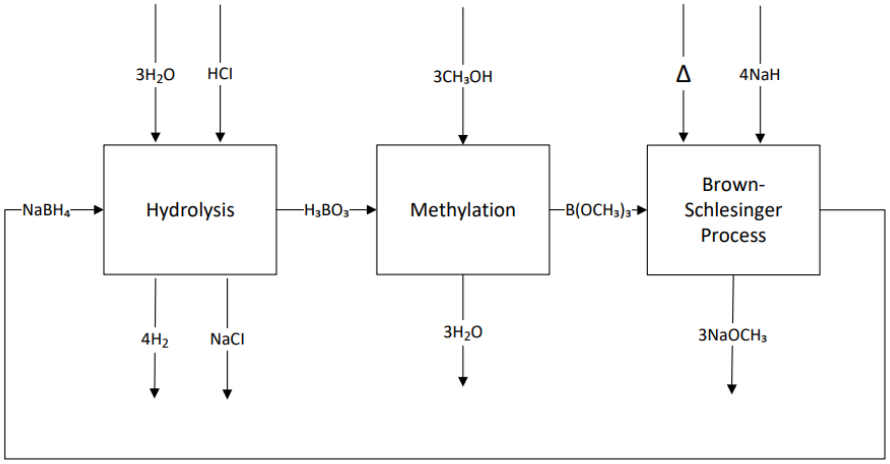

Scheme 7: Block diagram of the hydrolysis reaction pathway with stochiometric amounts of acid.

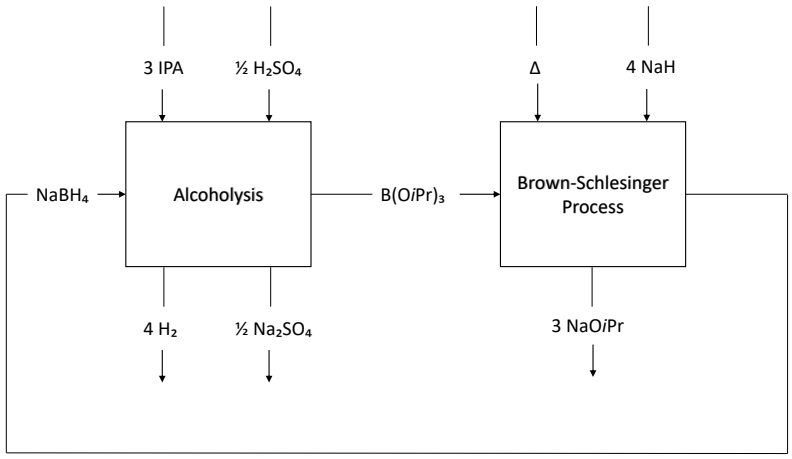

Scheme 8: Block diagram of the envisioned alcoholysis system using IPA and and stochiometric amounts of acid.

Process optimizations that have been described in the latter chapters by introducing the envisioned alcoholysis pathway include the circumvention of the crystallization stage to purify H_3BO_3 after hydrogen release in the hydrolysis pathway and the circumvention of the azeotropic distillation between methanol and $B(OCH_3)_3$. As mentioned above, the crystallization stage is used to separate boric acid from water subsequent to hydrogen release. The use of IPA as the solvent for the hydrogen release stage in the alcoholysis pathway results in the direct formation of the trialkylborate, obsoleting the need for an additional alcohol addition step following boric acid purification in the hydrolysis pathway. It is calculated with the involvement of the UvA Scientific Team that this alteration reduces energy consumption from 40.47 kWh/kg of $NaBH_4$ to 23.24 kWh/kg of $NaBH_4$ by executing the hydrogen release stage via alcoholysis with IPA instead of using the hydrolysis reaction pathway to release H_2 from $NaBH_4$. Additionally, the circumvention of the azeotropic distillation required to separate $B(OCH_3)_3$ from methanol, intrinsic to the hydrolysis pathway, also diminishes energy intensity. It is assumed that the energy required for the separation of $B(OiPr)_3$ from IPA within the alcoholysis pathway is less than the energy required for the separation of $B(OCH_3)_3$ from methanol.

It is proposed that this alteration in process design reduces energy consumption from 10.08 kWh/kg of $NaBH_4$ to 4.48 kWh/kg of $NaBH_4$. These estimations are based on similar distillation techniques used for distilling water/ethanol mixtures in which less distillation steps are required for different grades of purity [121].

It is important to note that the Brown-Schlesinger process is applicable to both the regeneration to $NaBH_4$ from $B(OCH_3)_3$, as well as for $B(OiPr)_3$, as demonstrated in section 3.2. As both reaction conditions are similar for both reagents, energy consumption is approximately equivalent for both the hydrolysis and alcoholysis systems with regards to the regeneration of $NaBH_4$. Calculations that have been made with the involvement of the UvA Scientific Team indicate that the Brown-Schlesinger process used within the described system necessitates an energy consumption of 26.25 kWh/kg of $NaBH_4$.

When combining the values for the energy consumption for both systems mentioned above, the aggregate energy consumption is decreased from 76.80 kWh/kg of $NaBH_4$ to 53.97 kWh/kg of $NaBH_4$ by using the alcoholysis pathway with IPA instead of the hydrolysis pathway. Table 3.8 shows an overview for the comparison of energy requirements of both systems. According to Scheme 5, 1 kg of hydrogen production necessitates 4.69 kg of $NaBH_4$. Consequently, the energy requirement for producing 1 kg of H_2 decreases from 360.2 kWh/kg of H_2 to 253.1 kWh/kg of H_2. Although this marks a substantial reduction in energy consumption, thereby minimizing the energy intensity of the use of $NaBH_4$ as a circular hydrogen carrier, it remains insufficient for this method to be economically competitive. If the average cost of 1 kWh within the Dutch energy market is €0,51 [122], then the production of 1 kg of hydrogen via the alcoholysis pathway amounts to €129,08/kg of H_2. Comparatively, the market price for green hydrogen ranges between €3,- and €8,- [123]. This illustrates that hydrogen storage using $NaBH_4$ as a circular hydrogen carrier still faces substantial barriers to attain competitive market pricing for hydrogen production and storage. Nonetheless, competitive circular hydrogen storage using $NaBH_4$ as a circular hydrogen carrier may become attainable with further optimization of the envisioned process.

Table 3.8: Energy balance for the hydrolysis reaction pathway and the alcoholysis reaction pathway with regards to the H_2 release stage, the distillation stage and the Regeneration stage.

	Hydrolysis		**Alcoholysis**	
	E [kWh/kg $NaBH_4$]	**E [kWh/kg H_2]**	**E [kWh/kg $NaBH_4$]**	**E [kWh/kg H_2]**
H_2 release stage	40.47	189.8	23.24	109.0
Distillation stage	10.08	47.28	4.48	21.01
Regeneration stage	26.25	123.1	26.25	123.1
Total	76.80	360.2	53.97	253.1

4

Experimental

4.1. General remarks

4.1.1. Preparative procedures

All reactions were performed under atmospheric pressure in a fumehood unless noted otherwise. Reactions under inert conditions were performed using standard Schlenk and glovebox techniques (Unilab MBraun Labmaster Pro). Glassware used for reactions under inert conditions were placed in the oven at 200 °C for minimum 1 hour before use. All alcohols were stored over molecular sieves (4 A°) which have been previously dried over night at $1 \cdot 10^{-2}$ mbar at 250 °C. THF(-d_8) was dried over Na instead of molecular sieves. NMR samples were either prepared under inert conditions or in the fumehood respective to the sensitivity of the product formed.

4.1.2. Technical Equipment and Experimental Design

The experimental work is described with sufficient detail to enable a researcher experienced in chemical synthesis with access to the respective technical equipment to perform the experiments for purposes of reproducing or extending the work.

4.1.3. Solution NMR spectra

^{1}H, ^{11}B, ^{11}B$\{^{1}$H$\}$ and ^{13}C NMR spectra were recorded at 300K on a 400 MHz/52mm Bruker NMR-spectrometer. Chemical shifts are given in parts per million (ppm) relative to trimethylsilane (TMS). They were referenced to the residual solvent signals (CD_3OD: ^{1}H δ_H=3.31, ^{13}C δ_C=49.00; CD_3CN: ^{1}H δ_H=1.94, ^{13}C δ_C=118.26 ; THF-d8: ^{1}H δ_H=1.73, ^{13}C δ_C=67.57; toluene-d8: ^{1}H δ_H=2.09, ^{13}C δ_C=20.40. NMR multiplicities are abbreviated as follows: s = singlet, d = doublet, t = triplet, quartet = q, quintet = qui, sext = sextet, sept = septet, m = multiplet, br = broad signal. All NMR measurements were done in Wilmad quartz NMR tubes (400 MHz, tube diam: 5 mm, L 7 in.).

4.1.4. IR spetra and melting points

IR spetra were recorded on a Bruker Alpha-p ATR FTIR spectrometer and melting points were determined on a Buchi M565-Melting Point system.

4.1.5. Starting Materials

All compounds were purchased from commercial sources and suppliers (Merck KGaA). Methanol, ethanol and isopropylalcohol were dried under molecular sieves (4°A). Sulphuric acid was used from Merck KGaA (97%). Sodiumborohydride was purchased from Merck KGaA. Sodium hydride was purchased from Merck KGaA. Trimethylborate and triisopropylborate that were used as reference were acquired from Merck KGaA.

THF-d_8 was dried over sodium and used only in a drybox. Naphtalene was sublimed under inert conditions prior use.

4.2. Preparation and procedure for trimethylborate

4.2.1. One-pot Methanolysis of $NaBH_4$ using 2,6-Lutidinium Triflate

.

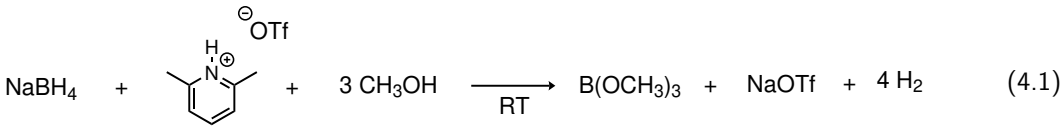

(4.1)

11.7 mg of $NaBH_4$ (0.31 mmol, 1 eq.) and 80.0 mg of 2,6-Lutidinium Triflate (0.31 mmol, 1 eq.) were added under inert conditions into a NMR tube at room temperature. Under standard atmosphere, 0.7 mL of deuterated methanol was added to the NMR tube. Bubble formation was observed for 2 minutes. After 2 minutes, an ^{11}B NMR spectrum was recorded (see Figure 6.1).

^{11}**B NMR** (128 MHz, 300K, CD_3OD): δ 18.47(s).

4.2.2. One-pot Methanolysis of $NaBH_4$ using HCl

.

$$NaBH_4 + 3\,CH_3OH + HCl \xrightarrow[RT]{} B(OCH_3)_3 + NaCl + 4\,H_2 \tag{4.2}$$

250 mg of $NaBH_4$ (6.61 mmol, 1 eq.) was added to a schlenk flask (100 mL) equipped with a magnetic stirring bar. 5.4 mL of 1.25 M HCl in methanol (6.61 mmol HCl, 1 eq.) was transferred to the schlenck by syringe while connected to the nitrogen port of a schlenk line to release the pressure build up from the hydrogen elevation originating from the reaction mixture. Bubble formation was observed during the first 4 minutes after acid addition. The reaction was stirred for 10 minutes at 500 rpm after which an ^{11}B NMR spectrum was recorded in CD_3OD (see Figure 6.2).

^{11}**B NMR** (128 MHz, 300K, CD_3OD): $\delta = 17.89$ (s), $\delta = 13.61$ (br).

4.2.3. One-pot Methanolysis of $NaBH_4$ using H_3PO_3

.

$$3\,NaBH_4 + 12\,CH_3OH + H_3PO_4 \xrightarrow[RT]{} 3\,B(OCH_3)_3 + Na_3PO_4 + 12\,H_2 \tag{4.3}$$

100 mg of $NaBH_4$ (2.64 mmol, 1 eq.) and 86.3 mg of H_3PO_4 (0.88 mmol, 0.333 eq.) were added to a standard 100 mL schlenk flask with a magnetic stirring bar. The schlenk was then transferred to a fumehood while connected to the nitrogen port of a schlenk line to release the pressure build up from the hydrogen elevation originating from the reaction mixture. 10 mL of methanol (247 mmol) was added to the schlenk with $NaBH_4$ and H_3PO_4 while stirring the reaction mixture at 500 rpm. Bubble formation was observed during the first 4 minutes after methanol addition. An ^{11}B NMR spectrum was recorded in CD_3OD (see Figure 6.3).

^{11}**B NMR** (128 MHz, 300K, CD_3OD): $\delta = 14.58$ (s), $\delta =$ -4.09 (br).

4.2.4. One-pot Methanolysis of $NaBH_4$ using H_2SO_4

$$2\,NaBH_4 + 6\,CH_3OH + H_2SO_4 \xrightarrow[RT]{} 2\,B(OCH_3)_3 + Na_2SO_4 + 8\,H_2 \tag{4.4}$$

282 mg of $NaBH_4$ (7.46 mmol, 1eq.) was added to a 50 mL RBF equipped with a magnetic stirring bar under standard atmosphere. 5 mL of methanol (124 mmol) was added while stirring. 0.2 mL of H_2SO_4 (62 mmol, 0.5 eq.) was added dropwise to the solution. Bubble formation was observed during the first 3 minutes after acid addition. NMR spectra were recorded in CD_3OD (see Figure 6.4, Figure 6.5 and Figure 6.6.)

^{11}**B NMR** (128 MHz, 300K, CD_3OD): $\delta = 18.52$ (s).
^{11}**B{**^{1}**H} NMR** (128 MHz, 300K, CD_3OD): $\delta = 18.53$ (s).
^{1}**H NMR** (400 MHz, 300K, CD_3OD): $\delta = 4.90$ (s), $\delta = 3.37$ (s).

4.2.5. Acidification of sodium tetramethoxyborate

.

$$2\,NaB(OCH_3)_4 + H_2SO_4 \xrightarrow[CH_3OH,\,RT]{} B(OCH_3)_3 + Na_2SO_4 + 2\,CH_3OH_3 \tag{4.5}$$

1178 mg of $NaBH_4$ (7.46 mmol, 1eq.) was added to a 100 mL RBF equipped with a magnetic stirring bar was under standard atmosphere, 15 mL of methanol (371 mmol) was added while stirring. 0.2 mL of H_2SO_4 (3.73 mmol, 0.5 eq.) was added dropwise to the solution. NMR spectra were recorded in THF-d_8 (see Figure 6.7, Figure 6.8 and Figure 6.9).

^{11}**B NMR** (128 MHz, 300K, CD_3OD): δ 18.48 (s).
^{11}**B{**^{1}**H} NMR** (128 MHz, 300K, CD_3OD): δ 18.48 (s).
^{1}**H NMR** (400 MHz, 300K, CD_3OD): $\delta = 4.87$ (s), $\delta = 3.36$ (s).

4.3. Preparation and procedure for sodium tetramethoxyborate

4.3.1. Methanolysis of $NaBH_4$ without an acid

.

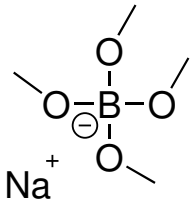

5g of $NaBH_4$ (132 mmol, 1 eq.) and 100 mL of methanol (2.47 mol, 19 eq.) were added in a 250 mL RBF equipped with a magnetic stirring bar and an attached cooler. The reaction was stirred at 500 rpm for 80 minutes at room temperature. The $NaBH_4$ dissolved and bubble formation was observed. NMR spectra were recorded in CD_3OD. The solvent in the RBF was then evaporated under reduced pressure. The remaining salt was heated at 110 ° C for 2 hours under reduced pressure to evaporate any remaining solvent. Product was isolated as a white powder (20.22 g, 128 mmol, 97% yield) (see Figure 6.10, Figure 6.11 and Figure 6.12, Figure 6.13).

^{11}**B NMR** (128 MHz, 300K, CD_3OD): $\delta = 2.97$ (s)
^{13}**C NMR** (101 MHz, 300K, CD_3OD): $\delta = 48.61$ (s)
^{1}**H NMR** (400 MHz, 300K, CD_3OD): $\delta = 3.37$ (s), $\delta = 4.92$ (s)
IR $_{max}$ (cm-1): 2936 (w), 2820 (w), 1457 (vw), 1192 (w), 1083 (s), 1063 (s), 986 (m) and 952 (m)

4.3.2. One-pot Methanolysis of $NaBH_4$ using methanol in IPA

.

$$NaBH_4 + 4\,CH_3OH \xrightarrow[IPA,\,RT]{} NaB(OCH_3)_4 + 4\,H_2 \tag{4.6}$$

23.4 mg of $NaBH_4$ (0.62 mmol, 1 eq.) and IPA (2 mL, 16.2 mmol, 26 eq.) were added in a 50 mL RBF equipped with a magnetic stirring bar after which 0.1 mL of methanol (2.47 mol, 4 eq.) was added dropwise to the reaction mixture. Little bubble formation was observed. NMR spectra were recorded in THF-d_8 (see Figure 6.14 and Figure 6.15).

^{11}**B NMR** (128 MHz, 300K, THF-d_8): $\delta = 3.08$ (s), $\delta =$ -40.98 (qui, J = 80 Hz).
^{11}**B{^{1}H} NMR** (128 MHz, 300K, THF-d_8): $\delta = 3.06$ (s), $\delta =$ -41.42 (s).
^{1}**H NMR** (400 MHz, 300K, THF-d_8): $\delta =$ -0.16 (q, J = 81 Hz, 6H), $\delta = 1.05$ (d, J = 6.70 Hz, 12H), $\delta =$ 3.24 (s), $\delta = 3.85$ (hept, J = 6.16 Hz, 1H), $\delta = 5.04$ (s).

4.3.3. One-pot Methanolysis of $NaBH_4$ with using methanol in THF

.

$$NaBH_4 + 4\,CH_3OH \xrightarrow[THF,\,RT]{} NaB(OCH_3)_4 + 4\,H_2 \tag{4.7}$$

23.4 mg of $NaBH_4$ (0.62 mmol, 1 eq.) and 2 mL of THF-d_8 (16.2 mmol, 26 eq.) were added in a 50 mL RBF with a magnetic stirring bar after which 0.1 mL of methanol (2.47 mol, 4 eq.) was added dropwise to the reaction mixture. Little bubble formation was observed. NMR spectra were recorded (see Figure 6.16, Figure 6.17 and Figure 6.18).

^{11}**B NMR** (128 MHz, 300K, THF-d_8): δ 3.05 (s), δ -43.44 (qui, J = 81 Hz).
^{11}**B{^{1}H} NMR** (128 MHz, 300K, THF-d_8): δ 3.04 (s), δ -43.42 (s).
^{1}**H NMR** (400 MHz, 300K, THF-d_8): -0.43 (q, J = 81 Hz, 4H). δ 1.76 (s), δ 3.13 (s), δ 3.31 (s), δ 3.38 (s), δ 3.62 (s).

4.3.4. Stabilizer experiments with KOH and NaOMe

.
10 mL of methanol was added to 8 RBFs (50 mL) equipped with magnetic stirring bars under standard atmosphere. KOH was added to 4 RBFs and NaOMe was added to the other 4 RBFs according to Table 4.1 to acquire solutions with 2, 5, 7 and 10 molpercent of stabilizer, respectively. 100 mg of $NaBH_4$ (2.64 mmol, 1 eq.) was added to all reaction mixtures. NMR spectra were recorded in CD_3OD after 5 hours and after 24 hours.

Table 4.1: Amount of stabilizer added to methanol solutions.

Molpercent (%)	n (mmol)	mass of NaOMe (mg)	mass of KOH (mg)
2	5.09	275	204
5	13.14	710	526
7	18.78	1015	751
10	27.73	1498	1109

4.4. Preparation and procedure for triisopropylborate

4.4.1. One-pot alcoholysis of $NaBH_4$ with IPA using H_2SO_4

.

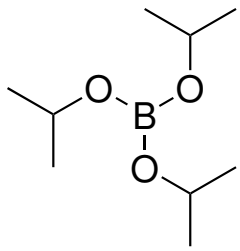

212 mg of $NaBH_4$ (5.6 mmol, 1.0 eq.) and 10 mL of IPA (131 mmol, 23 eq.) were added in a 100 mL three-neck RBF with attached cooler and equipped with a stirring bar. 0.15 mL of H_2SO_4 (2.8 mmol, 0.5 eq.) was added to the reaction mixture over 20 minutes at 50 °C with an Aladdin AL-4000 double syringe pump. The reaction mixture was evaporated under reduced pressure to remove the precipitate. The reaction mixture was captured in a cooling trap. The triisopropylborate was separated from the IPA through distillation at 230 °C for 2 hours in a vigreux column after which NMR spectra were recorded (see Figure 6.19, Figure 6.20 and Figure 6.21). A yield was obtained of 14 mL (46 %).

^{11}**B NMR** (128 MHz, 300K, Tol-d_8): $\delta = 17.72$ (s).
^{13}**C NMR** (101 MHz, 300K, Tol-d_8): $\delta = 24.15$ (s), $\delta = 64.69$ (s).
^{1}**H NMR** (400 MHz, 300K, Tol-d_8): $\delta = 1.10$ (d, J = 6.3 Hz, 18H), $\delta = 4.43$ (sext, J = 6.4 Hz, 3H).*
*This spectrum was only acquired a single time. Follow-up experiments showed signals that correspond to the presence of IPA: $\delta = 1.06$ (d, J = 5.8 Hz, 6H) $\delta = 3.82$ (sext, J = 6.3 Hz, 1H)

4.4.2. Conversion reactions to triisopropylborate

.

$$2\,NaBH_4 + H_2SO_4 + 6\,IPA \xrightarrow[RT]{} 2\,B(O\mathit{i}Pr)_3 + Na_2SO_4 + 8\,H_2 \tag{4.8}$$

5g of $NaBH_4$ (132 mmol, 1.0 equiv) and 61 mL of IPA (792 mmol, 6.0 eq.) were each added in 11 100 mL three-neck RBFs equipped with stirring bars and with attached cooler. 3.54 mL of H_2SO_4 (66 mmol, 0.5 eq.) was added to the reaction mixture with an Aladdin AL-4000 double syringe pump. The acid addition time was 20 minutes in 6 RBFs at room temperature, 30 °C, 40 °C, 50°C, 60 °C and 70 °C, respectively. 3.54 mL of H_2SO_4 (66 mmol, 0.5 eq.) was added over 30 minutes in 3 RBFs at room temperature, 30 °C, 40 °C, respectively. Lastly, 3.54 mL of H_2SO_4 (66 mmol, 0.5 eq.) was added over 35 minutes in 2 RBFs at room temperature and at 30 °C, respectively. Severe salt formation was observed in all RBFs. All reaction mixtures were evaporated under reduced pressure to remove the precipitate and were captured in cooling

traps. NMR spectra were recorded.

^{11}**B NMR** (128 MHz, 300K, Tol-d_8): δ = 17.72 (s), δ = -41.35 (qui, J = 80 Hz)*
* For reaction samples with the following parameters (Time (min)|Temp.): (20, RT), (30, RT), (20, 30 °C), (30, 30 °C), (20, 40 °C).

4.5. Preparation and procedure for $NaBH_4$ through the Brown-Schlesinger process

$$B(O\textit{i}Pr)_3 + 4\,NaH \xrightarrow[250\,^\circ C]{} NaBH_4 + 3\,NaO\textit{i}Pr \tag{4.9}$$

2 mL of mineral oil was added to a Kemtech glass Schlenk storage tube with high vacuum valve (25 mL) equipped with a stirring bar under inert conditions. 46 mg of NaH (1.91 mmol, 4.4 eq.) was added to the mineral oil together with 0.1 mL of $B(O\textit{i}Pr)_3$ (0.433 mol, 1eq.). The reaction mixture was then heated to 230 °C for 5 hours while stirring. D_2O with 40% NaOD (4 mL) was added to the reaction mixture for extraction. The glass tube was shaken three time with intermediate pressure release to prevent potential pressure build up. An ^{11}B NMR spectrum was recorded (see Figure 6.22).

^{11}**B NMR** (128 MHz, 300K, Tol-d_8): δ = 1.51 (s), δ = -41.84 (qui, J = 80 Hz, 4H).

4.6. Borohydride formation through radical activation

4.6.1. Borohydride formation with Sodium naphthalene and $B(OiPr)_3$ in mineral oil.

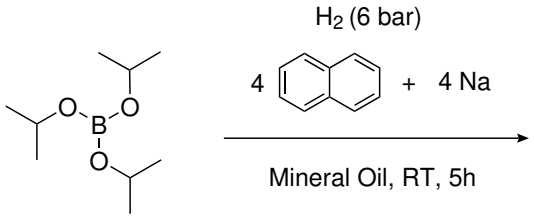

(4.10)

A glass reactor "tinyclave" (Büchiglasuster) (25 mL) equipped with a magnetic stirring bar was brought under inert conditions (see Figure 6.39). 3 mL of mineral oil was put in the glass reactor, after which 20g of Na (0.87 mmol, 4 eq.) and 111 mg of naphthalene (0.87 mmol, 4 eq.) was added to the mineral oil. The solution was then stirred. 0.05 mL of $B(O\textit{i}Pr)_3$ (0.22 mmol, 1 eq.) was added. The tinyclave was subjected to hydrogen pressure (6 bar). The solution was stirred for 5 hours at room temperature after which the hydrogen pressure was released and the tinyclave was dissembled. D_2O with 40% NaOD (4 mL) was added to the reaction mixture for extraction. The glass reactor was shaken three time with intermediate pressure release steps to prevent potential pressure build up. An ^{11}B NMR spectrum was recorded.

^{11}**B NMR** (128 MHz, Toluene-d_8): δ = 17.65 (s).

4.6.2. Borohydride formation with sodium naphthalene, hydrogen and B(OiPr)$_3$ in THF-d$_8$

4.6.2.1. 4 equivalents of sodium naphthalene, hydrogen and B(OiPr)$_3$ in THF-d$_8$

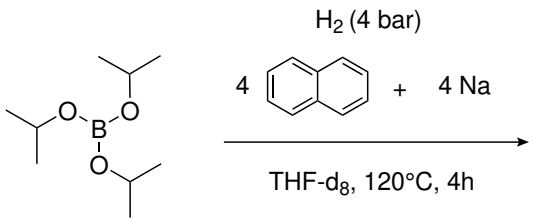

(4.11)

3 mL of THF-d$_8$ was added to a glass reactor "tinyclave" (Büchiglasuster) (25 mL) equipped with a magnetic stirring bar under inert conditions. 20 mg of Na (0.87 mmol, 4 eq.) and 111 mg of naphthalene (0.87 mmol, 4 eq.) was added to the THF-d$_8$. The solution was then stirred. 0.05 mL of B(O*i*Pr)$_3$ (0.22 mmol, 1 eq.) was added to the reaction mixture. The tinyclave was subjected to hydrogen pressure (4 bar). The solution was stirred for 4 hours at 120 °C after which the hydrogen pressure was released and the tinyclave was dissembled. A NMR spectra was recorded (see Figure 6.24).

^{11}**B NMR** (128 MHz, Toluene-d$_8$): δ = -28.73 (d, J = 81 Hz), δ = -19.00 (t, J = 80 Hz), δ = -16.88 (t, J = 76 Hz), δ = -16.30 (s), δ = -16.00 (s), δ = -15.74 (s), δ = -15.42 (s), δ = -15.12 (s), δ = -14.83 (s), δ = -10.04 (d, J = 71 Hz), δ = -7.64 (d, J = 63 Hz), δ = 5.27 (d, J = 121 Hz).

4.6.2.2. 8 equivalents of sodium naphthalene, hydrogen and B(OiPr)$_3$ in THF-d$_8$

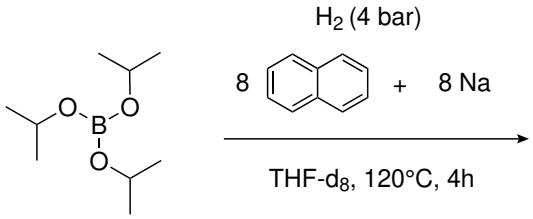

(4.12)

3 mL of THF-d$_8$ was added to a glass reactor "tinyclave" (Büchiglasuster) (25 mL) equipped with a magnetic stirring bar under inert conditions. 40 mg of Na (1.73 mmol, 8 eq.) and 222 mg of naphthalene (1.73 mmol, 8 eq.) was added to the THF-d$_8$. The solution was then stirred. 0.05 mL of B(O*i*Pr)$_3$ (0.22 mmol, 1 eq.) was added to the reaction mixture. The tinyclave was subjected to hydrogen pressure (4 bar). The solution was stirred for 4 hours at 120 °C after which the hydrogen pressure was released and the tinyclave was dissembled. NMR spectra were recorded (see Figure 6.25 and Figure 6.26).

^{11}**B NMR** (128 MHz, THF-d$_8$): δ = -14.05 (d, J = 67 Hz) , δ = -15.44 (d, J = 73 Hz), δ = -16.90 (t, J = 73 Hz), δ = -19.03 (t, J = 79 Hz), δ = -29.04 (q, J = 80 Hz)
^{11}**B{^{1}H} NMR**: (128 MHz, 300K, THF-d$_8$): δ = -13.63 (s), δ = -15.35 (s), δ = -16.83 (s), δ = -18.96 (s), δ = -29.01 (s)

4.6.2.3. 16 equivalents of sodium naphthalene, hydrogen and B(OiPr)$_3$ in THF-d$_8$

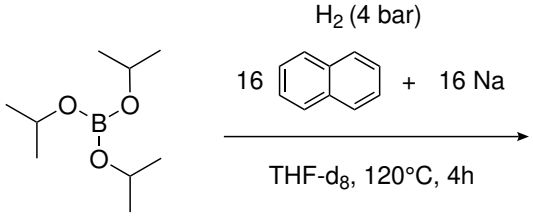

(4.13)

3 mL of THF-d_8 was added to a glass reactor "tinyclave" (Büchiglasuster) (25 mL) equipped with a magnetic stirring bar under inert conditions. 80 mg of Na (3.46 mmol, 16 eq.) and 444 mg of naphthalene (3.46 mmol, 16 eq.) was added to the THF-d_8. The solution was then stirred. 0.05 mL of B(O*i*Pr)$_3$ (0.22 mmol, 1 eq.) was added. The tinyclave was subjected to hydrogen pressure (4 bar). The solution was stirred for 4 hours at 120 °C after which the hydrogen pressure was released and the tinyclave was dissembled. NMR spectra were recorded (see Figure 6.27 and Figure 6.28).

^{11}B NMR (128 MHz, THF-d_8): δ = -13.43 (d, J = 73 Hz), δ = -15.44 (d, J = 73 Hz), δ = -16.90 (t, J = 73 Hz), δ = -19.03 (t, 81 Hz), δ = -29.11 (q, J = 81 Hz).
^{11}B{^{1}H} NMR (128 MHz, THF-d_8): δ = -13.72 (s), δ = -15.43 (s), δ = -16.90 (s), δ = -19.03 (s), δ = -29.11 (s).

4.6.3. Borohydride formation with of sodium biphenyl, hydrogen and B(OiPr)$_3$ in THF-d_8

4.6.3.1. 4 equivalents of sodium biphenyl, hydrogen and B(OiPr)$_3$ in THF-d_8

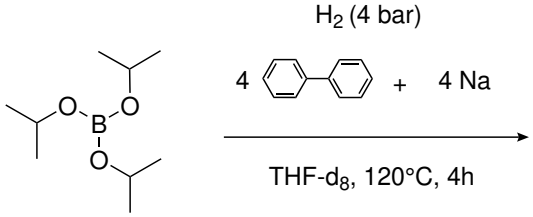

(4.14)

3 mL of THF-d_8 was added to a glass reactor "tinyclave" (Büchiglasuster) (25 mL) equipped with a magnetic stirring bar under inert conditions. 20 mg of Na (0.87 mmol, 4 eq.) and 133 mg of biphenyl (0.87 mmol, 4 eq.) was added to the THF-d_8. The solution was then stirred. 0.05 mL of B(O*i*Pr)$_3$ (0.22 mmol, 1 eq.) was added. The tinyclave was subjected to hydrogen pressure (4 bar). The solution was stirred for 4 hours at 120 °C after which the hydrogen pressure was released and the tinyclave was dissembled. NMR spectra were recorded (see Figure 6.29 and Figure 6.30).

^{11}B NMR (128 MHz, THF-d_8): δ = 5.82 (d, J = 126 Hz), δ = 2.67 (s)
^{11}B{^{1}H} NMR (128 MHz, THF-d_8): δ = 5.86 (s), δ = 2.67 (s)

4.6.3.2. 8 equivalents of sodium biphenyl, hydrogen and B(OiPr)$_3$ in THF-d_8

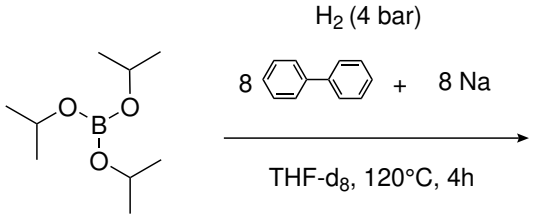

(4.15)

3 mL of THF-d_8 was added to a glass reactor "tinyclave" (Büchiglasuster) (25 mL) equipped with a magnetic stirring bar under inert conditions. 40 mg of Na (1.73 mmol, 8 eq.) and 266 mg of biphenyl (1.73 mmol, 8 eq.) was added to the THF-d_8. The solution was then stirred. 0.05 mL of B(O*i*Pr)$_3$ (0.22 mmol, 1 eq.) was added. The tinyclave was subjected to hydrogen pressure (4 bar). The solution was stirred for 4 hours at 120 °C after which the hydrogen pressure was released and the tinyclave was dissembled. NMR spectra were recorded (see Figure 6.31 and Figure 6.32).

^{11}B NMR (128 MHz, THF-d_8): δ = 5.70 (d , J = 122 Hz), δ = -16.07 (t, J = 73 Hz)
^{11}B{^{1}H} NMR (128 MHz, THF-d_8): δ = 5.66 (s), δ = 16.04 (s)

4.6.3.3. 16 equivalents of sodium biphenyl, hydrogen and B(OiPr)$_3$ in THF-d$_8$

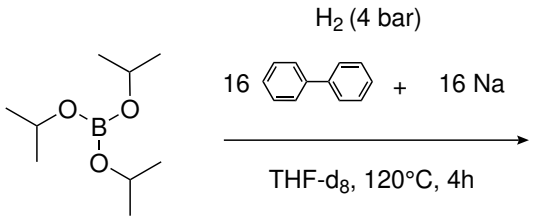

(4.16)

3 mL of THF-d$_8$ was added to a glass reactor "tinyclave" (Büchiglasuster) (25 mL) equipped with a magnetic stirring bar under inert conditions. 80 mg of Na (3.46 mmol, 16 eq.) and 522 mg of biphenyl (3.46 mmol, 16 eq.) was added to the THF-d$_8$. The solution was then stirred. 0.05 mL of B(O*i*Pr)$_3$ (0.22 mmol, 1 eq.) was added. The tinyclave was subjected to hydrogen pressure (4 bar). The solution was stirred for 4 hours at 120 °C after which the hydrogen pressure was released and the tinyclave was dissembled. NMR spectra were recorded (see Figure 6.33 and Figure 6.34).

^{11}**B NMR** (128 MHz, THF-d$_8$): δ = 5.71 (d , J = 123 Hz)
^{11}**B{^{1}H} NMR** (128 MHz, THF-d$_8$): δ = 5.65 (s)

4.7. Borohydride formation with Sodium naphthalene and mono alkoxydiethylborane in THF-d$_8$

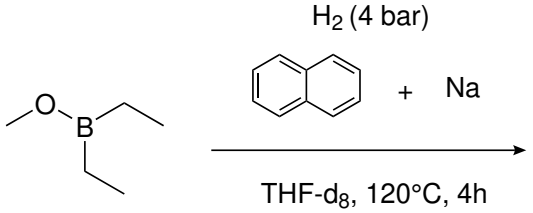

(4.17)

3 mL of THF-d$_8$ was added to a glass reactor "tinyclave" (Büchiglasuster) (25 mL) equipped with a magnetic stirring bar under inert conditions. 17.5 mg of Na (0.76 mmol, 1 eq.) and 98 mg of naphtalene (0.76 mmol, 1 eq.) was added to the THF-d$_8$. The solution was then stirred. 0.1 mL of monoalkoxydiethylmonomethoxyborate (0.76 mmol, 1 eq.) was added to the reaction mixture. The tinyclave was subjected to hydrogen pressure (4 bar). The solution was stirred for 4 hours at 120 °C after which the hydrogen pressure was released and the tinyclave was dissembled. NMR spectra were recorded (see Figure 6.35 and Figure 6.36).

^{11}**B NMR** (128 MHz, THF-d$_8$): δ = 6.58 (s), δ = -11.50 (d, J = 72 Hz), δ = -14.23 (d, J = 73 Hz), δ = -17.53 (t, J = 72 Hz)
^{11}**B{^{1}H} NMR** (128 MHz, THF-d$_8$): δ = 6.56 (s), δ = -11.51 (s), δ = -14.24 (s), δ = -17.54 (s)

4.7.1. Brown method for borohydride synthesis

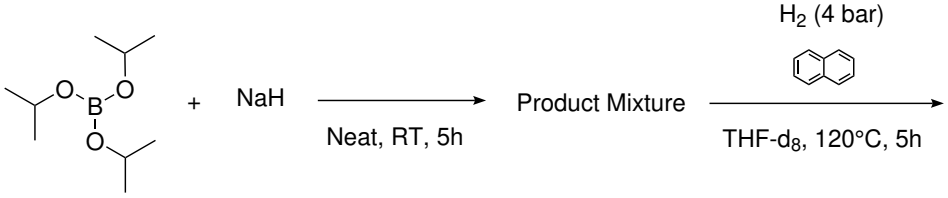

(4.18)

2.11 mL of B(O*i*Pr)$_3$ (9.16 mmol, 1.1 equivalents) was added to 200 mg of NaH (8.33 mmol, 1 eq.) in a schlenck flask under inert c onditions. The reaction mixture was stirred for 5 hours at room t emperature. The reaction mixture was then transferred to a glass reactor "tinyclave" (Büchiglasuster) (25 mL) with a magnetic

stirring bar. 3 mL of THF-d_8 was added to the reaction mixture after which 1.07 g of naphtalene (8.35 mmol, 1 eq.) was added to the reaction mixture. The solution was then stirred. The tinyclave was subjected to hydrogen pressure (4 bar). The solution was stirred for 5 hours at 120 °C after which the hydrogen pressure was released and the tinyclave was dissembled. NMR spectra were recorded (see Figure 6.37 and Figure 6.38).

^{11}**B NMR** (128 MHz, THF-d_8): δ = 17.66 (s), δ = 6.36 (d, J = 117 Hz), δ = 2.82 (s), δ = 2.15 (s), δ -42.37 (qui, J = 82 Hz)
^{11}**B{^{1}H} NMR** (128 MHz, THF-d_8): δ = 17.64 (s), δ = 5.89 (s), δ = 2.82 (s), δ = -42.37 (s)

4.7.2. Heat transfer experiments

$NaBH_4$ (according to Table 4.2) and IPA (according to Table 4.2) were respectively added to 3 three-neck RBFs (250 mL, 500 mL and 1000mL) equipped with stirring bars. A cooler was attached to each RBF together with a nitrogen inlet at the the top of the cooler to prevent ignition of the elevated hydrogen emerging from the reaction mixture. A Chauvin Arnoux C.A. 10101 thermocouple was attached to the RBFs. H_2SO_4 was added to the reaction mixture with an Aladdin AL-4000 double syringe pump to each RBF (according to Table 4.3). The temperature increase of the reaction mixture was then monitored during a period of 30 minutes.

Table 4.2: Amounts of starting material for the test reactions needed for the heat transfer limitation model. All reactions were performed at room temperature under atmospheric pressure. the standard reaction time was 20 minutes.

Reaction: $2\,NaBH_4 + H_2SO_4 + 6\,IPA \longrightarrow B(OiPr)_3 + Na_2SO_4 + 8\,H_2$			
Three-neck RBF volume (mL)	**$NaBH_4$ (gr)**	**IPA (mL)**	**H_2SO_4 (mL)**
250	10	121	7.1
500	15	182	10.6
1000	20	242	14.2

Table 4.3: Acid addition rates of sulfuric acid corresponding to the amount of reacting $NaBH_4$.

$NaBH_4$ (grams)	**$r_{H_2SO_4,addition}$ (mL/s)**
10	0.00592
15	0.00883
20	0.01184

5 Conclusion

To date, there is a lack of commercially viable methods for using $NaBH_4$ as a circular hydrogen carrier for energy storage applications. The primary objective of this thesis was to minimize the energy requirements for circular hydrogen storage in $NaBH_4$ and establish an efficient, economically viable, scalable, and sustainable reaction pathway for this purpose. The research focused on improving the hydrogen release through alcoholysis using methanol and IPA, along with stoichiometric amounts of an acid to synthesize $B(OCH_3)_3$ and $B(OiPr)_3$, respectively. Additionally, this research focused on realizing an improved method for the regeneration of spent fuel to $NaBH_4$. Efforts were made to reduce the energy intensity of $NaBH_4$ synthesis through novel reaction pathways.

5.1. Hydrogen release through selective formation of $B(OCH_3)_3$

Hydrogen release and synthesis of $B(OCH_3)_3$ was successfully accomplished through a one-pot reaction pathway. Full conversion to $B(OCH_3)_3$ was achieved by adding stoichiometric amounts of LuHOTf in methanol to $NaBH_4$ as indicated by ^{11}B NMR. Similar results were obtained with stoichiometric amounts of H_2SO_4, which is a more cost-effective proton donor compared to LuHOTf. The hydrogen release of methanolysis of $NaBH_4$ to $B(OCH_3)_3$ was also performed in a two step reaction by first subjecting $NaBH_4$ to methanol to form $NaB(OCH_3)_4$ and release 4 equivalents of hydrogen, after which 0.5 equivalent of H_2SO_4 was added to form $B(OCH_3)_3$. A two step reaction does increase reaction steps, but could provide more control over the hydrogen release. However, alternative solutions for the hydrogen release through alcoholysis were explored due to the azeotropic nature of methanol with $B(OCH_3)_3$ and the inability to stabilize a pre-mixed solution of methanol with $NaBH_4$. According to Brown-Schlesinger, the reaction between NaH and $NaB(OCH_3)_4$ is an option to regenerate $NaBH_4$ under similar conditions instead of using $B(OCH_3)_3$ [18].

5.2. Hydrogen release through selective formation of $B(OiPr)_3$

The retainment of stable $NaBH_4$ in IPA was observed over a period of 5 days, enabling a premixed solution of $NaBH_4$ and IPA. By gradually adding stoichiometric amounts of H_2SO_4 to this pre-mixed solution of excess IPA and $NaBH_4$ using a syringe pump, full conversion to $B(iOPr)_3$ was achieved after 35 minutes at room temperature and 20 minutes at 50 °C, as indicated by ^{11}B NMR. It was determined that the minimum addition time was 20 minutes on 212 mg $NaBH_4$ scale for H_2SO_4 to avoid the formation of intermediate compounds. A minimum of 6 equivalents of IPA was required from refraining the reaction mixture of becoming too viscous due to Na_2SO_4 formation. Furthermore, the significant difference in boiling points between IPA and the respective alkylborate $B(iOPr)_3$ was assumed to facilitate easier separation relative to the separation of a $B(OCH_3)_3$/methanol mixture. A single experiment in separating $B(OiPr)_3$ resulted in a 46% yield. However, follow up experiments showed that IPA was still present in the distillate in a IPA/$B(OiPr)_3$ molar ratio of 1:10 according to ^{1}NMR. Nonetheless, separation of $B(OiPr)_3$ from IPA still poses to be a less energy intensive process relative to the separation of $B(OCH_3)_3$ and methanol, which attains a $B(OCH_3)_3$/methanol molar ratio of 1:1.2.

5.3. $NaBH_4$ regeneration through the Brown-Schlesinger process

The Brown-Schlesinger process, which is widely used for industrial-scale $NaBH_4$ synthesis, was used to convert $B(OCH_3)_3$ to $NaBH_4$. By adopting these reaction conditions to the use of $B(i OPr)_3$ as a reagent instead of $B(OCH_3)_3$, resulting from the alcoholysis of $NaBH_4$ with IPA, full conversion to $NaBH_4$ was observed according to ^{11}B NMR. Extraction of $NaBH_4$ on lab-scale was experienced to be challenging due to lack of formed polar/apolar boundary layers in the solution. Thus, no yield could be determined within the scope of this thesis.

5.4. Borohydride bond activation through a boron radical anion pathway

Due to the high energy requirements associated with the Brown-Schlesinger process, which makes use of 4 equivalents of NaH and operates at high temperatures, alternative routes for $NaBH_4$ synthesis were investigated in order to improve the energy efficiency of the circular hydrogen storage process using $NaBH_4$. The emphasis was directed towards reducing the reaction temperature for $NaBH_4$ synthesis through the use of radical activation, which facilitates homolytic hydrogen cleavage that would initiate the formation of B-H bonds.

4 equivalents of sodium and naphthalene were mixed in THF, after which 1 equivalent of $B(OiPr)_3$ was added. The reaction was heated for 4 hours at 120 °C under 4 bar of hydrogen pressure. Signals that correspond to B-H, B-H_2 and B-H_3 compounds were synthesized according to ^{11}B NMR. Notably, no sodium borohydride compound was synthesized. Additional side products were observed, suggesting hydroboration to form naphthalene adducts with boron. No variations in reaction products were witnessed upon changing reaction temperature (ranging from 80 °C to 160 °C), reaction time (ranging from 3 to 12 hours) or adjusting the hydrogen pressure (from 3 to 6 bar). To mitigate potential naphthalene adduct formation, biphenyl was employed as the initial radical source in the presence of sodium. Signals corresponding to B-H formation and $NaB(OiPr)_4$ formation were observed. Upon increasing the amount of hydrides in solution to 8 equivalents, a signal occured corresponding to the formation of a BH_2 compound. Selective formation of a B-H compound was achieved by adding 16 equivalents of sodium and biphenyl to one equivalent of $B(OiPr)_3$ according to ^{11}B NMR.

Reactions were also performed with 8 and 16 equivalents of naphthalene and sodium to see whether di- or trisubstituted borohydrides could be formed selectively when exposed to an excess of hydrides in solution. However, no BH compound is formed upon increasing the amount of hydrides in solution to 8 equivalents relative to $B(OiPr)_3$ according to ^{11}B NMR. In addition, stronger signals of BH_2 and BH_3 compound were perceived in comparison to the reaction with only 4 equivalents of hydrides. Finally, no signal that potentially is attributed to the hydroboration of the boron and the naphtalene was observed. However, no difference in product formation was found when performing a reaction using 16 equivalents of naphtalene and sodium relative to the reaction with 8 equivalents of hydrides in solution.

In order to drive the reaction to a higher selectivity with regards to the amount of formed products, mono alkoxy substituted diethylmonomethoxyborate was utilized as reagent as it can only yield a quartenary salt, monohydride and dihydride boron compounds due to its fixated boron-carbon bond, which might drive the reaction to a more selective product formation. Autoclave reactions in THF were performed with 4 equivalents of naphthalene and sodium. The reaction showed a higher selectivity relative to the trialkylborate as reagent, but did not show selective formation of a single borohydride product. The same reaction was done with a reaction time of 12 hours to see whether a longer reaction time could drive the reaction to a more selective product formation. However, the reaction mixture degraded over time and did not show distinctive borohydride peaks after 12 hours.

Finally, a method was adopted from other members of the Slootweg research group where a neat reaction with $B(OCH_3)_3$ and NaH at room temperature showed a relative formation of 30% of a BH_3 compound according to ^{11}B NMR. These reaction conditions were adopted to the latter system with $B(OiPr)_3$ as a reagent. The reaction product was then put in an autoclave and subjected to 4 equivalents of sodium and naphthalene under 4 bar of hydrogen pressure. No signal was observed that correspond to a BH_3 compound

after addition of 4 equivalents of hydrides, which indicates that the latter reaction conditions dissociates the initially formed BH_3. A signal that corresponds to a BH_4 compound was observed, which was the result of an increase in temperature during the work up to evaporate any remaining $B(OiPr)_3$ still left in the product mixture, resulting in BH_4 formation with any remaining NaH in the reaction mixture through the Brown-Schlesinger process.

5.5. Heat Transfer Limitation Model

The potential limitations of heat transfer were investigated with regards to the hydrogen release process in order to comprehensively evaluate the energy intensity of the novel circular hydrogen storage pathway using $NaBH_4$ as a hydrogen carrier. As the hydrogen release through selective alkylborate formation is an exothermic process characterized by a substantial enthalpy change, a heat transfer limitation model was developed to analyze the corresponding heat transfer phenomena.

An overall energy balance of the system was derived, which entailed the heat production from the reaction mixture and the heat flux from the reaction mixture through the reactor wall into the flowing cooling water within the cooling mantle. The heat production in the reaction mixture was determined through the heat of reaction and the reaction rate which in turn was determined through the addition rate of H_2SO_4. The heat flux through the reactor wall was determined through Newton's law of cooling through an interface from which the total heat transfer coefficient (U_{tot}) and the temperature of stagnant cooling water (T_c) was determined. Subsequently, real-time temperature increment experiments were performed for the alcoholysis of 10, 15 and 20 grams of $NaBH_4$ with IPA and stochiometric amounts of H_2SO_4. The exothermic behavior of the reaction remained consistent when the reaction parameters were proportionally scaled. The real-time temperature data was processed using a power regression algorithm to derive heat transfer mechanisms through convection and conduction in a single formula. From this, the mass flow rate of the cooling water was predicted through a microbalance of the cooling mantle through a single pipe heat exchanger model. A minimum scale up factor of 580 was derived from the minimum mass flow rate to reach turbulent flow regime in the cooling mantle, which allows for plug flow behavior, thereby enabling the validity of the heat transfer model. Finally, a macro energy balance of the cooling mantle was derived to predict the outflowing temperature of the cooling water, from which the temperature of the cooled reaction mixture was derived over time.

From this analysis, it is deducible that under the existing operational parameters of the heat exchanger, the conveyance of thermal energy from reactor wall to the heat exchanger, and subsequently out of the system occurs without any heat transfer constraints as long as PFR conditions are met. Consequently, the models applicability remains confined to a specific turnover number of 12 kg $NaBH_4$/batch reaction of 20 minutes, requiring 812 L of cooling water, which can be easily recycled. In view of these insights, the current envisioned hydrogen release process does not pose a problem for the reactor design upon up scaling with regards to heat transfer limitations.

5.6. Techno-Economic Analysis

An economic analysis on the envisioned process described in the latter was required in order to validate the research question at hand. First, a process flow diagram was derived for the alcoholysis reaction pathway for both the hydrogen release process, as well as for the $NaBH_4$ regeneration. The regeneration of $NaBH_4$ was based on the Brown-Schlesinger process as no borohydride formation from H_2 activation through boron radical anions was realized. The process flow diagram of the hydrogen release process and the applied $NaBH_4$ regeneration process were then used to predict an overall energy balance, which enabled the comparison between the hydrolysis pathway and the alcoholysis pathway with regards to energy consumption to access the merit in the use of the alcoholysis pathway instead of the hydrolysis pathway. It was observed that the energy requirement of the hydrolysis pathway being 360.2 kWh/kg of H_2, was decreased to 253.1 kWh/kg of H_2, required by the alcoholysis system. From this energy balance, a monetary assessment can be deduced that clarifies that the alcoholysis system shows a merit with regards to energy consumption, but remains too energy intensive for competitive market pricing.

5.7. Research Assessment

Upon answering the research question at hand: **"How can the recyclability of the spent fuel from the hydrogen release via the alcoholysis of $NaBH_4$ and the regeneration of 'spent fuel' be optimised to minimize the energy intensity of the use of $NaBH_4$ as a circular hydrogen carrier?"**, it can be concluded that the envisioned system proposed in this thesis provides a less energy intensive circular reaction pathway compared to pre-existing methodologies. Specifically, It was observed that the energy requirement of the hydrolysis pathway being 360.2 kWh/kg of H_2, was decreased to 253.1 kWh/kg of H_2, required by the proposed alcoholysis system. This was realised through the optimization of multiple reaction steps.

First of all, the release of hydrogen from $NaBH_4$ has been optimized through the development of a one-pot synthesis method for hydrogen release, along with the selective synthesis of a spent fuel that can be regenerated to $NaBH_4$ through a single reaction. This approach reduces the number of reaction steps and reduces energy intensity associated with conventional hydrogen release methods from $NaBH_4$. Secondly, successful regeneration of the spent fuel was achieved by adopting a conventional $NaBH_4$ synthesis methodology within a novel reaction system, closing the loop for circular hydrogen storage in $NaBH_4$ through the proposed system. Furthermore, a basis was established for optimizing $NaBH_4$ regeneration through radical chemistry, which successfully synthesized BH, BH_2, and BH_3 compounds, with selective formation of a BH compound upon an excess of hydrides in the reaction mixture according to ^{11}B NMR. In addition, the scalability of the proposed hydrogen release method was investigated, considering the limitations imposed by heat transfer. Finally, a monetary assessment was developed to compare the proposed circular reaction pathway to the circular hydrolysis pathway. As part of this general strategy, some experimental details of this thesis contribute to an initial patent application (NL Patent No. P192550NL00, 2023-04-11) by H_2 Fuel Systems B.V. with F.Buß, G.B. de Jong and J.C. Slootweg as inventors.

Thus, it can be concluded that that the conventional circular hydrogen storage methodology has been revised and improved through the proposed envisioned system presented in this thesis, providing a groundwork for further research to ultimately achieve commercial-scale circular hydrogen storage through the use $NaBH_4$ as a circular hydrogen carrier.

5.8. Recommendations

This thesis introduces a comprehensive framework for a circular approach to hydrogen storage through the use of $NaBH_4$. Nevertheless, further studies are required to elaborate on the proposed reaction pathways in order to fully comprehend the envisioned system. An extension of this research paves the way for potential realization of a consecutive system, which interlinks the various reaction stages on lab scale. Moreover, a more profound analysis of reaction kinetics and chemical behavior across these reaction stages is required. Both these extensions collectively create a potential realization for the implementation of scale-up processes. From the perspective of the author, there exists a need for further research across the independent reaction stages, which can be categorized into the hydrogen release stage, the $NaBH_4$ regeneration stage, and the heat transfer model.

Regarding the hydrogen release stage, it is of particular interest to investigate the feasibility of hydrogen release via alternative alcoholysis routes using different alcohols based on the findings for methanol and IPA within this thesis. For instance, exploring the alcoholysis system with ethanol or n-butanol may yield distinct advantages concerning process implementation or the circumvention of side-product and intermediate compound formation. An example of such is the circumvention of intermediate compound formation upon rapid acid addition during hydrogen release, thereby increasing the reaction turnover number. Furthermore, the methanolysis of $NaBH_4$ also requires more extensive research as regenerating $NaBH_4$ from $NaB(OCH_3)_4$ could potentially offer a viable alternate regeneration pathway, as this specific reaction is known in literature [18], and has also expanded to $NaAlH_4$, which reacts with $NaB(OCH_3)_4$ yielding $NaBH_4$ [76]. This requires a deeper understanding of the methanol system and its concerning product formation. Therefore, a detailed patent and literature analysis is needed, concomitant with the freedom to operate analysis as the current Brown-Schlesinger process using $Na(OCH_3)_4$ and $B(OCH_3)_3$ is literature known and can therefore not be patented without substantial improvement the current system. Furthermore, the assumed hydrogen

gas produced has yet to be substantively examined. A better understanding of the hydrogen gas released is necessary, which requires further research in gas analytics.

The described system for the regeneration of $NaBH_4$ through H_2 activation via boron radical anions has been only briefly addressed due to the limited time and the scope of this work. Isolating and examining various BH compounds from the described system can bring valuable insights into the reaction kinetics and the chemical behavior of the proposed system. Therefore, further research should be conducted towards the selective formation of BH compounds, preferably the selective formation of BH_3 compounds. This can be achieved by for example further changing the aromatic compound that initially interacts with sodium. Such alterations in the proposed system could also potentially facilitate the overcoming of the energy threshold that corresponds to a fourth hydride transfer, potentially resulting in $NaBH_4$ synthesis under milder reaction conditions relative to the Brown-Schlesinger process. A fourth hydride transfer would not necessarily have to be done through a synthetic chemical route. Other fields of research such a the potentiality for an electrochemical pathway should also be explored and is already under current investigation in the Slootweg research group.

The heat transfer model requires further exploration with the emphasis on eliminating assumptions, such as the assumption of a cylindrical reactor shape, the absence of internal heat transfer, and uniform heat production within the reaction mixture. In addition, note that the heat of solvation is not accounted for within the heat transfer model, particularly with respect to sulfuric acid in alcohols, which is substantial in comparison to that of the heat of reaction [124]. Consequently, The increase in enthalpy change due to the latter exerts a substantial influence on heat transfer dynamics, thereby requiring higher cooling demands in reality. Furthermore, the integration of computational fluid dynamics could predict local Reynolds numbers, flow regimes, and local concentration profiles. This could eliminate the assumption of ideal mixing, thereby making the heat transfer model more realistic.

6 Appendix

6.1. Appendix A - NMR Sepctra

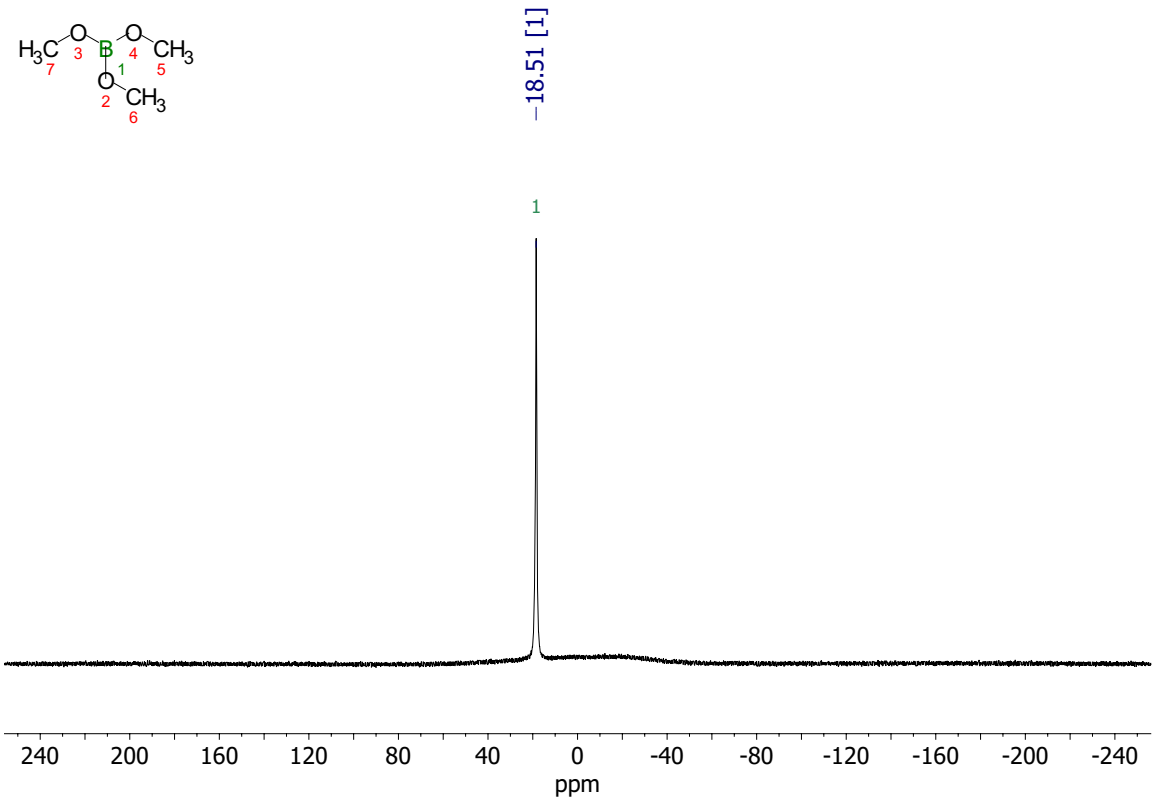

Figure 6.1: ^{11}B NMR spectrum of the reaction mixture of subsection 4.2.1.

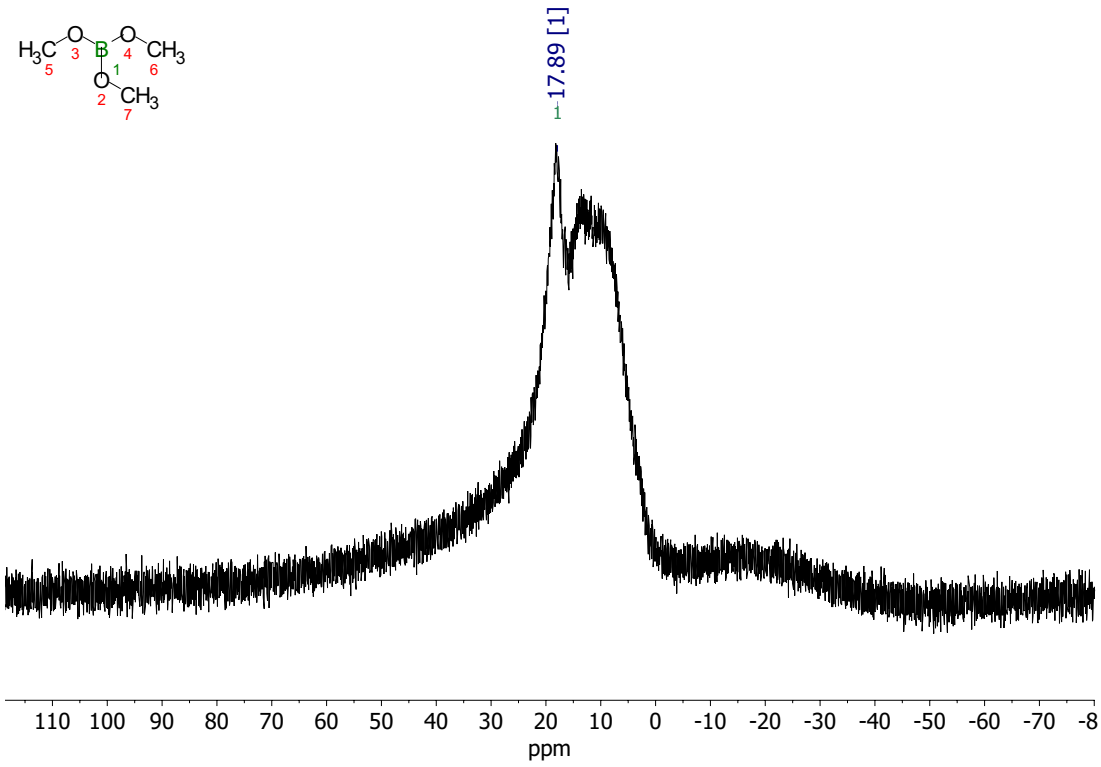

Figure 6.2: ^{11}B NMR spectrum of the reaction mixture of subsection 4.2.2.

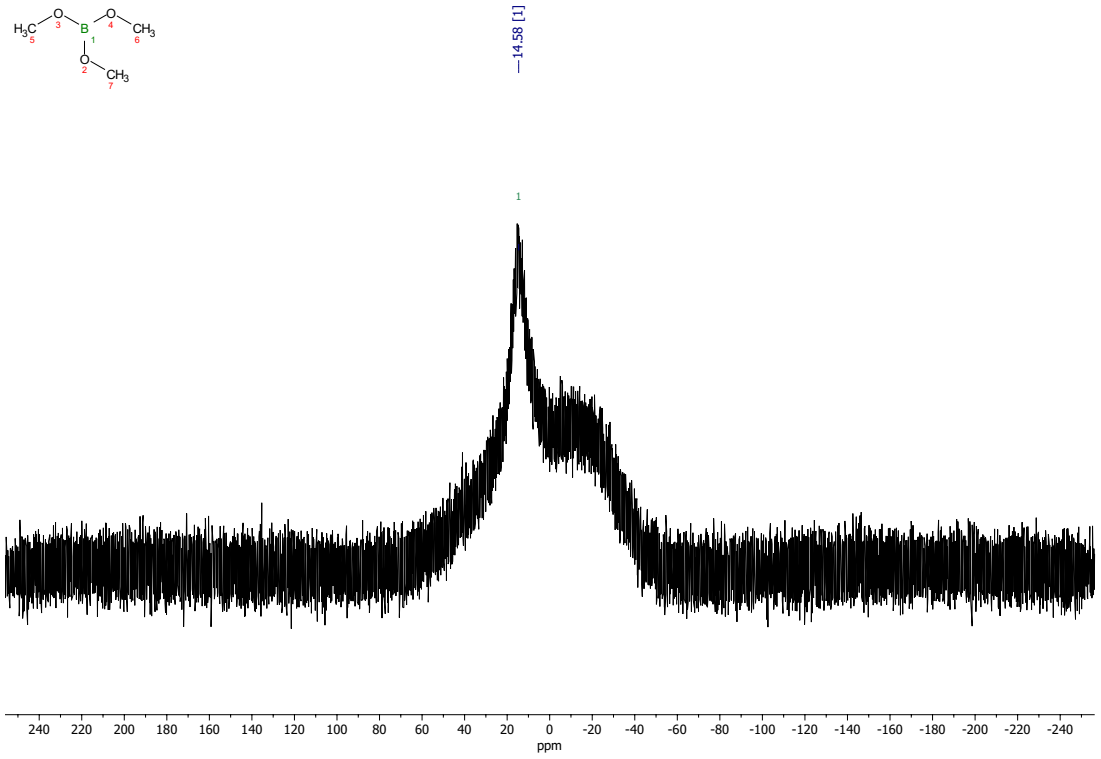

Figure 6.3: ^{11}B NMR spectrum of the reaction mixture of subsection 4.2.3.

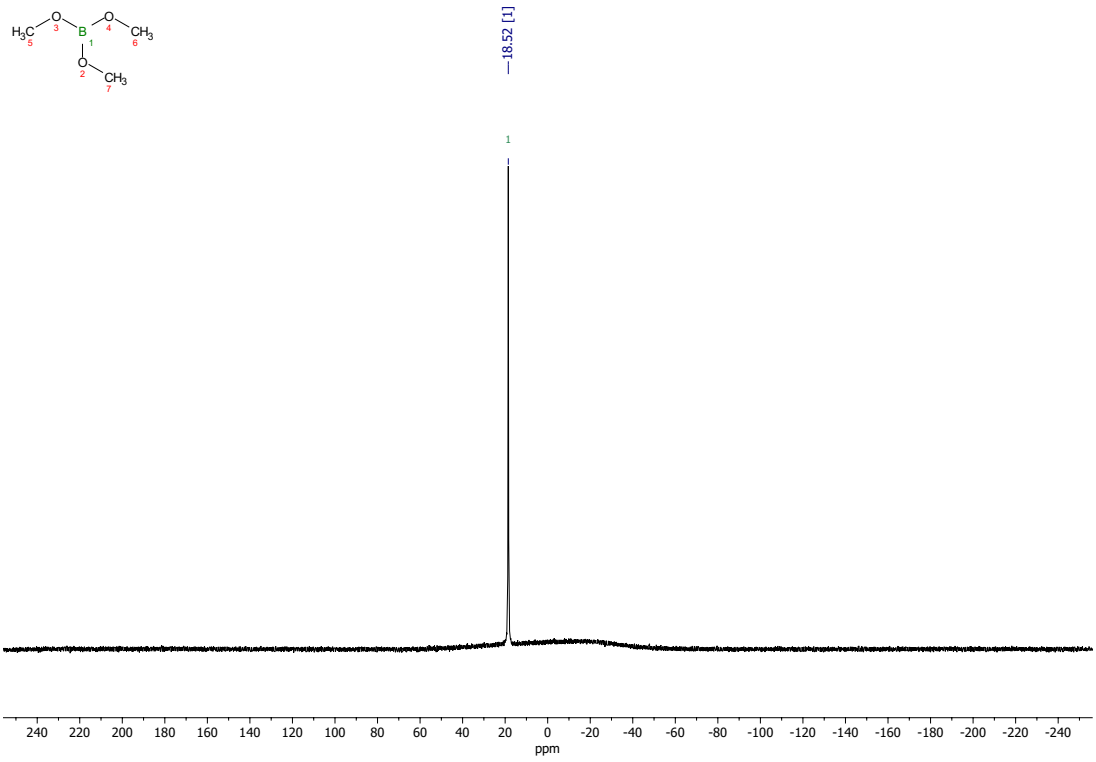

Figure 6.4: ^{11}B NMR spectrum of the reaction mixture of subsection 4.2.4.

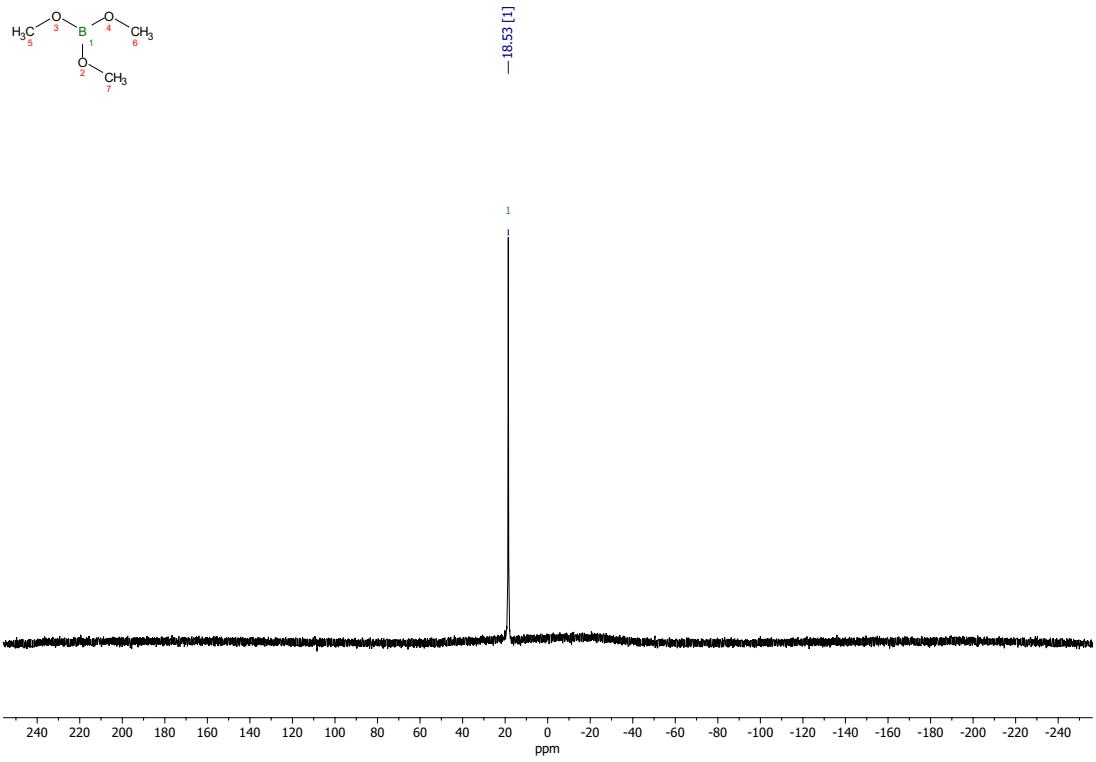

Figure 6.5: ^{11}B{^{1}H} NMR spectrum of the reaction mixture of subsection 4.2.4.

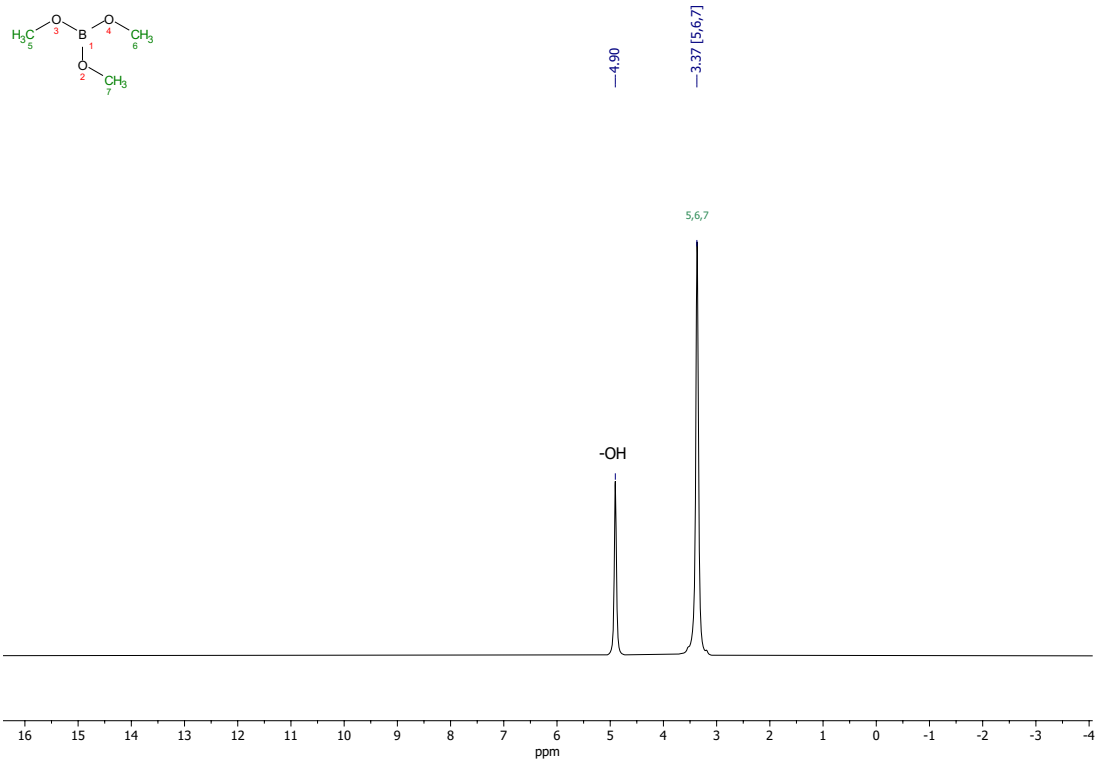

Figure 6.6: ^{1}H NMR spectrum of the reaction mixture of subsection 4.2.4.

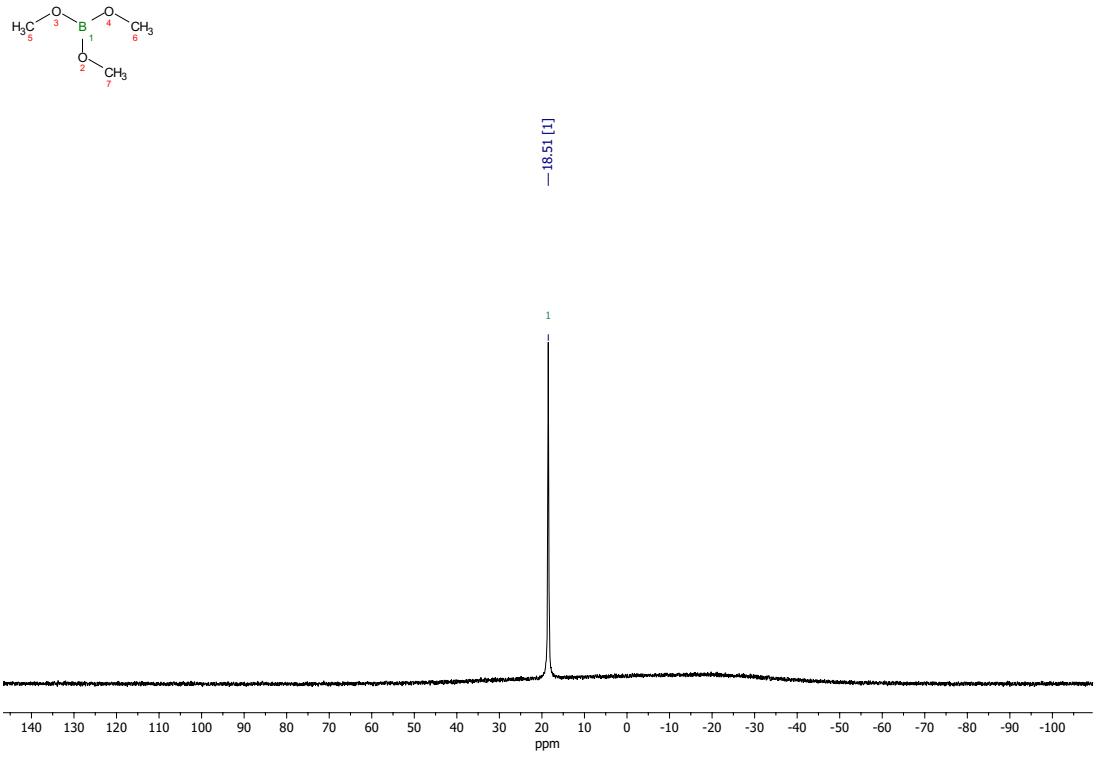

Figure 6.7: ^{11}B NMR spectrum of the reaction mixture of subsection 4.2.5.

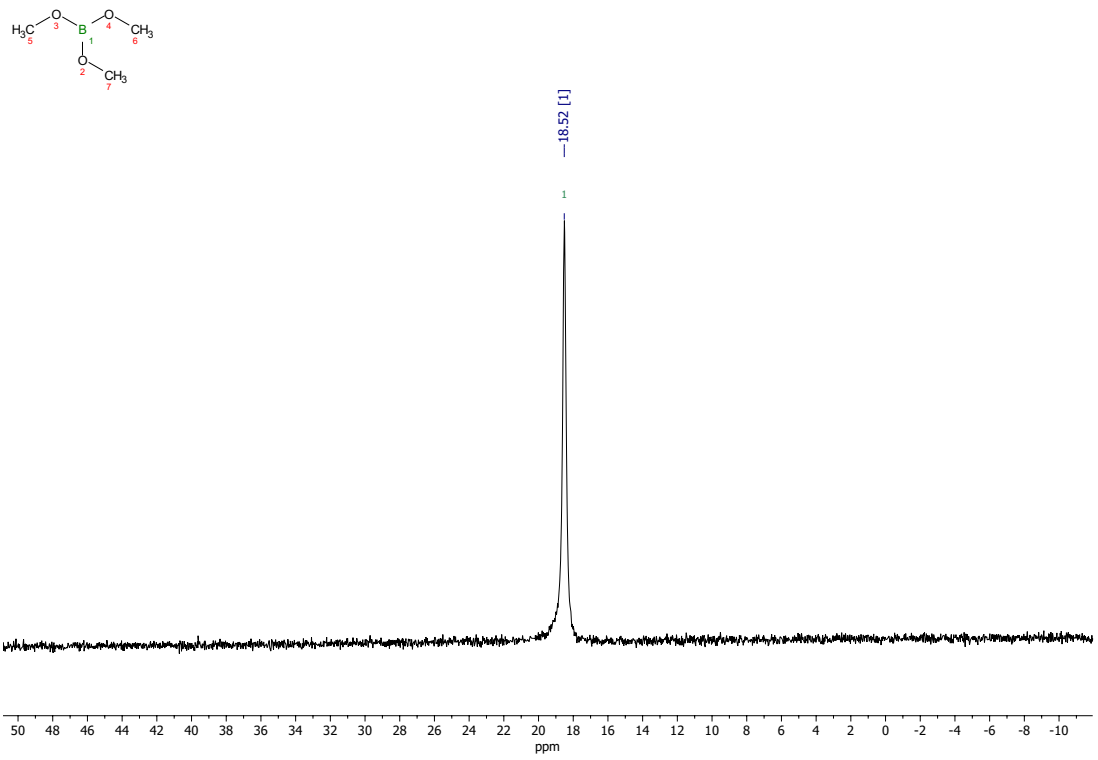

Figure 6.8: $^{11}B\{^{1}H\}$ NMR spectrum of the reaction mixture of subsection 4.2.5.

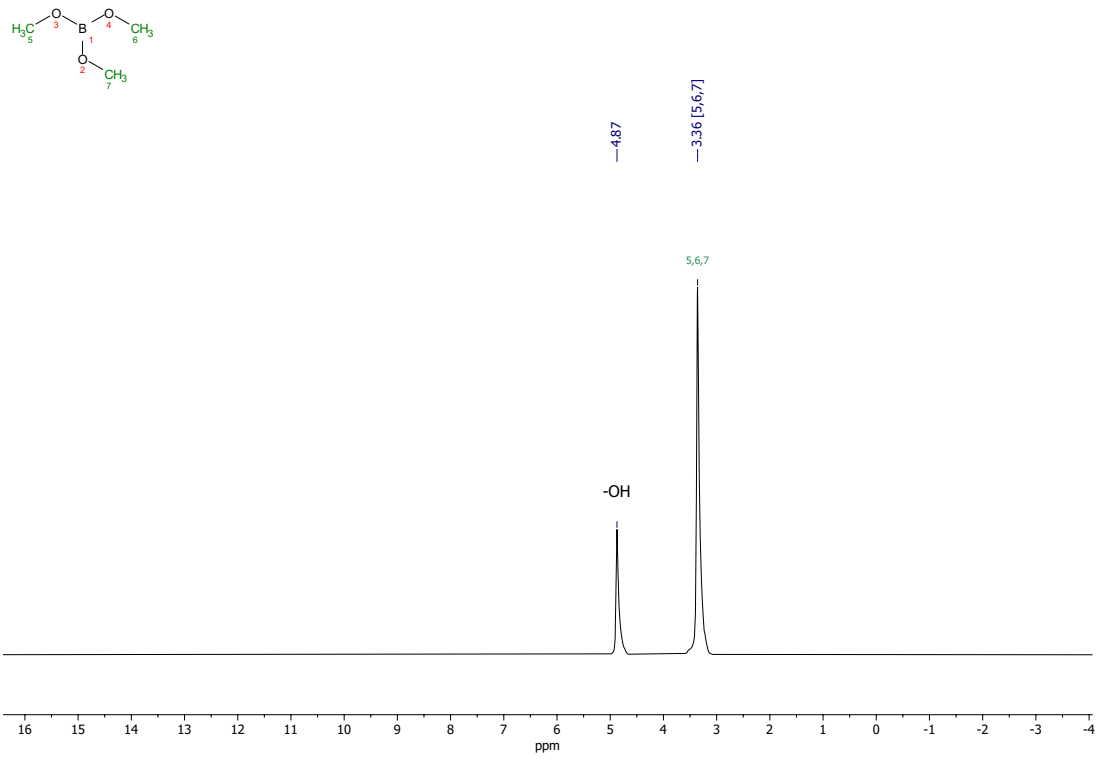

Figure 6.9: ^{1}H-NMR spectrum of the reaction mixture of subsection 4.2.5.

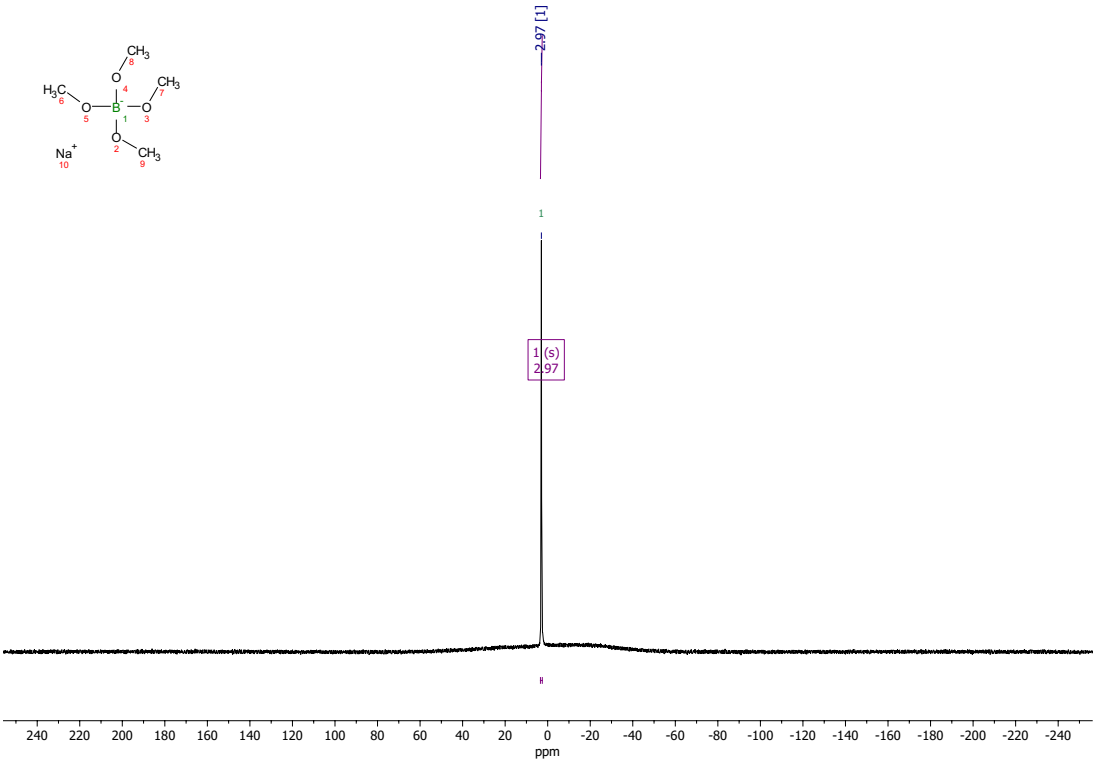

Figure 6.10: ^{11}B NMR spectrum of the reaction mixture of subsection 4.3.1.

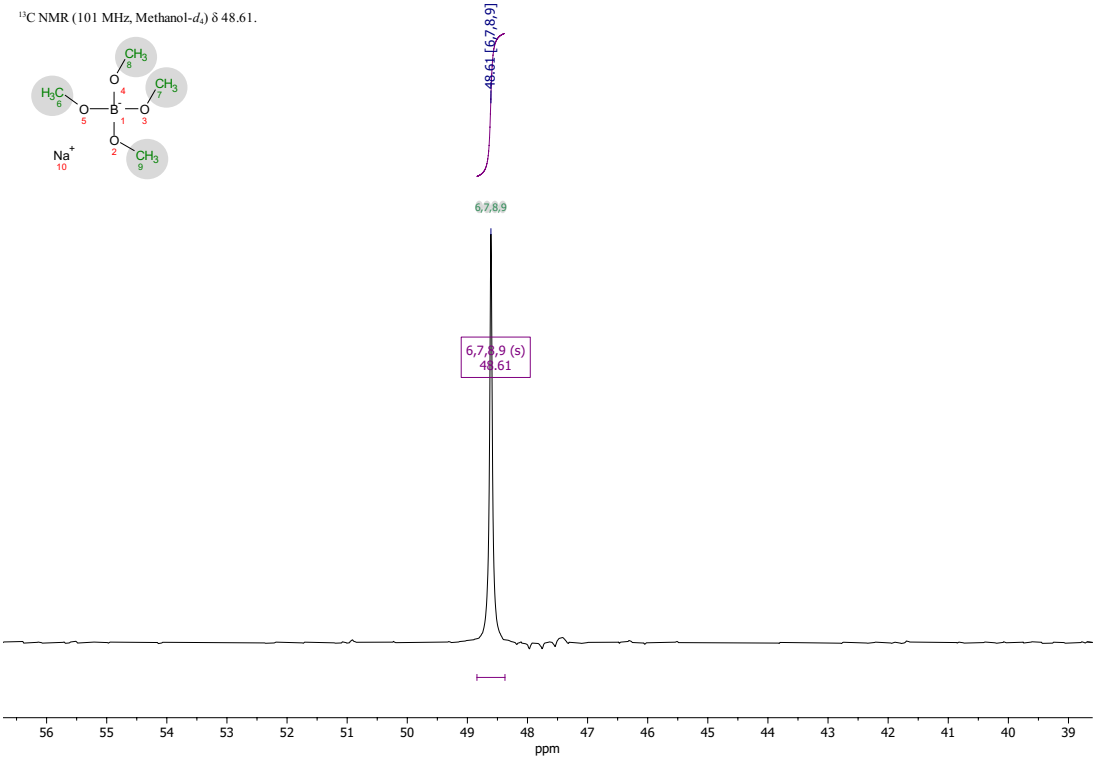

Figure 6.11: ^{13}C NMR spectrum of the reaction mixture of subsection 4.3.1.

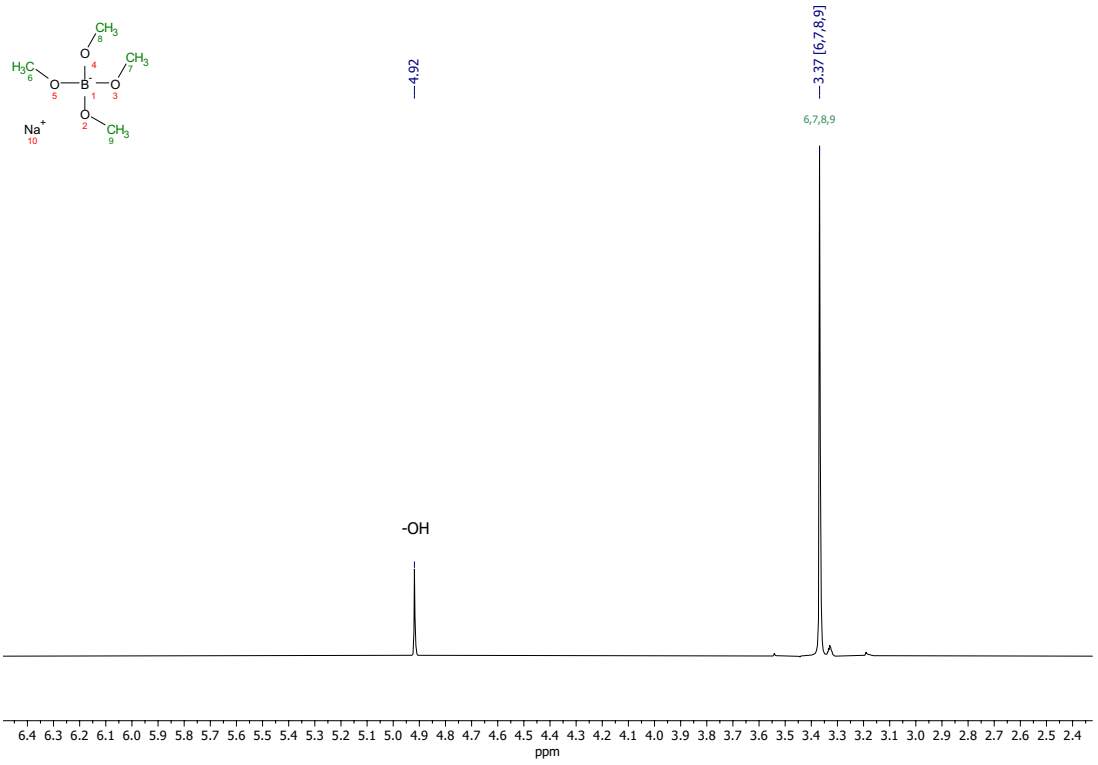

Figure 6.12: ^{1}H-NMR spectrum of the reaction mixture of subsection 4.3.1.

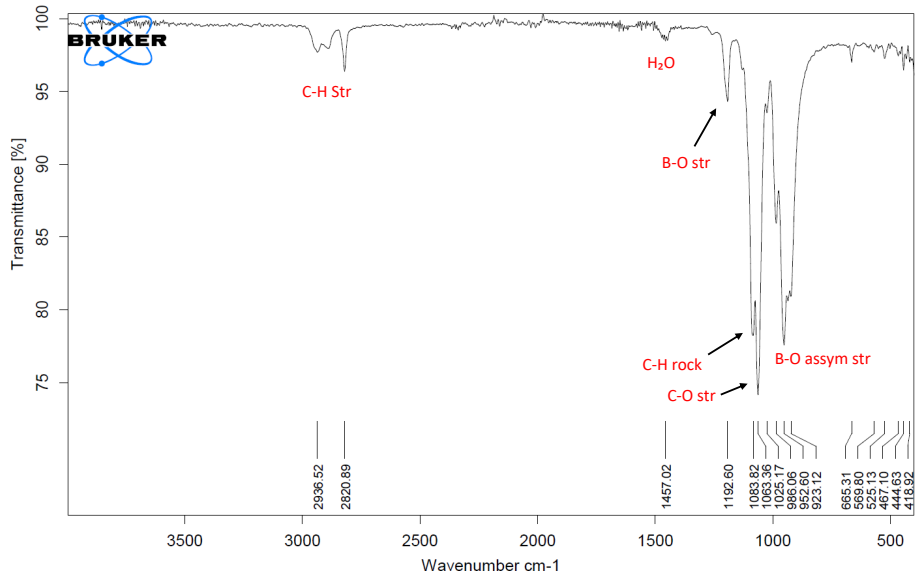

Figure 6.13: IR spectrum of the reaction mixture of subsection 4.3.1.

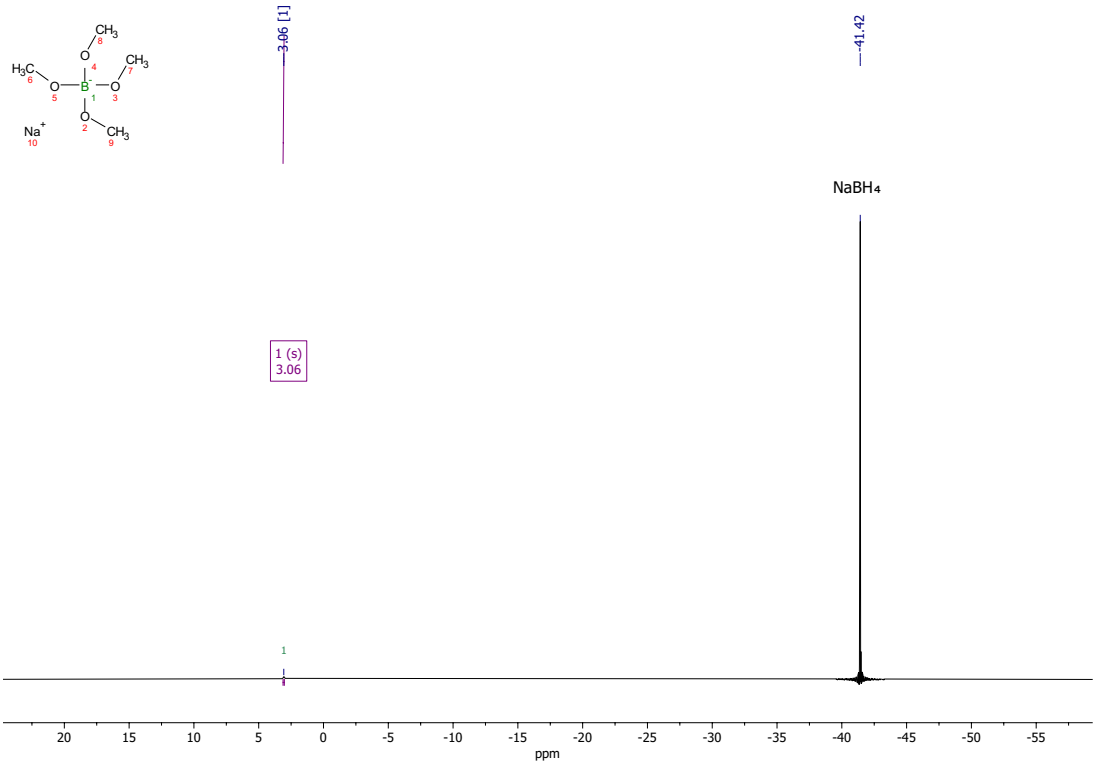

Figure 6.14: $^{11}B\{^{1}H\}$ NMR spectrum of the reaction mixture of subsection 4.3.2.

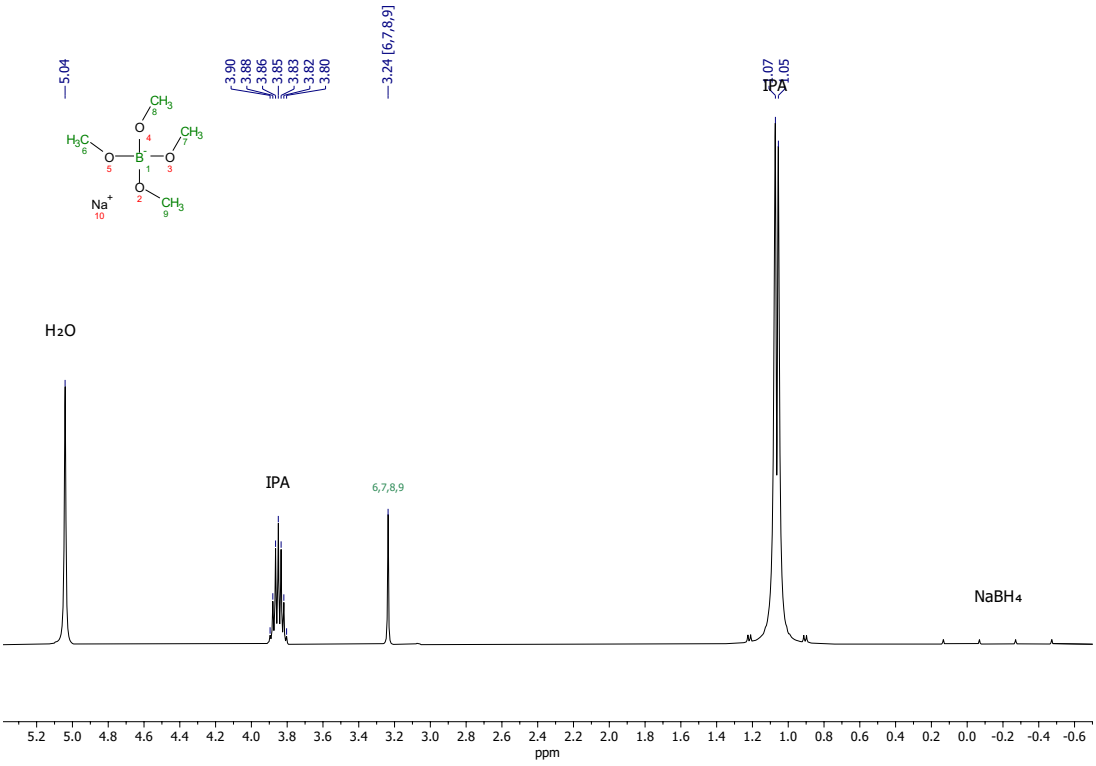

Figure 6.15: ^{1}H NMR spectrum of the reaction mixture of subsection 4.3.2.

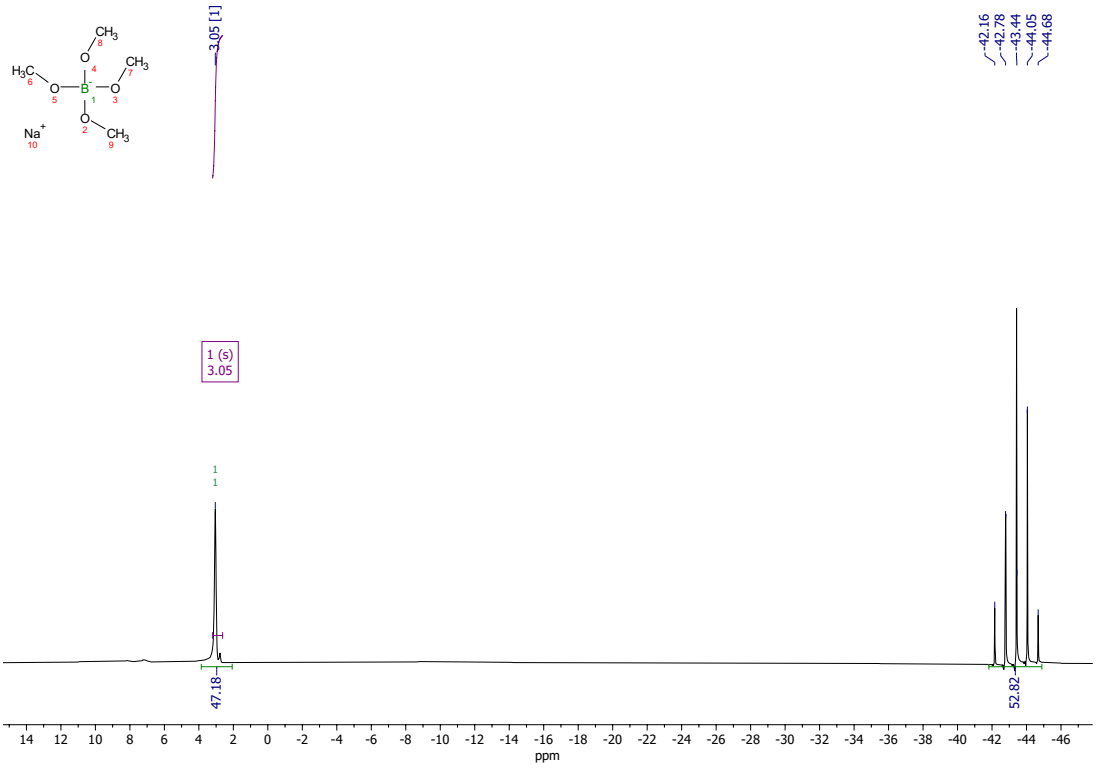

Figure 6.16: ^{11}B NMR spectrum of the reaction mixture of subsection 4.3.3.

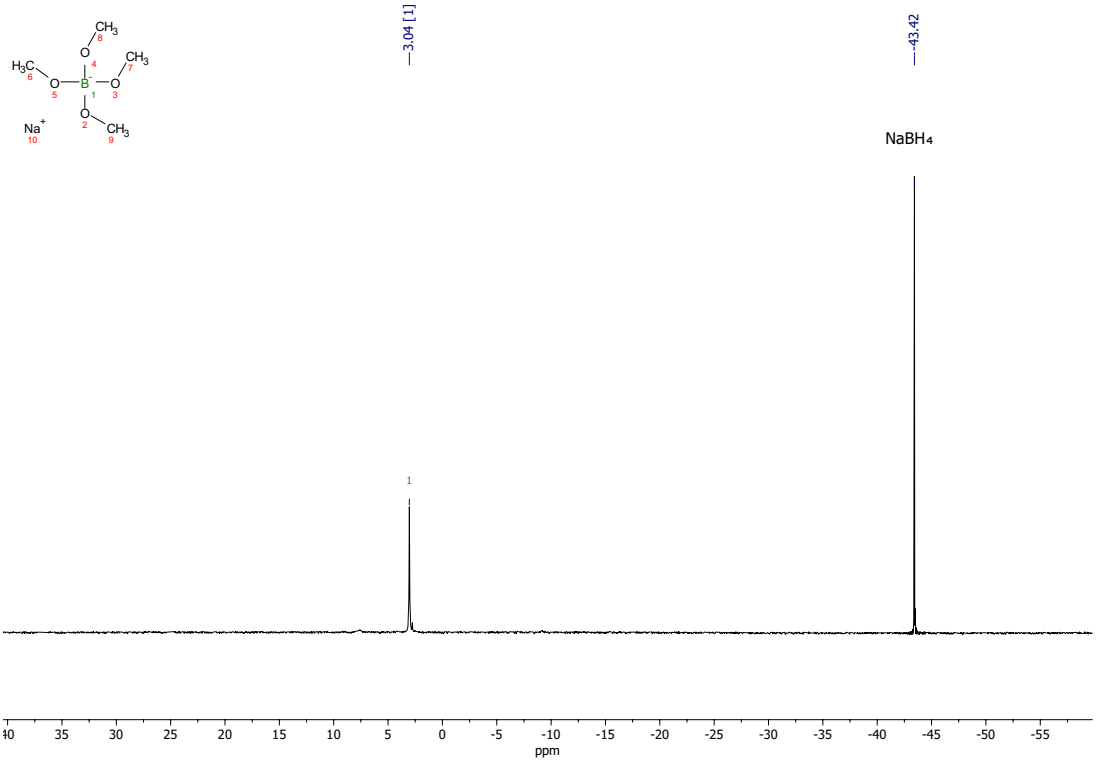

Figure 6.17: ^{11}B$\{^{1}$H$\}$ NMR spectrum of the reaction mixture of subsection 4.3.3.

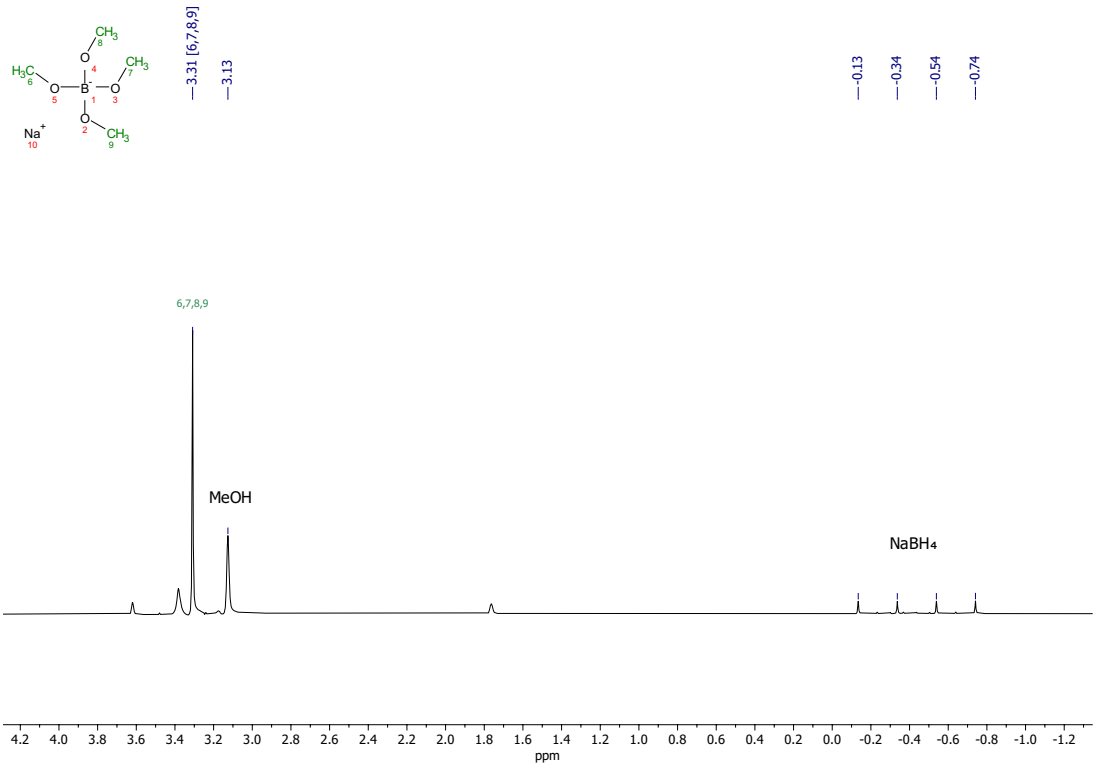

Figure 6.18: ^{1}H NMR spectrum of the reaction mixture of subsection 4.3.3.

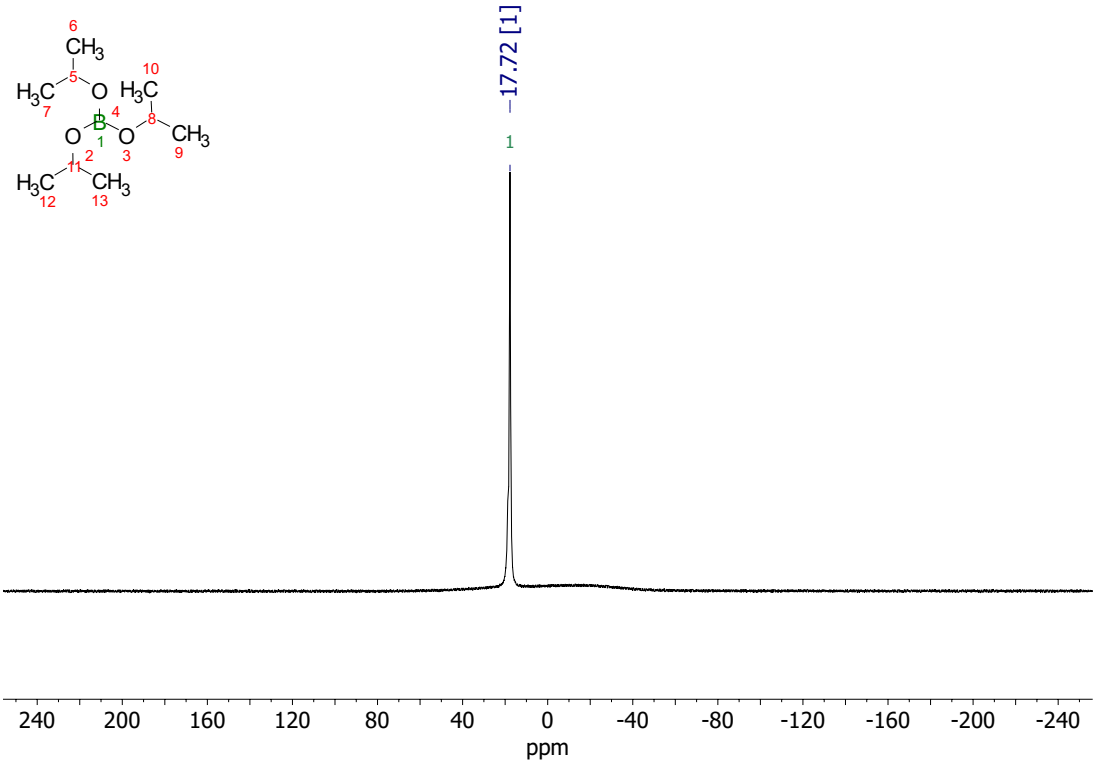

Figure 6.19: ^{11}B NMR spectrum of the reaction mixture of subsection 4.4.1.

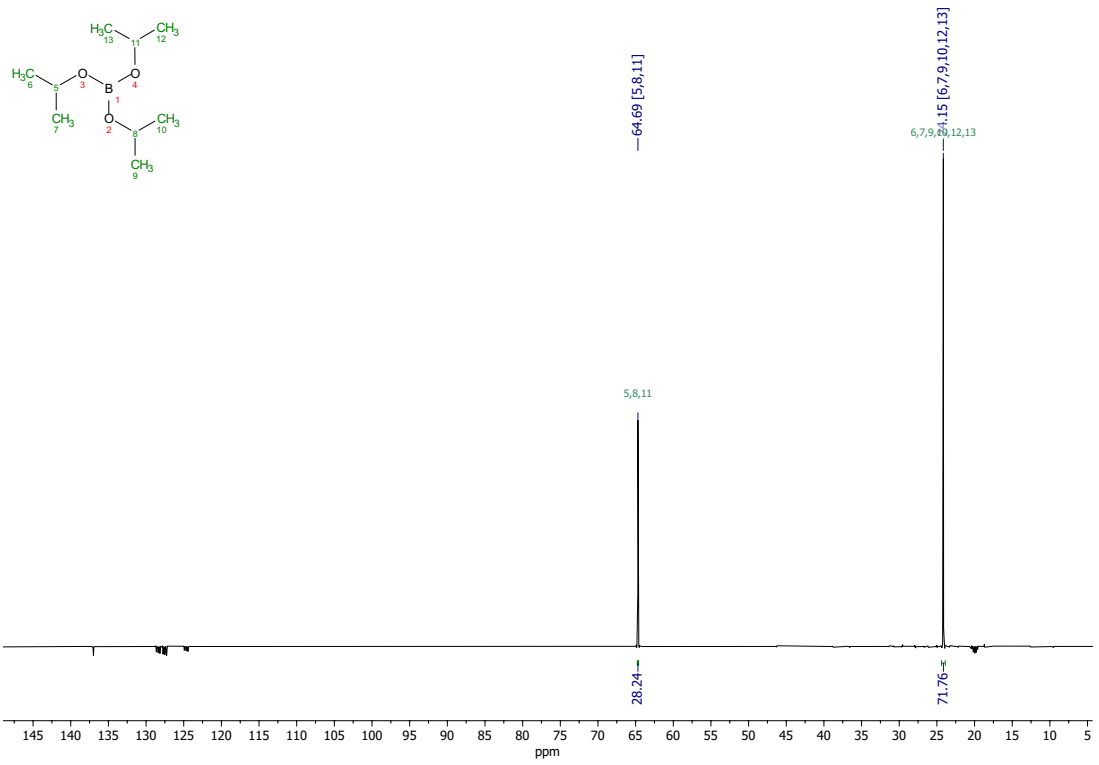

Figure 6.20: ^{13}C NMR spectrum of the reaction mixture of subsection 4.4.1.

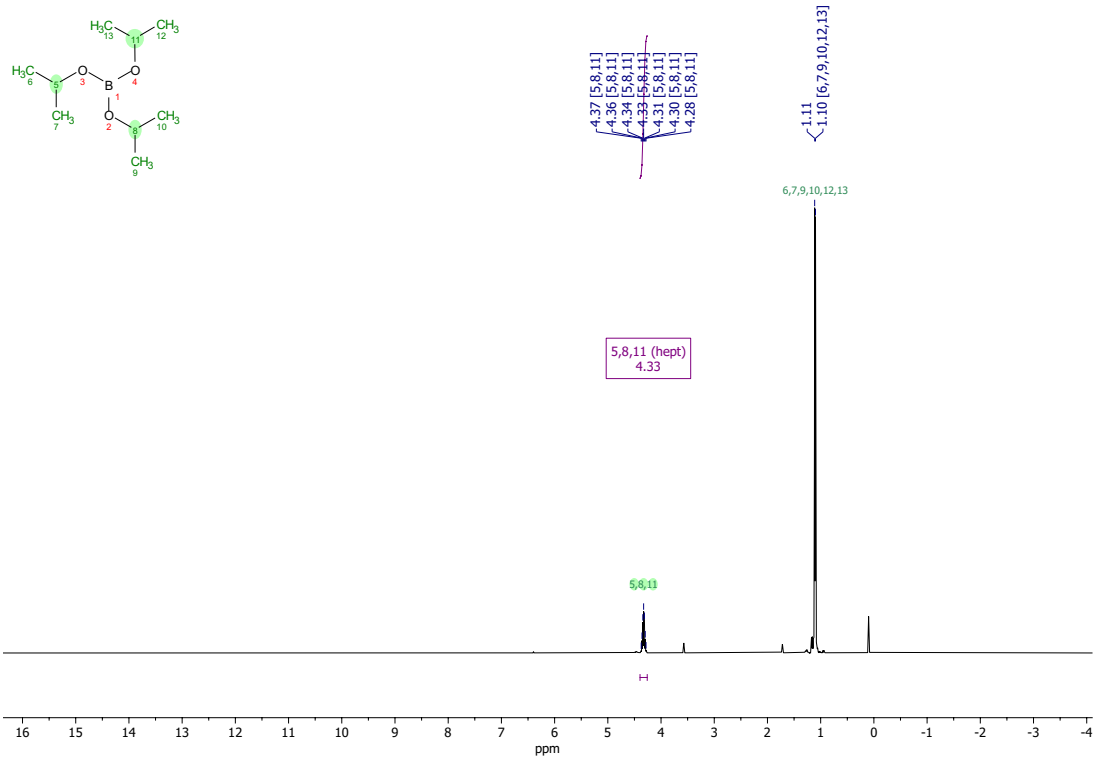

Figure 6.21: ^{1}H-NMR spectrum of the reaction mixture of subsection 4.4.1.

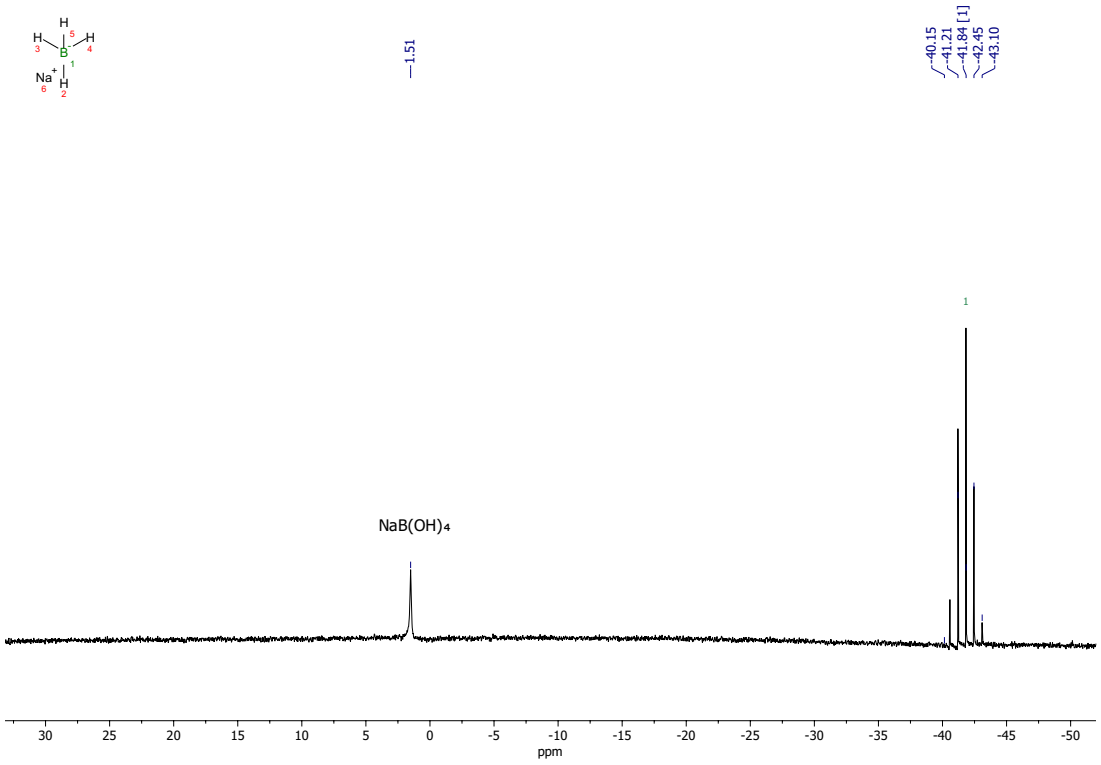

Figure 6.22: ^{11}B NMR spectrum of the reaction mixture of section 4.5.

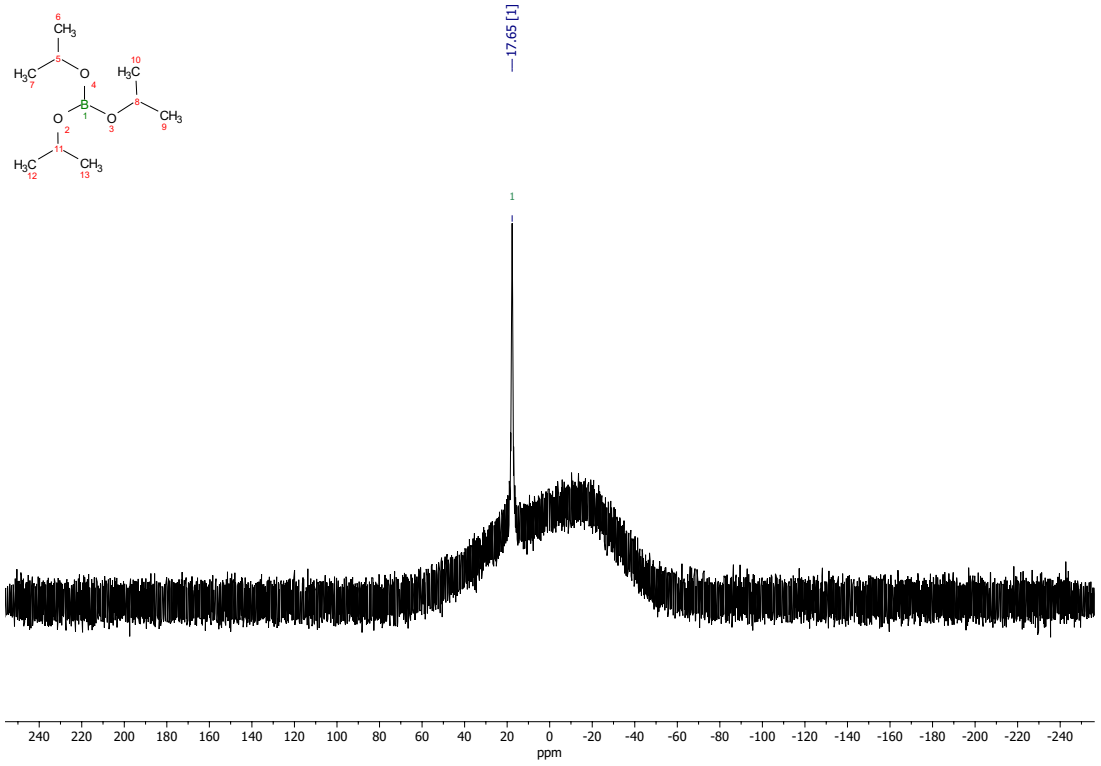

Figure 6.23: ^{11}B NMR spectrum of the reaction mixture of subsection 4.6.1.

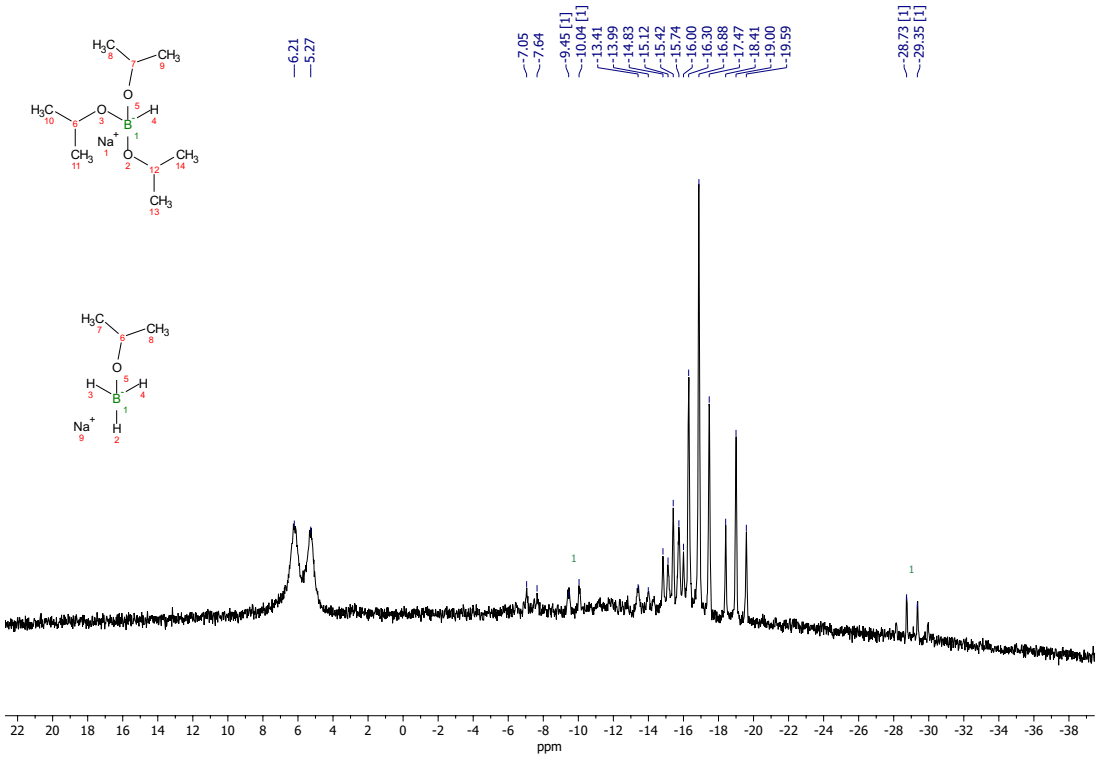

Figure 6.24: ^{11}B NMR spectrum of the reaction mixture of subsubsection 4.6.2.1.

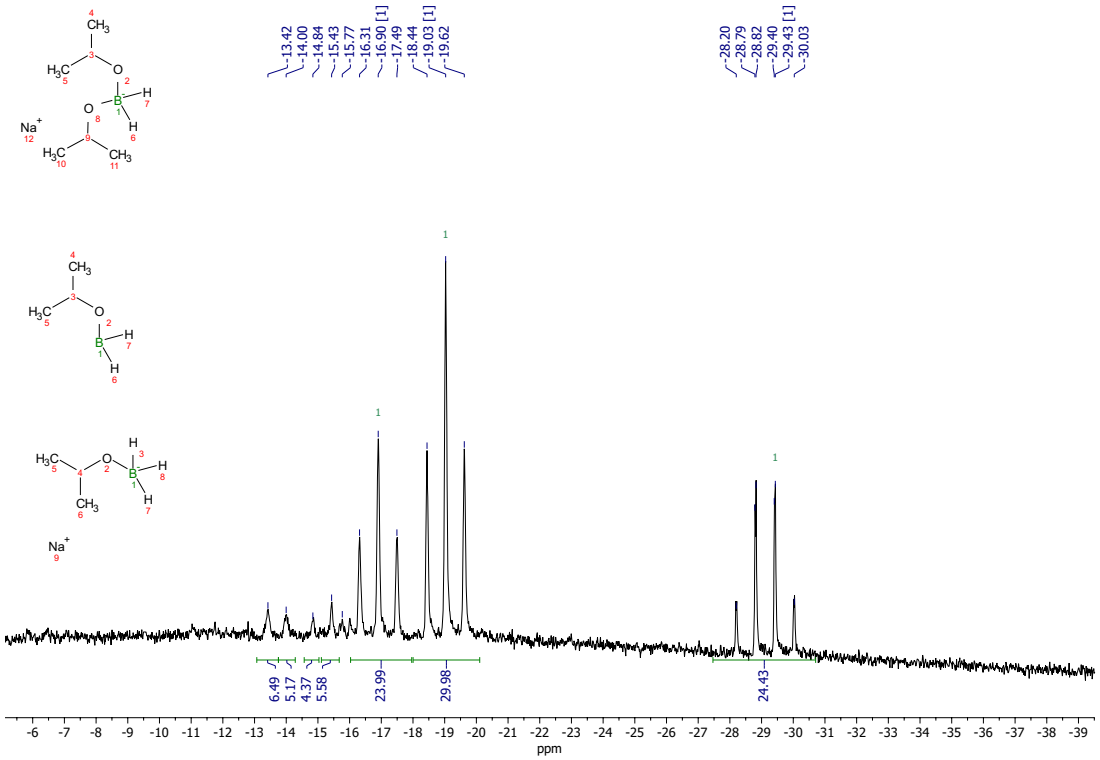

Figure 6.25: ^{11}B NMR spectrum of the reaction mixture of subsubsection 4.6.2.2.

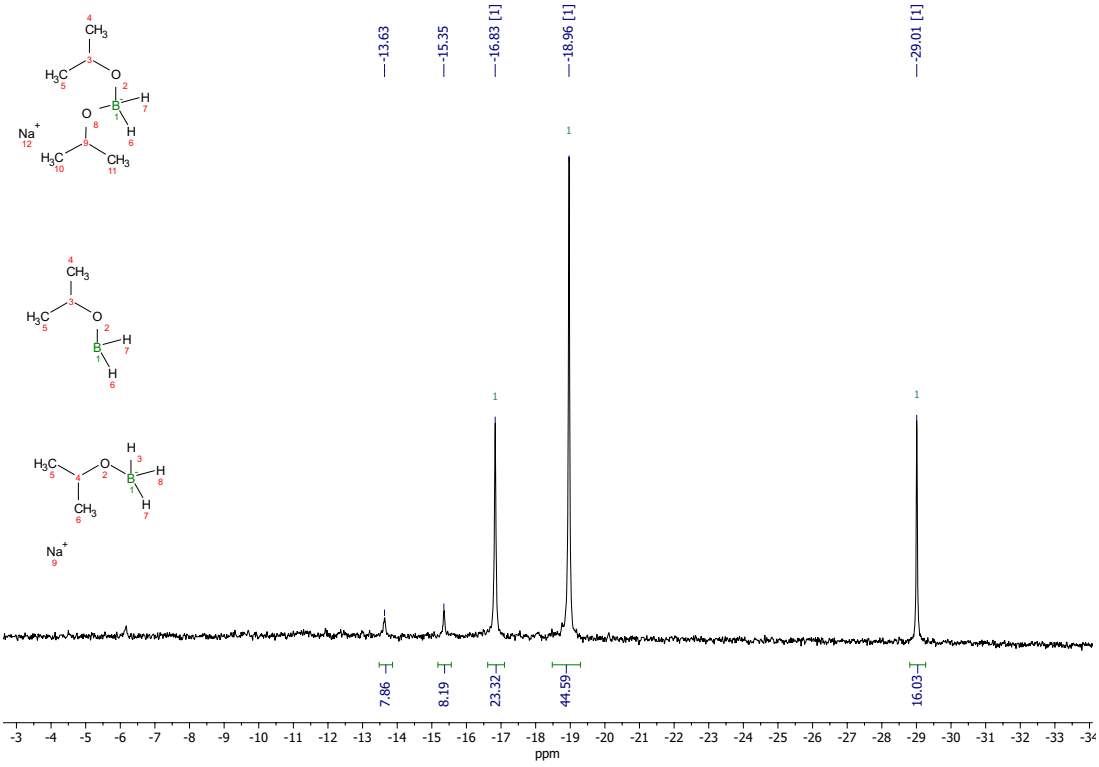

Figure 6.26: $^{11}B\{^{1}H\}$ NMR spectrum of the reaction mixture of subsubsection 4.6.2.2.

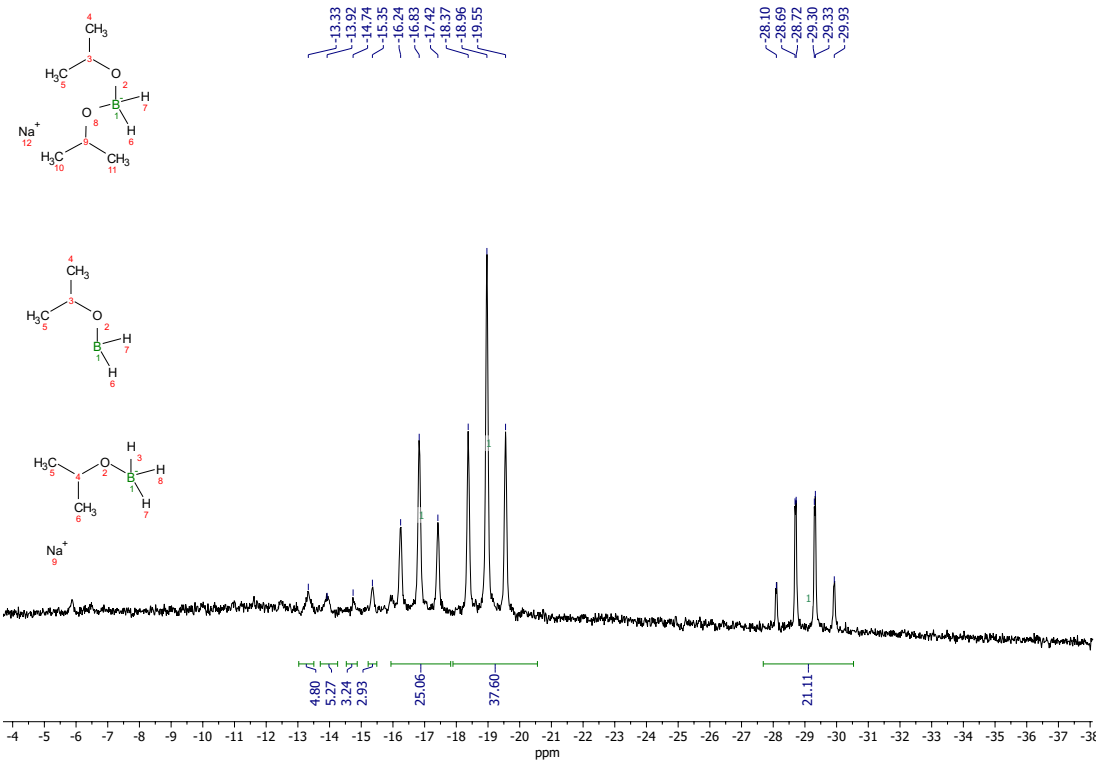

Figure 6.27: ^{11}B NMR spectrum of the reaction mixture of subsubsection 4.6.2.3.

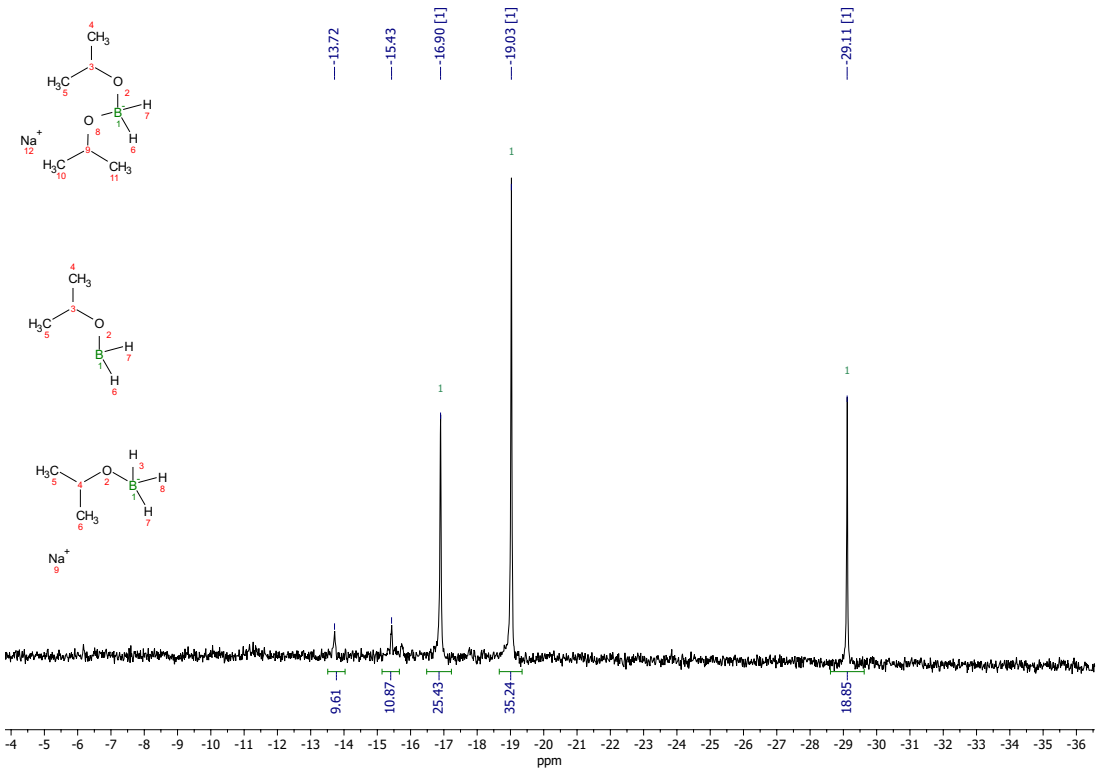

Figure 6.28: $^{11}B\{^{1}H\}$ NMR spectrum of the reaction mixture of subsubsection 4.6.2.3.

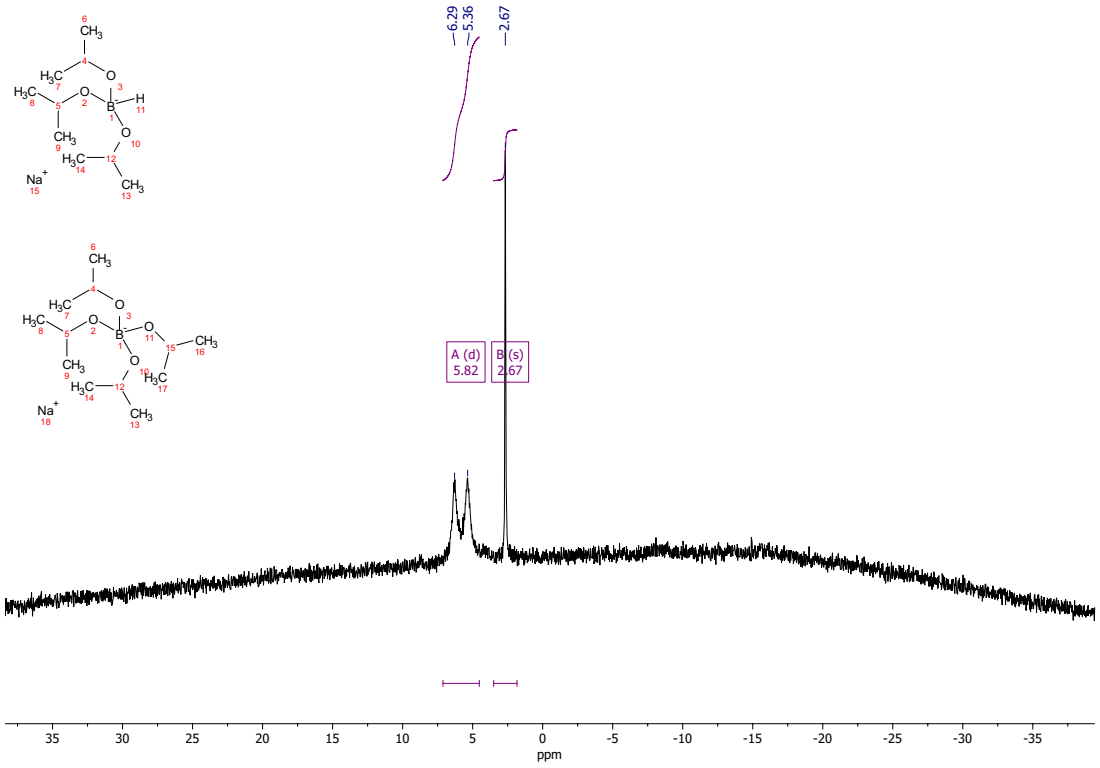

Figure 6.29: ^{11}B NMR spectrum of the reaction mixture of subsubsection 4.6.3.1.

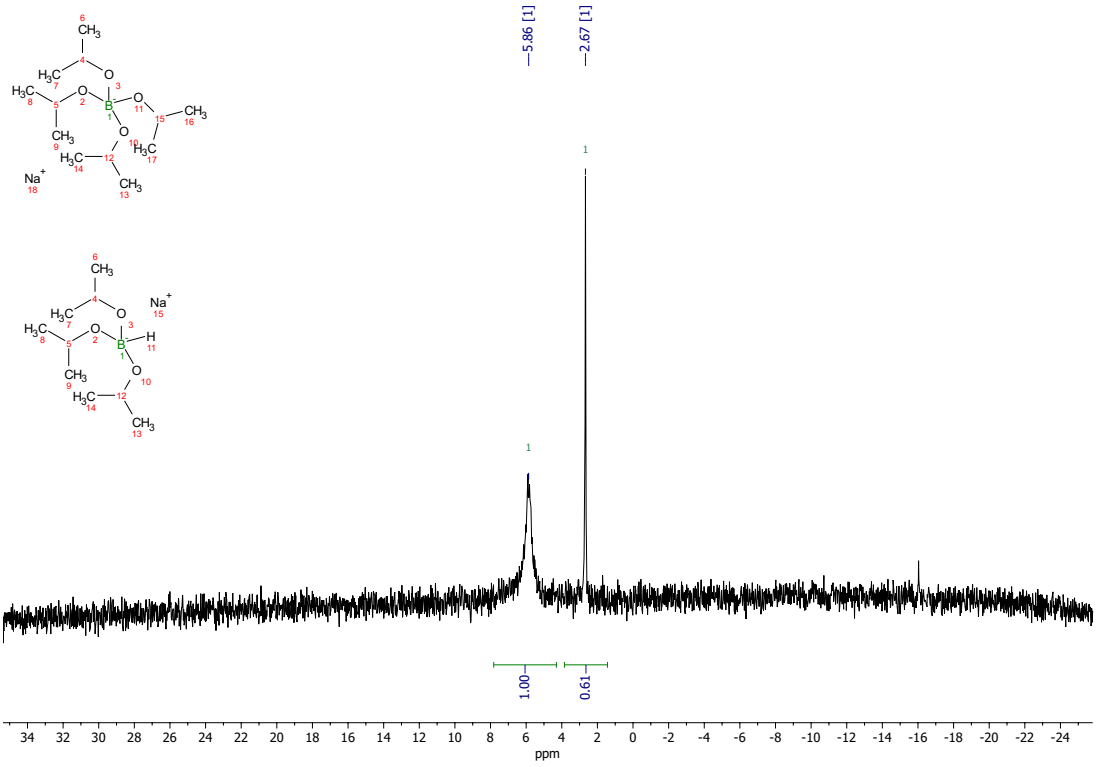

Figure 6.30: $^{11}B\{^{1}H\}$ NMR spectrum of the reaction mixture of subsubsection 4.6.3.1.

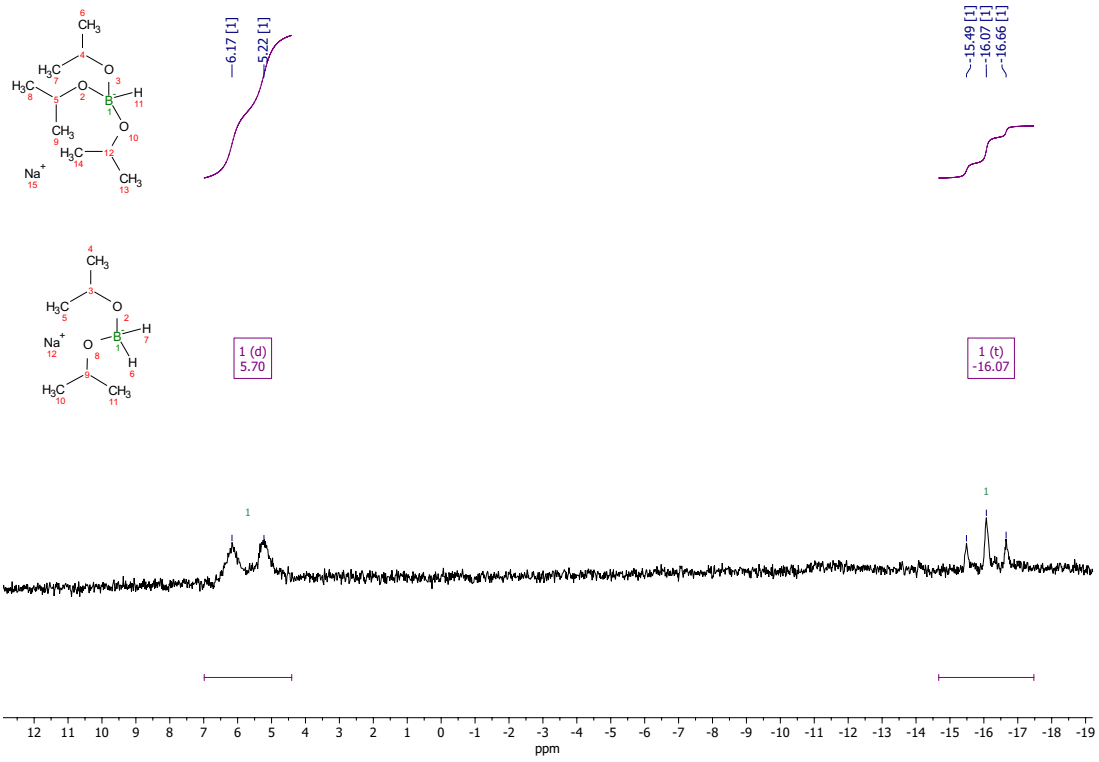

Figure 6.31: ^{11}B NMR spectrum of the reaction mixture of subsubsection 4.6.3.2.

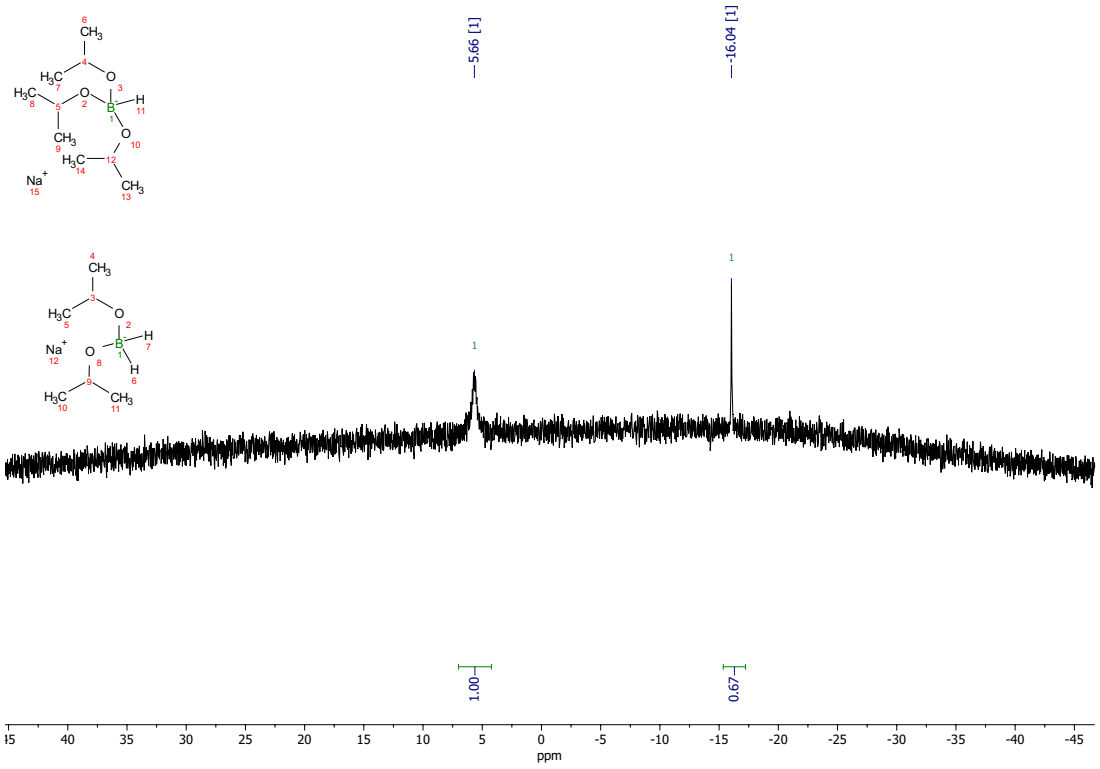

Figure 6.32: $^{11}B\{^{1}H\}$ NMR spectrum of the reaction mixture of subsubsection 4.6.3.2.

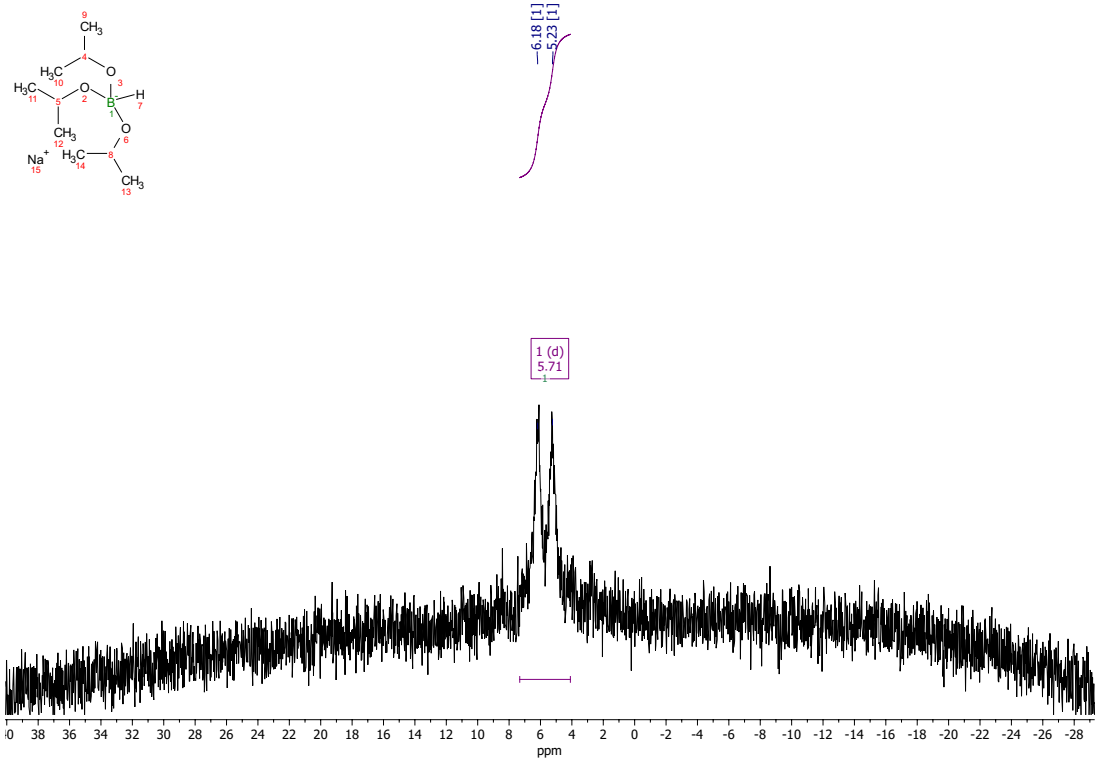

Figure 6.33: ^{11}B NMR spectrum of the reaction mixture of subsubsection 4.6.3.3.

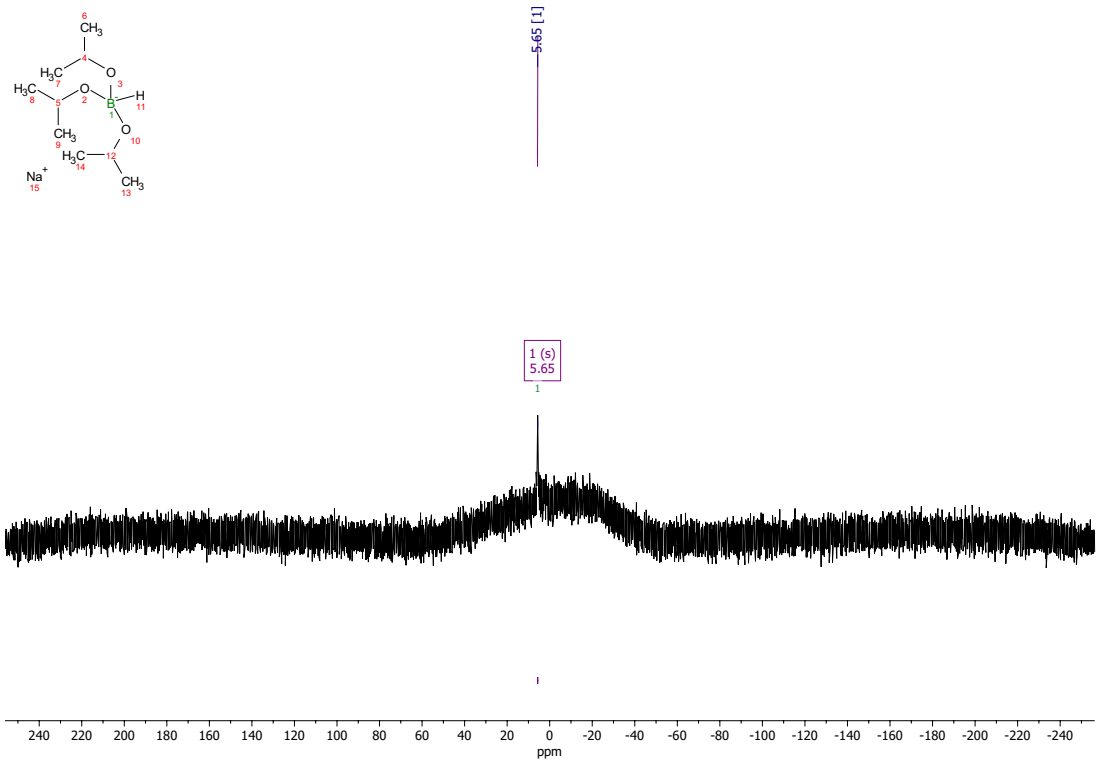

Figure 6.34: $^{11}B\{^{1}H\}$ NMR spectrum of the reaction mixture of subsubsection 4.6.3.3.

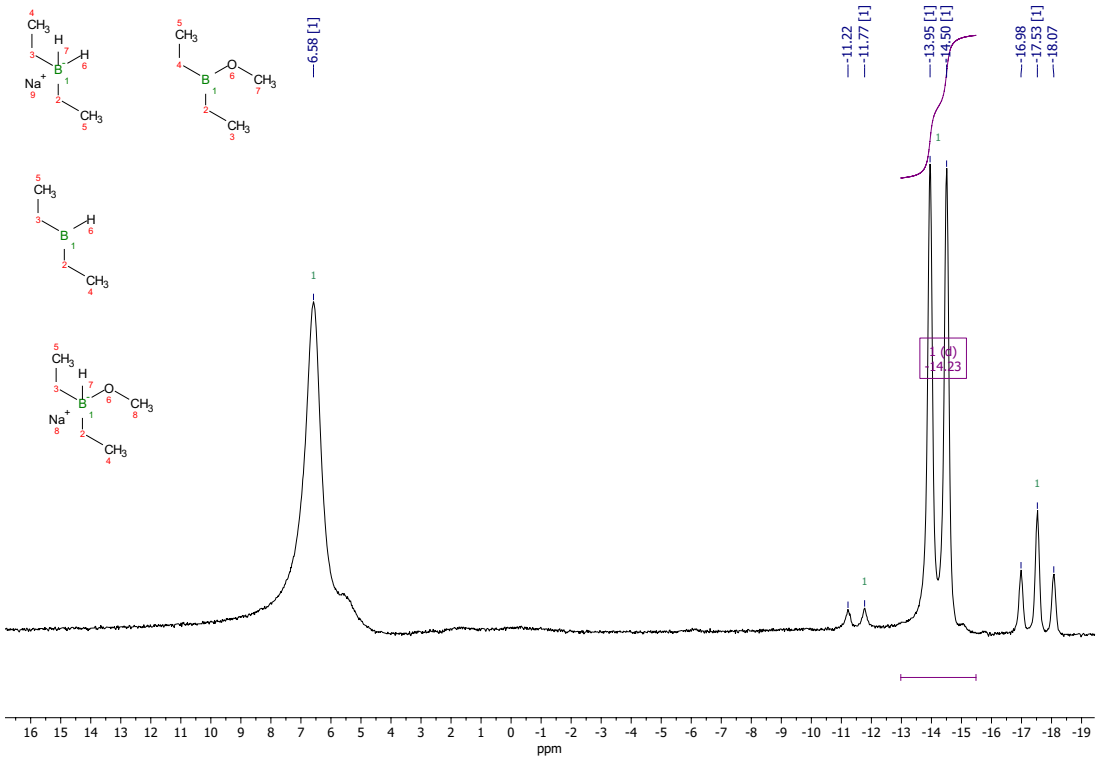

Figure 6.35: ^{11}B NMR spectrum of the reaction mixture of section 4.7.

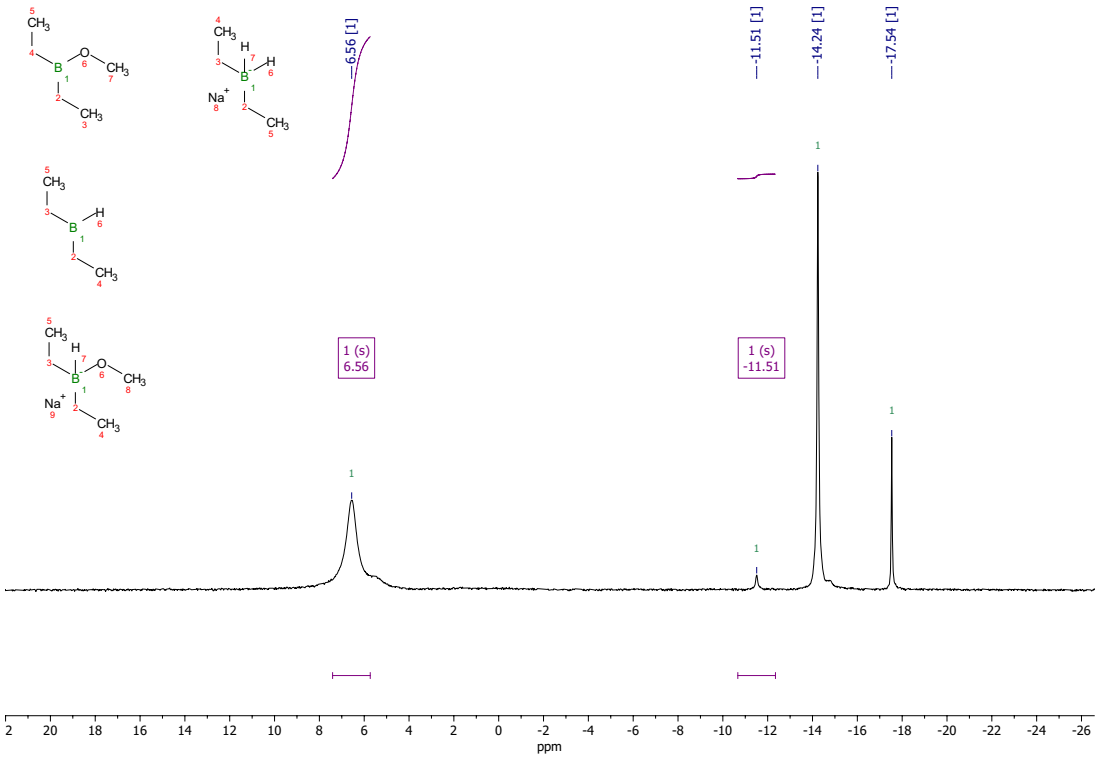

Figure 6.36: $^{11}B\{^{1}H\}$ NMR spectrum of the reaction mixture of section 4.7.

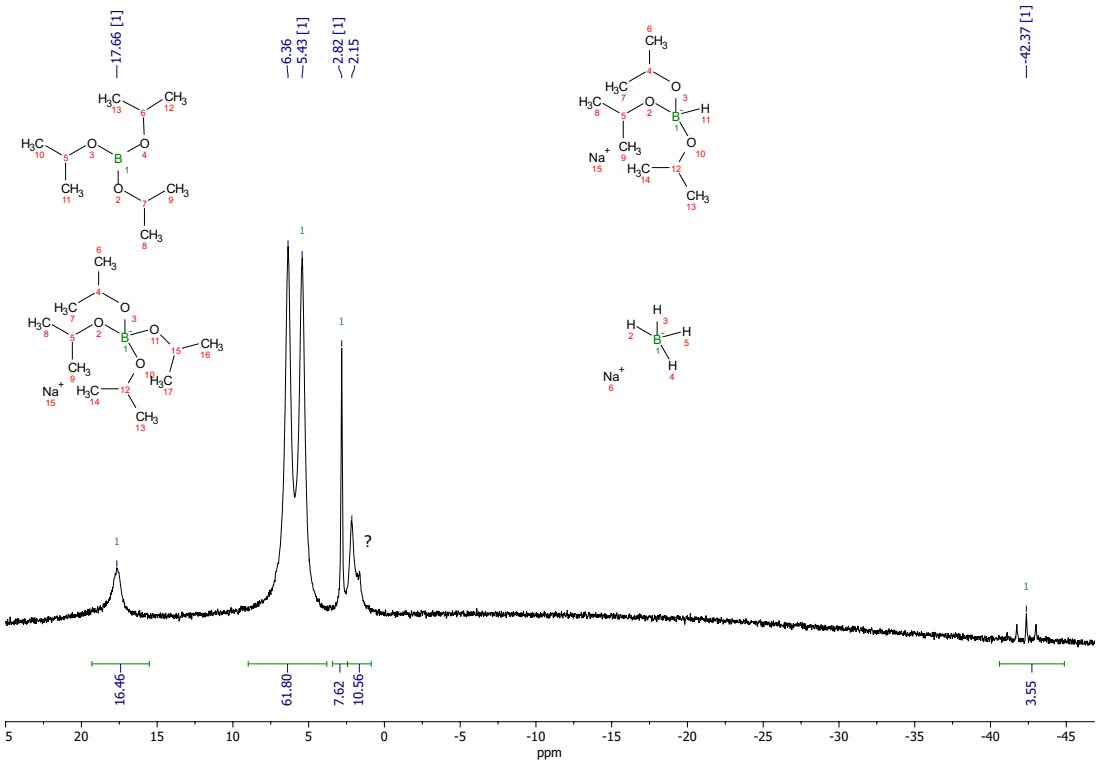

Figure 6.37: ^{11}B NMR spectrum of the reaction mixture of subsection 4.7.1.

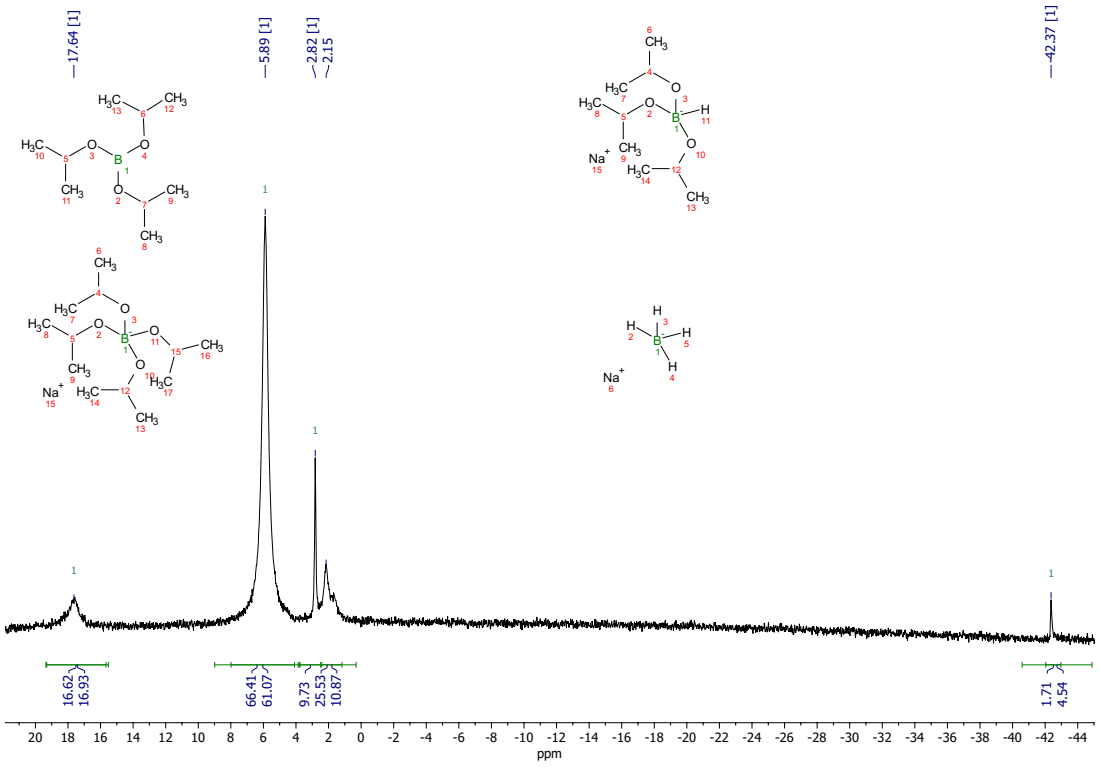

Figure 6.38: $^{11}B\{^{1}H\}$ NMR spectrum of the reaction mixture of subsection 4.7.1.

6.2. Appendix B - Laboratory Set-Up

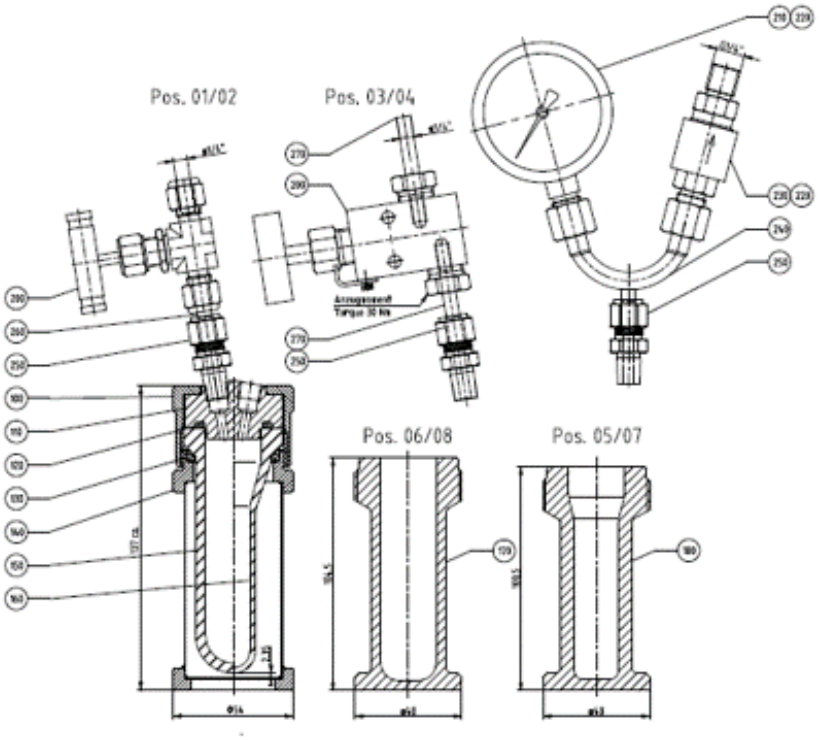

Figure 6.39: Schematic of the tiny clave.

Figure 6.40: Fed-batch hydrogen release system through acid addition by syringe pump.

Figure 6.41: Distillation set-up with packed bed column to separate triisopropylborate from IPA.

Figure 6.42: Autoclave used for boron radical activation reactions.

6.3. Appendix C - Python code

```
1
2   import math as m
3   import numpy as np
4   import matplotlib.pyplot as plt
5   import sys
6
7   np.set_printoptions(threshold=sys.maxsize)
8
9   "Fixed parameters"
10  "-----------------------------------------------------------------------------
11  T_in = 298 #[K] Temperature of inflowing cooling water
12  C_pwater= 4181 #[J/kgK] Specific heat of water at constant pressure
13  C_psol = 2350 #[J/kgK] Specific heat of Isopropanol
14  C_psteel = 540 #[J/kgK] Specific heat of Stainless steel.
15  C_pN2 = 1040 #[J/kgK] Specific heat of dinitrogen.
16  rho_N2 = 1.16 #[kg/m^3] Density of N2 at RT
17  rho_ss = 8000 #[kg/m^3] Density of stainless steel
18  rho_w = 997 #[kg/m^3] Density of water
19  rho_sol = 786 #[kg/m^3] Density of IPA
20  labda_N2 =  0.0265 #[W m^-1 K^-1] Thermal conductivity of nitrogen
21  labda_ss = 15 #[W m^-1 K^-1] Thermal conductivity of stainless steel
22  labda_w = 0.6 #[W m^-1 K^-1] Thermal conductivity of water
23  labda_ipa = 0.16 #[W m^-1 K^-1] Thermal conductivity of IPA from datacompani
24  r = 0.9088 #[mol/m^3/s] Reaction rate and acid addition rate.
25  DeltaH = -536.3 #[kJ/mol] Enthalpy of reaction of alcoholysis reaction with
26
27  "Adjustable parameters"
28  "-----------------------------------------------------------------------------
29  D_out = 0.15 #[m] Outer diameter of reactor
30  L = 0.2 #[m] Length of the reactor
31  L_real = 0.15 # [m] Length of the reactor which is in contact with the react
32  D_w = 0.001 #[m] Thickness of the reactor wall
33  D_he = 0.005 #[m] Thickness of the heat exchanger
34  m_sol = 0.191 #[kg] Mass of solvent, in this case isopropanol
35  D_in = D_out - D_w
36  V_2 = np.pi*(L-L_real)*(0.5*D_in)**2  #[m^3] Excess volume in the reactor
37  V_wall = np.pi*(L_real)*(0.5*D_out)**2-np.pi*(L_real)*(0.5*D_in)**2
38  A_bottom = np.pi*(0.5*D_in)**2 #[m^2] Area of the reactor vessel
39  A_wall = D_out*np.pi*L_real
40
```

Figure 6.43: Python code for the heat transfer limitation model - Page 1.

```
41
42  "Load Data"
43  "------------------------------------------------------------------------
44
45  DATA3 = np.genfromtxt('data 10g p2 (K).csv')
46  f3 = DATA3[:]
47  f3 = f3[1:]
48
49
50  DATA5 = np.genfromtxt('data 20g (K).csv')
51  f5 = DATA5[:]
52  f5 = f5[1:]
53
54
55  DATA7 = np.genfromtxt('data 15g 3 (K).csv')
56  f7 = DATA7[:]
57  f7 = f7[1:]
58
59
60  time3 = np.array(range(1185))
61  time5 = np.array(range(1295))
62  time7 = np.array(range(1240))
63  timeave = np.array(range(1295))
64
65  plt.figure(1)
66  plt.plot(time5,f5,'-', color='red')
67  plt.ylabel('Temperature of solution (K)')
68  plt.xlabel('Time (s)')
69  plt.title('Temperature of solution over time')
70  plt.show()
71
72  plt.figure(2)
73  plt.plot(time3,f3,'-', label='10 gr', color='blue')
74  plt.plot(time7,f7,'-', label='15 gr', color='red')
75  plt.plot(time5,f5,'-', label='20 gr', color='purple')
76  plt.ylabel('Temperature of solution (K)')
77  plt.xlabel('Time (s)')
78  plt.title('Temperature of solution over time')
79  plt.legend(['10 gr','15 gr','20 gr'])
```

Figure 6.44: Python code for the heat transfer limitation model - Page 2.

```
80  plt.show()
81
82
83  "Create mean function out of datapoints"
84  '--------------------------------------------------------------------------------
85  T20g = np.zeros(len(timeave))
86  dT20g = np.zeros(len(timeave))
87  Q = np.zeros(len(timeave))
88  phi_m = np.zeros(len(timeave))
89  #T_wall = np.zeros(len(time5))
90  T_c = np.zeros(len(time5))
91  u_he = np.zeros(len(timeave))
92  Re = np.zeros(len(timeave))
93
94  #Qdot = np.zeros(len(dT20g))
95
96  for k in range(0,len(time5)):
97      T20g[k] = -np.exp((744.154374 - k)/196.447342) + 345.5391 # + 106 for fi
98      dT20g[k] = (1/196.447342) * np.exp((744.154374 - k)/196.447342) # + 106
99
100 plt.figure(3)
101 plt.plot(time5,f5,'-', color='red')
102 plt.plot(time5,T20g,'-', color = 'blue')
103 plt.ylabel('Temperature of solution (K)')
104 plt.xlabel('Time (s)')
105 plt.title('Temperature of solution over time')
106 plt.legend(['Mean data set', 'Power regression'], loc='upper right')
107 plt.show()
108
109 plt.figure(4)
110 plt.plot(time5,dT20g,'-', color = 'blue')
111 plt.ylabel('Temperature change of solution (K)')
112 plt.xlabel('Time (s)')
113 plt.title('Temperature change of solution over time')
114 plt.show()
115
116 "Challenge 1 - Static Model to obtain the overall heat transfer coefficient"
117 '--------------------------------------------------------------------------------
118 U_ss = 2*labda_w/(D_out*np.log(D_out/(D_in))) #[W m^-2 k^-1]Thermal resistan
119 U_wat = 2*labda_ss/((D_out+D_he)*np.log((D_out+D_he)/(D_out))) #[W m^-2 k^-1
```

Figure 6.45: Python code for the heat transfer limitation model - Page 3.

```
120
121 U_tot = 1/(1/U_ss + 1/U_wat)
122
123 def Q_func(dT):
124     Q = r*-DeltaH*1000*m_sol/rho_sol
125     return Q
126
127 for k in range(len(dT20g)):
128     Q[k] = Q_func(dT20g[k])
129
130
131 plt.figure(5)
132 plt.plot(time5,T20g,'-', color = 'blue')
133 plt.plot(time5,f5,'-', color='red')
134 plt.ylabel('Temperature of solution (K)')
135 plt.xlabel('Time (s)')
136 plt.title('Temperature of solution over time')
137 plt.show()
138
139 "Challenge 2 - Dynamic Model to obtain the mass flow of the cooling water."
140 '--------------------------------------------------------------------------
141 def T_c_func(T_20g, Q):
142    Tc = T_20g-(Q/(U_tot*A_wall))
143    return Tc
144
145 for k in range(len(timeave)):
146     T_c[k] = T_c_func(T20g[k], Q[k])
147
148 def phi_m_func(T_20g, Q, T_c):
149    #T_c(x) = (T_20g-(Q/(U_tot*A_wall)))
150    phi_m = (-U_wat*m.pi*D_he*L_real)/(C_pwater*np.log((T_20g-T_c)/(T_20g-T_i
151    return phi_m
152
153 for k in range(len(timeave)):
154     phi_m[k] = phi_m_func(T20g[k], Q[k], T_c[k])
155
156 phi_v = phi_m*997 # ml/s
157
158 plt.figure(6)
159 plt.plot(time5,phi_v,'-', color = 'blue')
```

Figure 6.46: Python code for the heat transfer limitation model - Page 4.

```
plt.ylabel('Volume flow of cooling water (mL/s)')
plt.xlabel('Time (s)')
plt.title('Volume flow of cooling water over time')
plt.show()



"Challenge 3 - Determining Flow Regime"
'-------------------------------------------------------------------------------

plt.figure(7)
plt.plot(time5,T_c,'-', color = 'blue')
plt.ylabel('Temperature of cooling water')
plt.xlabel('Time (s)')
plt.title('Temperature of cooling water over time')
plt.show()

def u_he_func(phim):
    u = phim/(rho_w*(np.pi*0.5*(D_he)**2))
    return u

for k in range(len(timeave)):
    u_he[k] = u_he_func(phi_m[k])

Re_lim = np.zeros(len(timeave))

for k in range(len(timeave)):
    Re_lim[k] = 2040

mu = 0.00089 # Dynamic viscosity of water at 25 degrees (worst case scenario

def Re_func(uhe):
    Rey =  uhe*L/mu
    return Rey

for k in range(len(timeave)):
    Re[k] = Re_func(u_he[k])

plt.figure(8)
plt.plot(u_he,Re,'-', color = 'blue')
```

Figure 6.47: Python code for the heat transfer limitation model - Page 5.

```
200  plt.ylabel('Reynolds number')
201  plt.xlabel('Flow velocity (m/s)')
202  plt.title('Reynolds number for flow discipline approximation')
203  plt.show()
204
205  "Challenge 4 - Determining backcooling of reaction mixture by cooling water.
206  '--------------------------------------------------------------------------
207
208  T_cout = np.zeros(len(timeave))
209
210  def backcooling(Q, phi_m):
211      T_cout = Q/(phi_m*C_pwater) + T_in
212      return T_cout
213
214  for k in range(len(T_cout)):
215      T_cout[k] = backcooling(Q[k], phi_m[k])
216
217  Tsol = np.zeros(len(timeave))
218
219  def backcooling2(Q, T_cout):
220      Tsol = Q/(U_tot*A_wall) + T_cout
221      return Tsol
222
223  for k in range(len(Tsol)):
224      Tsol[k] = backcooling2(Q[k], T_cout[k])
225
226  plt.figure(9)
227  plt.plot(timeave,T_cout,'-', color = 'blue')
228  plt.ylabel('Cooling water temperature (T)')
229  plt.xlabel('Time (s)')
230  plt.title('Outflowing cooling water temperature')
231  plt.show()
232
233  plt.figure(10)
234  plt.plot(timeave, Tsol,'-', color = 'red')
235  plt.ylabel('Temperature of reaction mixture (T)')
236  plt.xlabel('Time (s)')
237  plt.title('Temperature of reaction mixture during active cooling')
238  plt.show()
239
```

Figure 6.48: Python code for the heat transfer limitation model - Page 6.

```
240  plt.figure(11)
241  plt.plot(timeave,T_cout,'-', color = 'blue')
242  plt.plot(timeave, Tsol,'-', color = 'red')
243  plt.ylabel('Temperature (T)')
244  plt.xlabel('Time (s)')
245  plt.legend(['T cooling water', 'T mixture'], loc='right')
246  plt.title('Reaction mixture temperature and cooling water temperature')
247  plt.show()
248
```

Figure 6.49: Python code for the heat transfer limitation model - Page 7.

Bibliography

[1] Georgios I. Maniatis and Nikolaos Milonas. "The impact of wind and solar power generation on the level and volatility of wholesale electricity prices in Greece". In: *SSRN Electronic Journal* (2022). DOI: 10.2139/ssrn.3998732.

[2] J O Bockris and A J Appleby. "Hydrogen Economy: An Ultimate Economy. A practical answer to the problem of energy supply and pollution." In: *Environmental This* 1.1 (July 1972), pp. 29–35. DOI: 10.1126/science.176.4041.1323.

[3] K. S. V. Kalathur S. V. Santhanam et al. *Introduction to hydrogen technology*. John Wiley et Sons, 2018.

[4] IRENA. *Hydrogen*. 2023. URL: https://www.irena.org/Energy-Transition/Technology/Hydrogen#:~:text=As%20at%20the%20end%20of,around%204%25%20comes%20from%20electrolysis..

[5] US Department of Energy. *Liquid Hydrogen Delivery: Hydrogen and Fuel Cell Technologies Office*. Sept. 2020. URL: https://www.energy.gov/eere/fuelcells/liquid-hydrogen-delivery#:~:text=Gaseous%20hydrogen%20is%20liquefied%20by,plant%20in%20large%20insulated%20tanks..

[6] D.K. Ross. "Hydrogen storage: The major technological barrier to the development of hydrogen fuel cell cars". In: *Vacuum* 80.10 (2006), pp. 1084–1089. DOI: 10.1016/j.vacuum.2006.03.030.

[7] Cevahir Tarhan and Mehmet Ali Çil. "A study on hydrogen, the clean energy of the future: Hydrogen Storage Methods". In: *Journal of Energy Storage* 40 (2021), p. 102676. DOI: 10.1016/j.est.2021.102676.

[8] Asbjørn Klerke et al. "Ammonia for hydrogen storage: Challenges and opportunities". In: *Journal of Materials Chemistry* 18.20 (2008), p. 2304. DOI: 10.1039/b720020j.

[9] W. Betteridge and J. Hope. "The Separation of Hydrogen from Gas Mixtures: A process of absorption and desorption by palladium." In: *Platinum Metals Review* 19 (Feb. 1975).

[10] Y.K. Ip, S.F. Chew, and D.J. Randall. "Ammonia toxicity, tolerance, and excretion". In: *Fish Physiology* (2001), pp. 109–148. DOI: 10.1016/s1546-5098(01)20005-3.

[11] M. Markiewicz et al. "Environmental and Health Impact Assessment of Liquid Organic Hydrogen Carrier (LOHC) systems – challenges and preliminary results". In: *Energy amp; Environmental Science* 8.3 (2015), pp. 1035–1045. DOI: 10.1039/c4ee03528c.

[12] Hani Nasser Abdelhamid. "A review on hydrogen generation from the hydrolysis of sodium borohydride". In: *International Journal of Hydrogen Energy* 46.1 (2021), pp. 726–765. DOI: 10.1016/j.ijhydene.2020.09.186.

[13] Mirela Dragan. "Hydrogen storage in complex metal hydrides nabh4: Hydrolysis reaction and experimental strategies". In: *Catalysts* 12.4 (2022), p. 356. DOI: 10.3390/catal12040356.

[14] Nejc Klopcic et al. "A review on metal hydride materials for hydrogen storage". In: *Journal of Energy Storage* 72 (2023), p. 108456. DOI: 10.1016/j.est.2023.108456.

[15] Jianjun Liu and Wenqing Zhang. "Improvement on hydrogen storage properties of complex metal hydride". In: *Hydrogen Storage* (2012). DOI: 10.5772/50153.

[16] Christian Hulteberg Bianca Rolim Josephine Digne. "H2Fuel Technology - White Paper". In: (Nov. 2022).

[17] Z.P. Li et al. "Protide compounds in hydrogen storage systems". In: *Journal of Alloys and Compounds* 356-357 (2003), pp. 469–474. DOI: 10.1016/s0925-8388(02)01241-0.

[18] H. I. Schlesinger, Herbert C. Brown, and A. E. Finholt. "The preparation of sodium borohydride by the high temperature reaction of sodium hydride with borate esters1". In: *Journal of the American Chemical Society* 75.1 (1953), pp. 205–209. DOI: 10.1021/ja01097a054.

[19] USED. "Go no or go recommendation for sodium borohydride for on-board vehicular hydrogen storage". In: (2007). DOI: 10.2172/1219597.

[20] Asım Balbay and Cafer Saka. "The effect of the concentration of hydrochloric acid and acetic acid aqueous solution for fast hydrogen production from methanol solution of nabh4". In: *International Journal of Hydrogen Energy* 43.31 (2018), pp. 14265–14272. DOI: 10.1016/j.ijhydene.2018.05.131.

[21] Asım Balbay and Cafer Saka. "Semi-methanolysis reaction of potassium borohydride with phosphoric acid for effective hydrogen production". In: *International Journal of Hydrogen Energy* 43.46 (2018), pp. 21299–21306. DOI: 10.1016/j.ijhydene.2018.09.167.

[22] Kang Chen et al. "Efficient hydrogen release from libh4 alcoholysis in methanol/ethylene glycol based solutions over a wide temperature range". In: *Journal of Alloys and Compounds* 905 (2022), p. 164030. DOI: 10.1016/j.jallcom.2022.164030.

[23] Marie-Helene Grosjean, Moussa Zidoune, and Lionel Roue. "Hydrogen generation via alcoholysis reaction using ball-milled MG-based materials". In: *ECS Meeting Abstracts* MA2005-01.1 (2006), pp. 2–2. DOI: 10.1149/ma2005-01/1/2.

[24] Na Yang et al. "Alcoholysis features of lithium aluminum hydrides for its hydrolysis reaction at low-temperature". In: *International Journal of Hydrogen Energy* 47.68 (2022), pp. 29382–29389. DOI: 10.1016/j.ijhydene.2022.06.262.

[25] Lin Yu and Michael A. Matthews. "Hydrolysis of sodium borohydride in concentrated aqueous solution". In: *International Journal of Hydrogen Energy* 36.13 (2011), pp. 7416–7422. DOI: 10.1016/j.ijhydene.2011.03.089.

[26] Cafer Saka. "Surface modification with oxygen doping of G-C3N4 nanoparticles by carbon vacancy for efficient dehydrogenation of sodium borohydride in methanol". In: *Fuel* 310 (2022), p. 122444. DOI: 10.1016/j.fuel.2021.122444.

[27] Cafer Saka and Asım Balbay. "Fast and effective hydrogen production from ethanolysis and hydrolysis reactions of potassiumnbsp;borohydride using phosphoric acid". In: *International Journal of Hydrogen Energy* 43.43 (2018), pp. 19976–19983. DOI: 10.1016/j.ijhydene.2018.09.048.

[28] H ATIYEH and B DAVIS. "Separation of sodium metaborate from sodium borohydride using nanofiltration membranes for hydrogen storage application". In: *International Journal of Hydrogen Energy* 32.2 (2007), pp. 229–236. DOI: 10.1016/j.ijhydene.2006.06.003.

[29] Qinglin Zhang et al. "Kinetics of catalytic hydrolysis of stabilized sodium borohydride solutions". In: *Industrial amp; Engineering Chemistry Research* 46.4 (2007), pp. 1120–1124. DOI: 10.1021/ie061086t.

[30] Qiwen Lai et al. "Hydrogen generation from a sodium borohydride–nickel core@shell structure under hydrolytic conditions". In: *Nanoscale Advances* 1.7 (2019), pp. 2707–2717. DOI: 10.1039/c9na00037b.

[31] Zhaolin Liu et al. "Pt and Ru dispersed on licoo2 for hydrogen generation from sodium borohydride solutions". In: *Journal of Power Sources* 176.1 (2008), pp. 306–311. DOI: 10.1016/j.jpowsour.2007.09.114.

[32] Sanjay Kumar Singh, Yasuo Iizuka, and Qiang Xu. "Nickel-palladium nanoparticle catalyzed hydrogen generation from hydrous hydrazine for chemical hydrogen storage". In: *International Journal of Hydrogen Energy* 36.18 (2011), pp. 11794–11801. DOI: 10.1016/j.ijhydene.2011.06.069.

[33] Duong Dinh Tuan and Kun-Yi Andrew Lin. "Ruthenium supported on Zif-67 as an enhanced catalyst for hydrogen generation from hydrolysis of sodium borohydride". In: *Chemical Engineering Journal* 351 (2018), pp. 48–55. DOI: 10.1016/j.cej.2018.06.082.

[34] Y.V. Larichev et al. "Comparative XPS study of Rh/Al2O3 and rh/tio2 as catalysts for Nabh4 Hydrolysis". In: *International Journal of Hydrogen Energy* 35.13 (2010), pp. 6501–6507. DOI: 10.1016/j.ijhydene.2010.04.048.

[35] Shuai Hao et al. "Self-supported Spinel Feco2O4nanowire array: An efficient non-noble-metal catalyst for the hydrolysis of nabh4toward on-demand hydrogen generation". In: *Nanotechnology* 27.46 (2016). DOI: 10.1088/0957-4484/27/46/46lt03.

[36] "00/02589 an ultrasafe hydrogen generator: Aqueous, Alkaline Borohydride Solutions and Ru Catalyst". In: *Fuel and Energy Abstracts* 41.5 (2000), p. 289. DOI: 10.1016/s0140-6701(00)96502-0.

[37] R. Peña-Alonso et al. "A picoscale catalyst for hydrogen generation from NABH4 for fuel cells". In: *Journal of Power Sources* 165.1 (2007), pp. 315–323. DOI: 10.1016/j.jpowsour.2006.12.043.

[38] G. Guella, B. Patton, and A. Miotello. "Kinetic features of the platinum catalyzed hydrolysis of sodium borohydride from 11B NMR measurements". In: *The Journal of Physical Chemistry C* 111.50 (2007), pp. 18744–18750. DOI: 10.1021/jp0759527.

[39] Leigang Li et al. "Hydrogen generation from hydrolysis and methanolysis of guanidinium borohydride". In: *The Journal of Physical Chemistry C* 116.27 (2012), pp. 14218–14223. DOI: 10.1021/jp3032989.

[40] Olga V. Netskina et al. *Hydrogen generation by both acidic and catalytic hydrolysis of sodium borohydride*. 2018. URL: https://www.degruyter.com/document/doi/10.1515/cse-2018-0006/html.

[41] Z.T. Xia and S.H. Chan. "Feasibility study of hydrogen generation from sodium borohydride solution for Micro Fuel Cell Applications". In: *Journal of Power Sources* 152 (2005), pp. 46–49. DOI: 10.1016/j.jpowsour.2005.03.002.

[42] Nurettin Sahiner, Alper O. Yasar, and Nahit Aktas. "An alternative to metal catalysts: Poly(4-vinyl pyridine)-based polymeric ionic liquid catalyst fornbsp;H2 generation from hydrolysis and methanolysis of NABH4". In: *International Journal of Hydrogen Energy* 41.45 (2016), pp. 20562–20572. DOI: 10.1016/j.ijhydene.2016.08.182.

[43] O.V. Komova et al. "LiCoO2-based catalysts for generation of hydrogen gas from sodium borohydride solutions". In: *Catalysis Today* 138.3-4 (2008), pp. 260–265. DOI: 10.1016/j.cattod.2008.06.030.

[44] Tai-Feng Hung et al. "An alternative cobalt oxide-supported platinum catalyst for efficient hydrolysis of sodium borohydride". In: *Journal of Materials Chemistry* 21.32 (2011), p. 11754. DOI: 10.1039/c1jm11720c.

[45] Xiaofeng Wang et al. "Preparation and catalytic activity of PVP-protected au/ni bimetallic nanoparticles for hydrogen generation from hydrolysis of basic NABH4 solution". In: *International Journal of Hydrogen Energy* 39.2 (2014), pp. 905–916. DOI: 10.1016/j.ijhydene.2013.10.122.

[46] Joydev Manna, Binayak Roy, and Pratibha Sharma. "Efficient hydrogen generation from sodium borohydride hydrolysis using silica sulfuric acid catalyst". In: *Journal of Power Sources* 275 (2015), pp. 727–733. DOI: 10.1016/j.jpowsour.2014.11.040.

[47] Nuran Selvitepe, Asım Balbay, and Cafer Saka. "Optimisation of sepiolite clay with phosphoric acid treatment as support material for COB catalyst and application to produce hydrogen from the NABH4 hydrolysis". In: *International Journal of Hydrogen Energy* 44.31 (2019), pp. 16387–16399. DOI: 10.1016/j.ijhydene.2019.04.254.

[48] Yi Wang and Xiang Liu. "Catalytic hydrolysis of sodium borohydride for hydrogen production using magnetic recyclable cofe2O4-modified transition-metal nanoparticles". In: *ACS Applied Nano Materials* 4.10 (2021), pp. 11312–11320. DOI: 10.1021/acsanm.1c03067.

[49] D Hua. "Hydrogen production from catalytic hydrolysis of sodium borohydride solution using nickel boride catalyst". In: *International Journal of Hydrogen Energy* 28.10 (2003), pp. 1095–1100. DOI: 10.1016/s0360-3199(02)00235-5.

[50] Yixiu Xin, Zeyuan Wang, and Yanyan Jiang. "Kinetic study of NABH4 catalytic hydrolysis using supported Nico2O4". In: *Materials Research Express* 6.12 (2019), p. 125530. DOI: 10.1088/2053-1591/ab5d4c.

[51] Zhenkai Cui, Yueping Guo, and Jiantai Ma. "In situ synthesis of graphene supported CO-SN-B alloy as an efficient catalyst for hydrogen generation from sodium borohydride hydrolysis". In: *International Journal of Hydrogen Energy* 41.3 (2016), pp. 1592–1599. DOI: 10.1016/j.ijhydene.2015.11.081.

[52] Sibel Duman and Saim Özkar. "Ceria supported manganese(0) nanoparticle catalysts for hydrogen generation from the hydrolysis of sodium borohydride". In: *International Journal of Hydrogen Energy* 43.32 (2018), pp. 15262–15274. DOI: 10.1016/j.ijhydene.2018.06.120.

[53] Cuili Xiang et al. "Hydrogen generation by hydrolysis of alkaline sodium borohydride using a cobalt–zinc–boron/graphene nanocomposite treated with sodium hydroxide". In: *International Journal of Hydrogen Energy* 40.11 (2015), pp. 4111–4118. DOI: 10.1016/j.ijhydene.2015.01.145.

[54] Sankaran Murugesan and Vaidyanathan (Ravi) Subramanian. "Effects of acid accelerators on hydrogen generation from solid sodium borohydride using small scale devices". In: *Journal of Power Sources* 187.1 (2009), pp. 216–223. DOI: 10.1016/j.jpowsour.2008.10.060.

[55] Olga V. Netskina et al. "Hydrogen generation by both acidic and catalytic hydrolysis of sodium borohydride". In: *Catalysis for Sustainable Energy* 5.1 (2018), pp. 41–48. DOI: doi:10.1515/cse-2018-0006. URL: https://doi.org/10.1515/cse-2018-0006.

[56] Umit B. Demirci, Philippe Miele, and François Garin. "Catalysis in hydrolysis of sodium borohydride and ammonia borane, and electrocatalysis in oxidation of sodium borohydride". In: *Catalysis Today* 170.1 (2011), pp. 1–2. DOI: 10.1016/j.cattod.2011.04.005.

[57] R. Willem. "Cheminform abstract: Possible mechanisms of the reaction between tetrahydroborate and hydrogen ions: A permutational analysis". In: *Chemischer Informationsdienst* 10.13 (1979). DOI: 10.1002/chin.197913034.

[58] George A. Olah et al. "Electrophilic reactions at single bonds. vii. hydrogen-deuterium exchange accompanying protolysis (deuterolysis) of borohydride and aluminum hydride anions with anhydrous strong acids. intermediacy of pentahydroboron and pentahydroaluminum and their structural relation with the Methonium Ion". In: *Journal of the American Chemical Society* 94.22 (1972), pp. 7859–7862. DOI: 10.1021/ja00777a031.

[59] M. M. Kreevoy and J. E. Hutchins. "H2BH3 as an intermediate in tetrahydridoborate hydrolysis". In: *Journal of the American Chemical Society* 94.18 (1972), pp. 6371–6376. DOI: 10.1021/ja00773a020.

[60] Olga V. Netskina et al. "Hydrogen generation by both acidic and catalytic hydrolysis of sodium borohydride". In: *Catalysis for Sustainable Energy* 5.1 (2018), pp. 41–48. DOI: 10.1515/cse-2018-0006.

[61] O. Akdim, U.B. Demirci, and P. Miele. "Acetic acid, a relatively green single-use catalyst for hydrogen generation from sodium borohydride". In: *International Journal of Hydrogen Energy* 34.17 (2009), pp. 7231–7238. DOI: 10.1016/j.ijhydene.2009.06.068.

[62] Cafer Saka and Asım Balbay. "Influence of process parameters on enhanced hydrogen evolution from alcoholysis of sodium borohydride with a boric acid catalyst". In: *International Journal of Hydrogen Energy* 45.32 (2020), pp. 16193–16200. DOI: 10.1016/j.ijhydene.2020.04.094.

[63] Liuzhang Ouyang et al. "Hydrogen production via hydrolysis and alcoholysis of light metal-based materials: A Review". In: *Nano-Micro Letters* 13.1 (2021). DOI: 10.1007/s40820-021-00657-9.

[64] G.M. Arzac and A. Fernández. "Hydrogen production through sodium borohydride ethanolysis". In: *International Journal of Hydrogen Energy* 40.15 (2015), pp. 5326–5332. DOI: 10.1016/j.ijhydene.2015.01.115.

[65] Cafer Saka and Asım Balbay. "Influence of process parameters on enhanced hydrogen generation via semi-methanolysis and semi-ethanolysis reactions of sodium borohydride using phosphoric acid". In: *International Journal of Hydrogen Energy* 44.57 (2019), pp. 30119–30126. DOI: 10.1016/j.ijhydene.2019.09.172.

[66] Cafer Saka and Asım Balbay. "Metal-free catalyst fabrication by incorporating oxygen groups on the surface of the carbonaceous sample and efficient hydrogen production from NABH4 methanolysis". In: *International Journal of Hydrogen Energy* 47.11 (2022), pp. 7242–7251. DOI: 10.1016/j.ijhydene.2021.12.070.

[67] Cafer Saka and Asım Balbay. "Ethylene glycol as an alternative solvent approach for very efficient hydrogen production from sodium borohydride with phosphoric acid and acetic acid catalysts". In: *International Journal of Hydrogen Energy* 47.19 (2022), pp. 10500–10507. DOI: 10.1016/j.ijhydene.2022.01.131.

[68] Dongyan Xu et al. "Hydrogen generation from methanolysis of sodium borohydride over CO/Al2O3 catalyst". In: *Journal of Natural Gas Chemistry* 21.5 (2012), pp. 488–494. DOI: 10.1016/s1003-9953(11)60395-2.

[69] Yao-Hui Huang et al. "Development of AL2O3 carrier-RU composite catalyst for hydrogen generation from alkaline nabh4 hydrolysis". In: *Energy* 46.1 (2012), pp. 242–247. DOI: 10.1016/j.energy.2012.08.027.

[70] Nurettin Sahiner and Sahin Demirci. "Natural microgranular cellulose as alternative catalyst to metal nanoparticles for H2 production from nabh4 methanolysis". In: *Applied Catalysis B: Environmental* 202 (2017), pp. 199–206. DOI: 10.1016/j.apcatb.2016.09.028.

[71] Nurettin Sahiner, Sultan Butun, and Tugce Turhan. "P(AAGA) Hydrogel Reactor for in Situ co and ni nanoparticle preparation and use in hydrogen generation from the hydrolysis of sodium borohydride". In: *Chemical Engineering Science* 82 (2012), pp. 114–120. DOI: 10.1016/j.ces.2012.07.032.

[72] Kun-Yi Andrew Lin and Hsuan-Ang Chang. "Efficient hydrogen production from NABH4 hydrolysis catalyzed by a magnetic cobalt/carbon composite derived from a zeolitic imidazolate framework". In: *Chemical Engineering Journal* 296 (2016), pp. 243–251. DOI: 10.1016/j.cej.2016.03.115.

[73] Kaiqiang Yan et al. "Effect of preparation method on NI2P/SIO2 catalytic activity for NABH4 methanolysis and phenol hydrodeoxygenation". In: *International Journal of Hydrogen Energy* 40.46 (2015), pp. 16137–16146. DOI: 10.1016/j.ijhydene.2015.09.145.

[74] Nurettin Sahiner and Alper O. Yasar. "A new application for colloidal silica particles: Natural, environmentally friendly, low-cost, and reusable catalyst material for H2 production from nabh4 methanolysis". In: *Industrial amp; Engineering Chemistry Research* 55.43 (2016), pp. 11245–11252. DOI: 10.1021/acs.iecr.6b03089.

[75] Jonathan Snover and Ying Wu. *Recycle of discharged sodium borate fuel*. 2005.

[76] T. Kemmitt and G.J. Gainsford. "Regeneration of sodium borohydride from sodium metaborate, and isolation of intermediate compounds". In: *International Journal of Hydrogen Energy* 34.14 (2009), pp. 5726–5731. DOI: 10.1016/j.ijhydene.2009.05.108.

[77] Elliot L. Bennett et al. "A new mode of chemical reactivity for metal-free hydrogen activation by Lewis acidic boranes". In: *Angewandte Chemie* (2019). DOI: 10.1002/ange.201900861.

[78] Gregory C. Welch et al. "Reversible, metal-free hydrogen activation". In: *Science* 314.5802 (2006), pp. 1124–1126. DOI: 10.1126/science.1134230.

[79] Howard Edan Katz. "Hydride sponge: 1,8-naphthalenediylbis(dimethylborane)". In: *Journal of the American Chemical Society* 107.5 (1985), pp. 1420–1421. DOI: 10.1021/ja00291a057.

[80] Junior M.W. Chase. "Janaf Thermochemical tables third edition". In: *Analytical Chemistry* 61.24 (1989). DOI: 10.1021/ac00199a720.

[81] University of Pittsburgh Department of Chemistry. *Pitt Quantum Repository: Trimethyl borate*. URL: http://pqr.pitt.edu/mol/WRECIMRULFAWHA-UHFFFAOYSA-N.

[82] J. A. Martinho Simões and M. E. da Piedade. "A short and illustrated guide to metal-alkyl bonding energetics". In: *Energetics of Organic Free Radicals* (1996), pp. 169–195. DOI: 10.1007/978-94-009-0099-8_6.

[83] M. Rivarolo et al. "Thermo-Economic Analysis of a hydrogen production system by sodium borohydride (NABH4)". In: *International Journal of Hydrogen Energy* 43.3 (2018), pp. 1606–1614. DOI: 10.1016/j.ijhydene.2017.11.079.

[84] Adam Allerhand and Robert E Moll. "Indirect determination of boron-proton coupling in trimethyl borate by proton spin-echo NMR". In: *Journal of Magnetic Resonance (1969)* 1.4 (1969), pp. 488–493. ISSN: 0022-2364. DOI: https://doi.org/10.1016/0022-2364(69)90084-5. URL: https://www.sciencedirect.com/science/article/pii/0022236469900845.

[85] Cher-Chiek Chia et al. "Aluminum-hydride-catalyzed hydroboration of carbon dioxide". In: *Inorganic Chemistry* 60.7 (2021), pp. 4569–4577. DOI: 10.1021/acs.inorgchem.0c03507.

[86] Paul A. Cox et al. "Base-catalyzed aryl-B(OH)2 Protodeboronation Revisited: From concerted proton transfer to liberation of a transient aryl anion". In: *Journal of the American Chemical Society* 139.37 (2017), pp. 13156–13165. DOI: 10.1021/jacs.7b07444.

[87] Georgenbsp; L Cunningham. *Separation of trimethyl borate from the trimethyl borate-methanol azeotrope*. 1961.

[88] Zhenyu Bao et al. "Design, optimization and control of extractive distillation for the separation of trimethyl borate–methanol". In: *Industrial amp;amp; Engineering Chemistry Research* 53.38 (2014), pp. 14802–14814. DOI: 10.1021/ie502022m.

[89] Janine M. Unterreiner, Mark A. McHugh, and Val J. Krukonis. "Breaking the trimethyl borate-methanol azeotrope with supercritical methane". In: *Industrial amp;amp; Engineering Chemistry Research* 30.4 (1991), pp. 740–745. DOI: 10.1021/ie00052a018.

[90] Cheng-Hong Liu et al. "Trimethyl borate regenerated from spent sodium borohydride after hydrogen production". In: *Industrial amp;amp; Engineering Chemistry Research* 49.20 (2010), pp. 9864–9869. DOI: 10.1021/ie101309f.

[91] Zhenyu Bao et al. "Design, optimization and control of extractive distillation for the separation of trimethyl borate–methanol". In: *Industrial amp; Engineering Chemistry Research* 53.38 (2014), pp. 14802–14814. DOI: 10.1021/ie502022m.

[92] Darren M. Ould et al. "Sodium borates: Expanding the electrolyte selection for sodium-Ion Batteries". In: *Angewandte Chemie* 134.32 (2022). DOI: 10.1002/ange.202202133.

[93] Xi-Meng Chen et al. "Brønsted and Lewis base behavior of sodium amidotrihydridoborate (Nanh2bh3)". In: *European Journal of Inorganic Chemistry* 2017.38-39 (2017), pp. 4541–4545. DOI: 10.1002/ejic.201700556.

[94] Herbert C. Brown, Edward J. Mead, and B. C. Subba Rao. "A study of solvents for sodium borohydride and the effect of solvent and the metal ion on borohydride reductions1". In: *Journal of the American Chemical Society* 77.23 (1955), pp. 6209–6213. DOI: 10.1021/ja01628a044.

[95] Werner Büchner and Hans Niederprüm. "Sodium borohydride and amine-boranes, commercially important reducing agents". In: *Boron Chemistry–3* (1977), pp. 733–743. DOI: 10.1016/b978-0-08-021206-7.50007-0.

[96] Paul A. Cox et al. "Base-Catalyzed Aryl-B(OH)2 Protodeboronation Revisited: From Concerted Proton Transfer to Liberation of a Transient Aryl Anion". In: *Journal of the American Chemical Society* 139.37 (2017). PMID: 28823150, pp. 13156–13165. DOI: 10.1021/jacs.7b07444. eprint: https://doi.org/10.1021/jacs.7b07444. URL: https://doi.org/10.1021/jacs.7b07444.

[97] W. David English and Roger L. Kidwell. "Azeotrope of isopropyl alcohol and isopropyl borate". In: *Science* 139.3552 (1963), pp. 341–342. DOI: 10.1126/science.139.3552.341.

[98] Çetin Çakanyıldırım and Metin Guru. "Alternative energy storage key component trimethylborate: Synthesis, dehydration and kinetic parameters". In: *0 Isı bilimi ve tekniği dergisi = Journal of Thermal Sciences and Technology* 35 (Jan. 2015), pp. 53–57.

[99] Wu Ying, Michael T. Kelly, and Jeffrey V. Ortega. "Review of Chemical Processes for the Synthesis of Sodium Borohydride". In: *Millennium Cell Inc.* (Aug. 2004), p. 26.

[100] Marko Bertmer et al. "Short and medium range order in sodium aluminoborate glasses. 2. site connectivities and cation distributions studied by rotational echo double resonance NMR spectroscopy". In: *The Journal of Physical Chemistry B* 104.28 (2000), pp. 6541–6553. DOI: 10.1021/jp9941918.

[101] Fritz Ephraim and Eduard Michel. "Ueber metallhydride I. Alkalihydride". In: *Helvetica Chimica Acta* 4.1 (1921), pp. 762–781. DOI: 10.1002/hlca.19210040182.

[102] Nur Izzati Iberahim, Tan Beng Choo, and Khairunissa Syairah Ahmad Sohaimi. In: *Hexane-isopropanol extraction and quality assessment of omega-3 fish oil from Atlantic Salmon (Salmo salar)* (2020). DOI: 10.20944/preprints202012.0203.v1.

[103] Wenqi Li et al. "Separation of bio-based chemicals using pervaporation". In: *Journal of Chemical Technology amp;amp; Biotechnology* 95.9 (2020), pp. 2311–2334. DOI: 10.1002/jctb.6434.

[104] N. D. Scott, J. F. Walker, and V. L. Hansley. "Sodium naphthalene. i. A new method for the preparation of addition compounds of alkali metals and polycyclic aromatic hydrocarbons". In: *Journal of the American Chemical Society* 58.12 (1936), pp. 2442–2444. DOI: 10.1021/ja01303a022.

[105] Yaelle Roina et al. "Sodium naphthalenide Diglyme solution for etching PTFE, characterizations and molecular modelization". In: *ChemistrySelect* 7.21 (2022). DOI: 10.1002/slct.202200153.

[106] Andreas Reiß, Carsten Donsbach, and Claus Feldmann. "Insights into the naphthalenide-driven synthesis and reactivity of zerovalent iron nanoparticles". In: *Dalton Transactions* 50.44 (2021), pp. 16343–16352. DOI: 10.1039/d1dt02523f.

[107] Martin J. Pitt. "Chemical Safety: Dangers of Diglyme". In: *American Chemical Society* 88 (28).

[108] Josyula V. Kanth and Herbert C. Brown. "Improved procedures for the generation of diborane from sodium borohydride and boron trifluoride". In: *Inorganic Chemistry* 39.8 (2000), pp. 1795–1802. DOI: 10.1021/ic0000911.

[109] H.C. Brown, M. Srebnik, and T. E. Cole. "Cheminform abstract: Organoboranes. part 48. improved procedures for the preparation of boronic and borinic esters." In: *ChemInform* 18.14 (1987). DOI: 10.1002/chin.198714252.

[110] Herbert C. Brown et al. "Addition compounds of alkali metal hydrides. Sodium Trimethoxyborohydride and related compounds1". In: *Journal of the American Chemical Society* 75.1 (1953), pp. 192–195. DOI: 10.1021/ja01097a051.

[111] Akker H.E.A van den and R.F Mudde. *Fysische Transportverschijnselen*. VSSD, 2005.

[112] Keith J Laidler. "A glossary of terms used in chemical kinetics, including reaction dynamics (IUPAC Recommendations 1996)". In: *Pure and applied chemistry* 68.1 (1996), pp. 149–192.

[113] *The Engineering ToolBox: Metals, Metallic Elements and Alloys - Thermal Conductivities.* Aug. 2005. URL: https://www.engineeringtoolbox.com/thermal-conductivity-metals-d_858.html.

[114] "NIST Chemistry WebBook". In: *Choice Reviews Online* 41.12 (2004). DOI: 10.5860/choice.41sup-0257.

[115] J. E. Bennett and H. A. Skinner. "413. thermochemistry of organoboron compounds. part VII. the heats of reaction of diborane with acetone and with propan-2-ol". In: *Journal of the Chemical Society (Resumed)* (1962), p. 2150. DOI: 10.1039/jr9620002150.

[116] C S Kim. "Thermophysical properties of Stainless Steels". In: (Sept. 1975). DOI: 10.2172/4152287.

[117] L.P.B.M Janssen and M.M.C.G Warmoeskerken. *Transport phenomena data companion*. VSSD, Jan. 2006.

[118] Richard Fitzgerald. "New experiments set the scale for the onset of turbulence in Pipe Flow". In: *Physics Today* 57.2 (2004), pp. 21–23. DOI: 10.1063/1.1688059.

[119] K. Gersten. *Boundary layer theory*. New York, Springer-Verlag, 2003.

[120] J. Roland Ortt and Linda M. Kamp. "A technological innovation system framework to formulate niche introduction strategies for companies prior to large-scale diffusion". In: *Technological Forecasting and Social Change* 180 (2022). ISSN: 0040-1625. DOI: 10.1016/j.techfore.2022.121671.

[121] D. Kunnakorn et al. "Techno-economic comparison of energy usage between azeotropic distillation and hybrid system for water–ethanol separation". In: *Renewable Energy* 51 (2013), pp. 310–316. DOI: 10.1016/j.renene.2012.09.055.

[122] Globalpetrolprices. Dec. 2022. URL: https://nl.globalpetrolprices.com/Netherlands/electricity_prices/.

[123] Iea. *Executive summary – global hydrogen review 2021 – analysis*. 2021. URL: https://www.iea.org/reports/global-hydrogen-review-2021/executive-summary.

[124] M. Bobtelsky and R. D. Larisch. "713. the heat of solution of halides, sulphuric acid, oxalic acid, sodium hydroxide, and urea in ethyl alcohol–water mixtures". In: *J. Chem. Soc.* 0.0 (1950), pp. 3612–3615. DOI: 10.1039/jr9500003612.